Universität Rostock Traditio et Innovatio

Catalysis Leibniz-Institut für Katalyse e.V.

Synthesis and Characterization of Modular Pyrimdopteridine Photoredox Catalysts.

Master's thesis

in partial fulfillment of the requirements for the degree of

Master of Science (M.Sc.)

at the University of Rostock

Faculty for Mathematics and Natural Sciences

submitted by

Niels Hildebrandt

born January 25th 2001

in Itzehoe, Germany.

Leibniz Institute for Catalysis

at the University of Rostock

2024

Statutory Declaration

I herewith declare that I have composed the present thesis myself and without use of any other than the cited sources and aids. Sentences or parts of sentences quoted literally are marked as such; other references with regard to the statement and scope are indicated by full details of the publications concerned.

The thesis in the same or similar form has not been submitted to any examination body and has not been published.

Rostock, 23.09.2024, _____

This Master's thesis was written from 07th 05 2024 to 24th 09 2024 at the Leibniz Institute for Catalysis e.V. at the University of Rostock under the supervision of Dr. Jola Pospech.

1. Reviewer: Dr. Jola Pospech
2. Reviewer: Prof. Torsten Beweries

Acknowledgments

I want to start by expressing my sincere thanks to Prof. Beweries and Dr. Jola Pospech for their warm welcome to the working group and for introducing me to this challenging and exciting topic. Thank you for your continuous support and professional advice.

I want to express my special gratitude to Jola for her incredible academic support and trust in my ideas and work. I do not take that for granted.

My most enormous thanks also goes to all my colleagues, who showed understanding for me and my problems even during the stressful end of the thesis, both inside and outside the lab.

Many thanks to Tobi for supporting me through the whole master's thesis and keeping me sane at the end of the thesis. Explaining everything from analytical methods over concepts of calculation to how to restore corrupted Word files. Thank you.

Furthermore, I would like to express my immense gratitude to the entire analytical department at LIKAT for recording all the analytical data. A special thanks to Dr. Hans-Joachim Drexler for recording and evaluating X-ray structures and to Dr. Marcus Klahn's insightful talks regarding mass spectrometry.

Last but definitely not least, I would also like to thank my family, all my friends, and my girlfriend for their support and patience during the entire duration of my studies, especially during the intense phases of this academic journey. Thank you, Mom and Dad. Without your unconditional support, obtaining this degree would be impossible. Thank you, Eddy, for being a friend for longer than 12 years and being an inspiring comrade along the whole way. Your faith in me never lacked, which pleasingly is not disturbing. Thank you, Lari, for being simply the best. I couldn't have asked for a better person to spend the last time with.

Table of contents

List of Abbreviations

[M+]	molecular ion peak	M	metall
A		mmol	millimol
Ac	acetyl	MeCN	acetonitrile
Alk	alkyl	MeOH	methanol
aq.	aqueous	min	minute
Ar	aryl	mL	milliliter
B		MS	mass spectrometry
BINOL	1,1'-Bi-2-naphthol	m.p.	melting point
C		**m/z**	mass-to-charge ratio
calcd.	calculated	**N**	
cat.	catalytic	NEt_3	Triethylamine
$(COCl)_2$	Oxalyl chloride	NMR	nuclear magnetic resonance spectroscopy
D		NOESY	nuclear Overhauser effect spectroscopy
DBU	1,8-diazabicyclo [5,4,0]undec-7-ene	**O**	
DG	directing group	OEt	ethoxy
DMAP	4- (Dimethylamino)pyridine	**P**	
DMF	*N*,*N*-dimethylacetamide dimethylsulfoxid	PCET	proton coupled electron transfer
d.r.	diastereomeric ratio	PIDA	phenyliodine(III) diacetate
E		POAT	photoinduced O-atom transfer
ee	enantiomeric excess	ppm	parts per million
e.r.	enantiomeric ratio	PPT	pyrimidopteridine
EDG	electron-donating group	PPTNO	pyrimidopteridine-N-oxide
EI	electron ionization	PT	proton transfer
ESI	electrospray ionization	Ph	Phenyl
Et	Ethyl	ppm	parts per million
EWG	electron-withdrawing group	**Q**	
equiv.	equivalent	**R**	
EI-MS	electron ionization mass spectroscopy	R	rest
eV	electron volt	rt.	room temperature
F		**S**	
G		S	singlet
g	gramm	sat.	saturated
GC	gas chromatography	SCE	saturated calomel electrode

H	
h	hours
HAT	Hydrogen atom transfer
HOMO	highest occupied molecular orbital
HPLC	high-performance liquid chromatography
HRMS	high resolution mass spectroscopy
Hz	Hertz
I	
IC	internal conversion
IR	infrared spectroscopy
ISC	intersystem crossing
J	
J	coupling constant
K	
L	
LC	liquid chromatography
LED	light-emitting diode
LUMO	lowest occupied molecular orbital
M	
m	multiplett
SET	single electron transfer
solv	solved
T	
t	time
T	temperature
t	triplett
TBAPF	Tetrabutylammonium hexafluorophosphate
TLC	thin layer chromatography
TOF	time-of-flight
t_R	retention time
U	
UV	ultraviolet
V	
VIS	visible
W	
X	
Y	
Z	
Symbols	
δ	chemical shift

1 Introduction

Light from the UV-VIS range is able to interact with the electrons in molecules. In general, when a molecule in its ground state (S_0) is exposed to light of a specific wavelength, an electron from the highest occupied molecular orbital (HOMO) can get promoted to the closest orbital in energy, the lowest unoccupied molecular orbital (LUMO), resulting in two single-occupied molecular orbitals (SOMO). This electronically excited (S_1) species fundamentally differs in its reactivity from the species in the ground state. Not only does the electron now reside in a higher lying, but also geometrically changed orbital. Both of these factors contribute to the change in reactivity.[1]

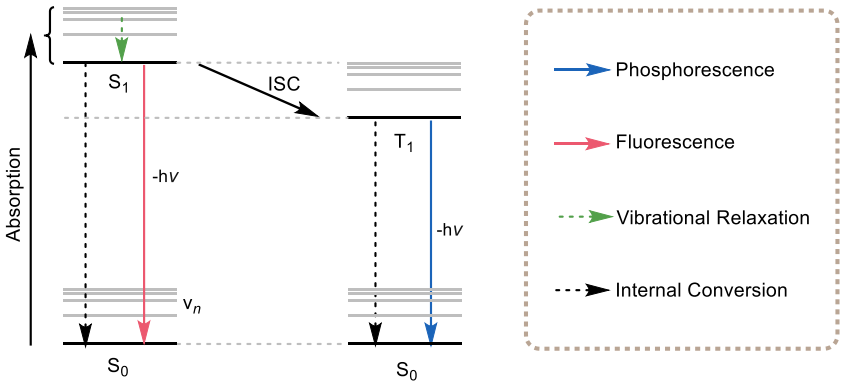

Scheme 1: Jablonski diagram.[1]

Concerning the now available photophysical pathways (Scheme 1), the excited species is able to relax to the S_0 ground state either by emitting the energy difference as radiation, formally known as fluorescence, or through an internal conversion (IC), a nonradiative transition (Scheme 1). Furthermore, the excited species is also able to populate the T_1 state through an intersystem crossing (ISC). The ISC is a radiationless, intramolecular energy transfer in which multiplicity is not maintained.[1] The T_1 state is also able to relax into the S_0 ground state by radiation-less or radiative spin-forbidden transition. This transition is known as phosphorescence. Notably, this relaxation process is spin-forbidden due to the change in multiplicity. Therefore, it is slower than the relaxation from the S_1 state to the S_0 ground state. As a result, the T_1 state is longer-lived than the S_1 state. If the T_1 and or S_1 states are sufficiently long-lived, bimolecular reactions become probable. Thus making highly reactive radical species accessible under mild conditions.[2]

1.1 Photoredox Catalysis

Photoredoxcatalysts (PCs) are based on the described behavior. Upon light irradiation, PCs reach an excited state, either S_1 or T_1, which is sufficiently long-lived to facilitate reactions. Furthermore, PCs are able to regenerate into their ground state after the reaction cycle is complete.[3] This leads to the general reaction pathways displayed in Scheme 2.

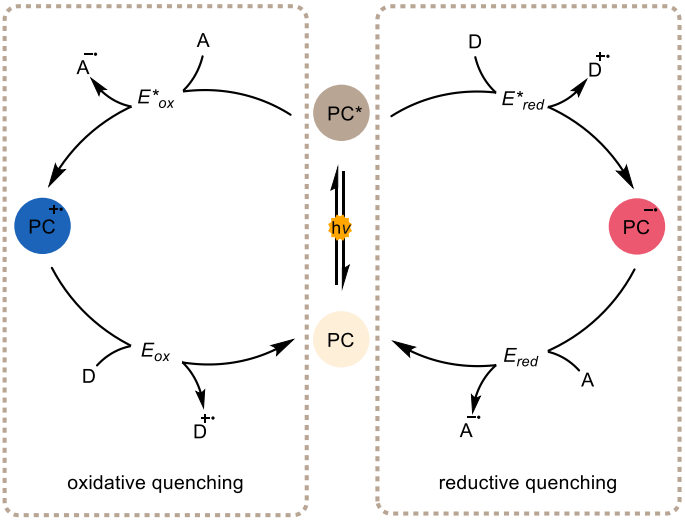

Scheme 2: General reaction pathway for photoredox catalysis.[4]

In both excited states (T_1 or S_1), the photocatalyst (PC*) is a stronger oxidizing and reducing agent. On the one hand, the promoted electron leaves a vacancy for a possible electron abduction from a substrate (D), leading to a reduction of the photocatalyst (right-hand path). Subsequently, the reduced $PC^{-\bullet}$ can get oxidized by an electron acceptor (A) to complete the cycle. This pathway is known as reductive quenching. On the other hand, the promoted electron from PC* can more efficiently reduce a substrate (A), simultaneously oxidizing the photocatalyst (left-hand path). The now oxidized $PC^{+\bullet}$ gets reduced again by an electron donor (D), fulfilling the cycle. This pathway is known as oxidative quenching. The redox potential in the excited state can be estimated via the energy of the excited states and the redox potential in the ground state.[4]

After the PC is excited, the PC* can react with an electron acceptor (A), and the latter is oxidized. If the PC* reacts with an electron donor, the PC is reduced. Subsequently, the $PC^{-\bullet}$ gets oxidized to complete the cycle. This pathway is known as reductive quenching (right-hand path).

Photoredox catalysts can be classified into two categories: organometallic complexes and organic molecules. In the recent past, metal-derived photocatalysts were predominantly based on iridium and ruthenium complexes. Examples of these are the well-established catalysts $Ru(bpy)_3^{2+}$ and *fac*-$Ir(ppy)_3$ (Scheme 3).[4]

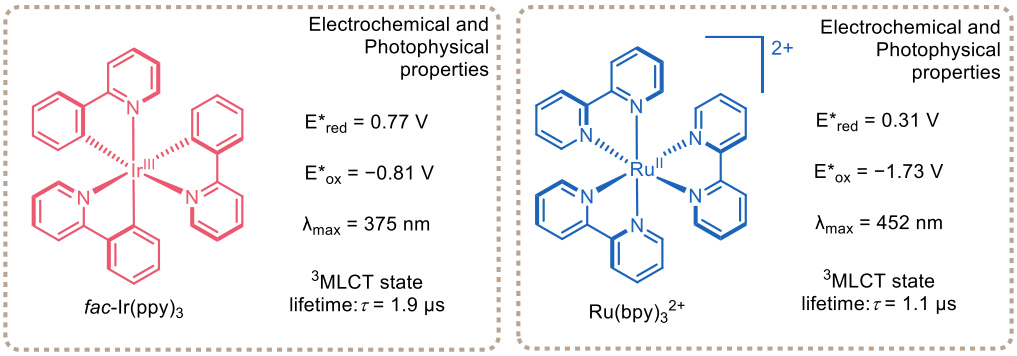

Scheme 3: Structure and properties of $Ru(bpy)_3^{2+}$ and *fac*-$Ir(ppy)_3$.[4]

Their popularity is grounded in their well-studied photochemical properties and their efficient ISC.[4,5] This leads to a high population of the T_1 state, resulting in a long time in the excited state. However, iridium and ruthenium, being second and third-row transition metals, are low in abundance.[6] Subsequently, two approaches to circumvent the use of these low-abundant elements are under investigation. Second and third-row -transition metals can be substituted with first-row transition metals like copper.[7,8]

Furthermore, second and third-row metal complexes can also be substituted with organic molecules. Organic molecules can be readily and meticulously fine-tuned to also efficiently promote photochemical reactions without the need for any metal at all.[9] It would be foolish, though, to reduce organic photoredox catalysis to a mere metal-free, more sustainable alternative to metal-based photocatalysts. Organic photocatalysts often react from the S_1 state, which is innately higher in energy compared to the T_1 state from which metal-based photocatalysts primarily react, allowing for a unique reactivity.[4] Subsequently, photoredox catalysis has already demonstrated a wide range of reactivities, including cycloadditions, bond cleavage, C–H functionalizations, alkene hydrofunctionalizations, and many more.[2] Still, exciting challenges remain. One of the more underdeveloped fields in photoredox catalysis, in general, is asymmetric photoredox catalysis.[10]

1.1.1 Asymmetric Photoredox Catalysis

Asymmetric synthesis using organo- or transition metal-based catalysts is a fundamental tool that is highly sought after among chemists. This has been apparent, particularly since two Nobel Prizes have already been awarded in this research area.[11–14] 2001, the first Nobel prize went to William S. Knowles and Ryoji Noyori “for their work on chirally catalyzed hydrogenation reactions” and the other half to K. Barry Sharpless “for his work on chirally catalyzed oxidation reactions”. In 2021, the second Nobel prize for asymmetric organic synthesis went to Benjamin List and David W.C. MacMillan "for the development of asymmetric organocatalysis”. Compared to this well-established research area, photocatalytic asymmetric catalysis is just emerging.[10]

Photocatalytic asymmetric catalysis offers enormous synthetic potential, opening the door for mild and, thus, environmentally friendly access to compounds and building blocks. However, compared to "classical" thermal asymmetric catalysis, an innate challenge has to be overcome. Comparing the general reactivity and enthalpy diagrams, the differences become evident (Scheme 4).

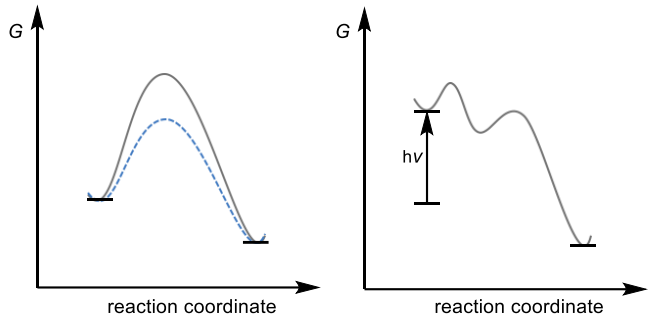

Scheme 4: Comparison between enthalpy diagrams of thermal catalysis (left-hand side) and photocatalysis (right-hand side).

In classical asymmetric catalysis, a close association between the catalyst and substrate is maintained through coordination and maintained throughout the catalytic cycle. This allows chiral catalysts to lower the energy barrier of a specific transition state (Scheme 4, left-hand side), resulting in an enantioselective process. However, this rationale is not easily translated to photoredox catalysis. In contrast, a photocatalyst facilitates the reaction through the increase of energy upon excitation (Scheme 4, right-hand side). After this rapid reaction, a close environment is no longer required to complete the catalytic cycle. However, enantioselectivity requires this chiral environment during the reaction.

Seeing that the close association does not come naturally to photocatalysis, two main approaches were developed:[15] The first one utilizes a dual or multi-catalytic system in which at least one component is chiral, dividing the task of the photochemical and enantioselective reaction. The second approach relies on a specific design or modification of the photocatalyst with functionalities that, through intermolecular binding, steric repulsion, and/or coordination, keep the substrate in a close environment and specific conformation. Through this functionalization, a chiral induction during the energy transfer or a later reaction step in the cycle is made possible in a single but bifunctional catalytic system.

Knowles and Miller *et al*. reported a key example of using a multi-catalytic system for the light-driven deracemization of unsymmetrical substituted imidazolinone derivatives (Scheme 5).[16]

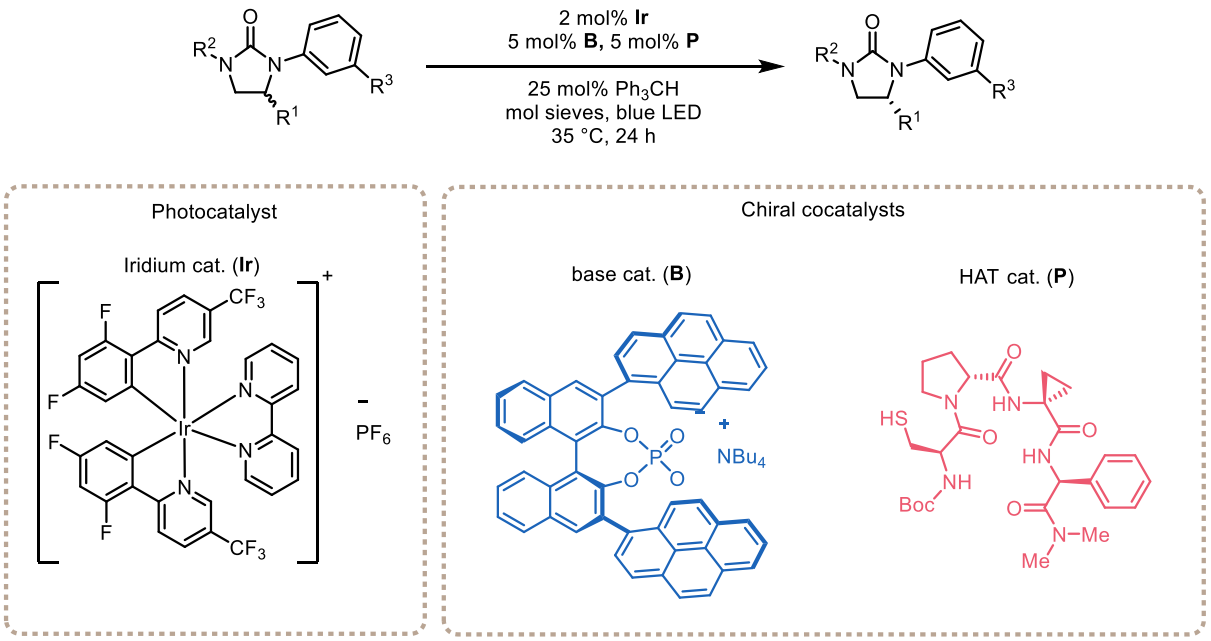

Scheme 5: Photo-mediated deracemization of imidazolinones.

Combining an iridium photocatalyst, a 1,1'-Bi-2-naphthol (BINOL) derived chiral phosphate base, and a cysteine-based peptide, 15 racemic imidazolinones were enantioenriched with an enantiomeric ratio between 81:19 and 96:5. They proposed that an iridium-catalyzed electron transfer (ET) resembling a classical photoredox event first creates a radical cation of both enantiomers (Scheme 6).

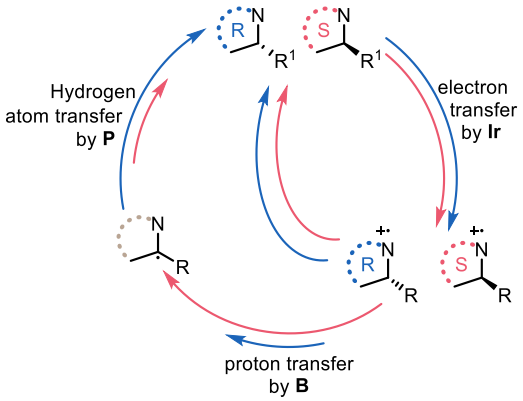

Scheme 6: Simplified reaction mechanism for the deracemization of racemic imidazolinones.
(The ratio of arrow lengths corresponds to the ratio of the reaction rate constant)

After deprotonation from the chiral phosphate base, the cysteine-catalyzed hydrogen atom transfer (HAT) to the prochiral methin radical obtains the product. Both of these independent steps are kinetically controlled. The proton transfer resembles a kinetic resolution in which the *S*-enantiomer reacts faster while the *R*-enantiomer is enriched, giving a chance for an ET back to the ground state. From the prochiral methin radical, the HAT preferably happens from the *re*-face forming the *R*-enantiomer. Consequently, in each cycle, the enantiomeric excess (*ee*) of the *R*-enantiomer is increased. Although independently only reaching mediocre enantioselectivity,

the combination of these seemingly mismatched steps creates the high enantioselectivities observed.

Combining classical transition metal catalysis with photochemistry, the group of Meggers utilized bis-cyclometalated photocatalysts for asymmetric reactions. [17,18] This demonstrates a variant of the bifunctional single catalytic system. The iridium and rhodium-based catalysts were equipped with two acetonitrile ligands, which were exchanged with the substrate prior to excitation, creating the photoactive species in situ.

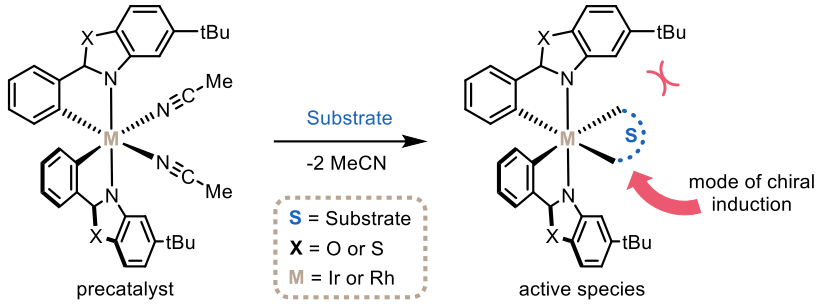

Scheme 7: Meggers *et al*. bis-cyclometalated photocatalysts for asymmetric induction.

Through the coordination of the substrate to the Lewis acidic metal center, a close association between the chiral environment could be ensured. This approach showed a broad reactivity, facilitating, among others, asymmetric Friedel-Crafts reactions, Micheal additions, cycloadditions, and radical radical couplings.[18]

In 2021, researchers led by Bach demonstrated a bifunctional approach using an all-organic framework (Scheme 8).[19] They discovered that by using chiral phosphoric acid and thioxanthone together in a single system rather than separately, it was possible to double the enantiomeric excess of a [2+2]-photocycloaddition of *N,O*-acetals derived from unsaturated aldehydes and olefines.

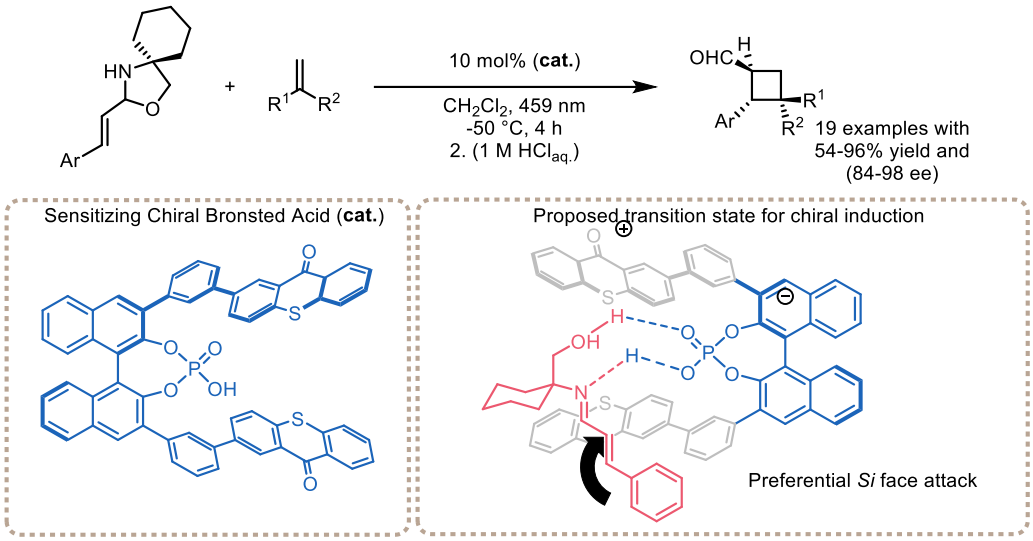

Scheme 8: [2+2]-photocycloaddition of *N*,*O*-acetals.

The scope encompassed 19 cyclobutanecarbaldehydes with yield ranging from 54% to 94% in 84 to 98% *ee*. Building on a model proposed by Akiyama and co-workers,[20] Bach *et al.*, in cooperation with the working group of Gschwind *et al.*, proposed that a *Si attack on the* in-situ generated iminium ion intermediate is favored, owing to the hydrogen bonding between the intermediate and phosphoric acid (Scheme 8). Extensive low-temperature NMR studies supported this claim.

1.2 Pyrimidopteridine as Photoredox Catalysts

Having a strong background in the field of heteroarene *N*-oxides and inspired by the potential of flavins, the Pospech group began the investigation of the structurally related pyrimidopteridines.[21,22] 3,7,9-tetrabutyl-2,4,6,8-tetraoxo-[5,4-*g*]pteridine (BuPPT *N*-oxide) was first reported in 1989 by Maki *et al.*, already demonstrating a broad reactivity of N-demethylation,[23] C-H oxygenation,[24–26] and oxidative C-C bond cleavage,[24,27,28] at this time still as a stochiometric oxygen atom transfer reagent.

The investigations of the Pospech group began with establishing a robust gram-scale synthesis of 4 *N*-substituted pyrimidopteridine. Notably, the former use of the toxic lead tetraacetate could be avoided instead using phenyliodine(III) diacetate (PIDA), a hypervalent iodine species. Subsequently, a thorough investigation of the photophysical properties of PPT *N*-oxides and PPTs revealed the potency of their excited state, exceeding reduction potentials of +2.0 V vs SCE.[29,30] The deoxygenated PPT derivatives were easily accessible through POAT.[29]

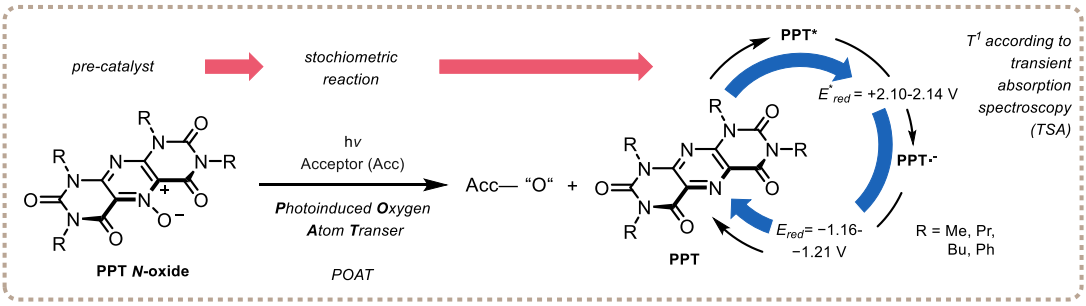

Scheme 9: Accessing PPTs through deoxygenation of PPT.

With these potent, metal-free photocatalysts in hand, a broad reactivity encompassing C–N,[31] C–C,[32] C–O,[33] and C–H/C–D[34] bond formation could be established (Scheme 10).

The photomediated hydroamination of stilbenes with chiral aliphatic amines is the first of its kind (Scheme 10A).[31] In fact, preserving the stereogenic center of aliphatic amines in oxidative transformation poses an innate challenge. When the amine is oxidized, the *α*-amino C–H bond is drastically acidified, resulting in *α*-deprotonation and, thus, racemization.[35] The scope of the hydroamination encompassed linear aliphatic, branched aliphatic, benzylic primary, and protected alcohol-containing amines. The preservation of the stereocenter was demonstrated utilizing *R*- and *S*-1-Phenylethylamine. No sign of stereo-degradation could be detected. Furthermore, the reaction does not require further additives or cocatalysts, which becomes apparent by looking at the evidence gathered for the proposed catalytic cycle. Not only does the PPT react as an efficient one-electron oxidant, but it most likely also acts as a HAT reagent. PPT *N*-oxide is deoxygenated, subsequently excited, and oxidizes the stilbene, forming a cationic stilbene radical. After the amine reacts with the stilbene intermediate, it forms the corresponding ammonium adduct carrying a *C*-centered radical in the beta position. Next, the PPT*- radical anion could act as a base, deprotonating the stilbene amine adduct to form a neutral PPTH* radical. The PPTH* radical subsequently performs the discussed HAT to the formed benzylic radical, closing the catalytic cycle. This step is supported by EPR and an absent side reaction, which otherwise would be likely to occur.

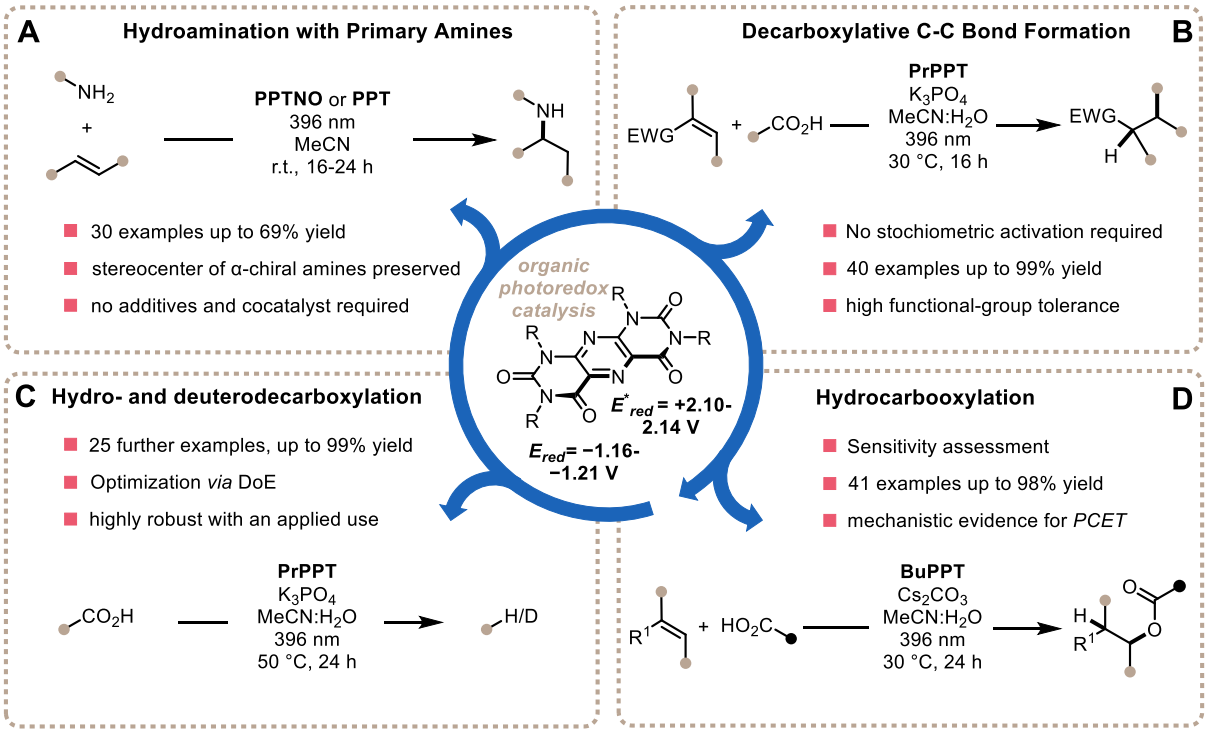

Scheme 10: Overview of the established reactivity of PPTs.

The C–C bond formation was facilitated through a decarboxylative Giese-type reaction (Scheme 10B).[32] This reaction, in general, offers C–C bond formation through a coupling of a nucleophilic radical and an electron-deficient alkene (Michael acceptor). The Giese reaction initially involved the transformation of Barton esters or alkyl halides into corresponding radicals using AIBN or tributylstannane.[36] In contrast to previously published photocatalytic approaches, Pospech *et al*. achieved this transformation photocatalytically without the need for stochiometric activation of the carboxylic acid. The scope encompasses 40 examples with up to 99% yield utilizing a multitude of different carboxylic acids and a variety of electron-deficient alkenes. Furthermore, evidence for the underlying mechanism was gathered. It was proposed that PrPPT *N*-oxide is deoxygenated in situ and subsequently excited through irradiation. The now excited PrPPT* performs a SET to the carboxylic acid, decarboxylating and oxidizing the acid in the process. The resulting alkyl radical then recombines with the alkene, creating a new C–C bond and a stabilized radical. The formerly reduced catalyst now reduces the radical, forming an anionic intermediate, which is protonated to yield the final product, closing the redox neutral cycle.

Strikingly, in some cases, rather than forming a C–C bond, a hydroacetoxylation product was obtained (Scheme 10D).[33] Further investigation of the oxidation potentials rationalized this reactivity. When the oxidation potential of the acid derivative is higher than that of the alkene, the alkene is oxidized and can then react with the carboxylic acid. This reactivity was utilized to carry out various hydrocarboxylations, resulting in a total of 41 products. These products included combinations of aromatic, heteroaromatic, alkenyl, and aliphatic carboxylic acids with

(*E*)-stilbene, as well as different alkenes with benzoic acid. Again, evidence of an HAT could be collected, underlining the multiple reaction facets of PPTs.

Moreover, it was demonstrated that PPTs, in combination with a base, are able to hydrodecarboxylate benzylic carboxylic acids (Scheme 10C).[34] This reactivity could be utilized to efficiently hydro- and deuterodecarboxylate various pharmaceutically and biologically active aliphatic carboxylic acids. In addition, the established method could also be performed on a large scale and form drugs in tablet form, highlighting its robustness. Consequently, the procedure presents a solution approach for the environmental contamination of drug residues.[37]

1.2.1 Towards asymmetric and functionalized Pyrimidopteridine

Given the multifaceted reactivity of PPTs, which act as photooxidants, proton acceptors, and HAT reagents, the next logical step is to explore the possibility of asymmetric photoredox catalysis.[38,39]

As discussed, there are multiple approaches to asymmetric photocatalysis. It is reasoned that through strategic *N*-substituent modification, repulsive steric or attractive noncovalent interactions will lead to chiral induction of prochiral substrates. To realize this approach, chiral peptide chains, inspired by Knowles, will be employed on the nitrogen atoms.[16] Consequently, this leads to three possibilities for arranging the chiral substituents: the *NNN*-face, the *NONON*-face, and the chiral substituents on both faces (Scheme 11). By dividing the close environment of the PPTs into eight octants, the conformation of these substituents is expected to follow the arrangement depicted in Scheme 11. As a result, chiral pockets, resembled by the clear space, will form in which the reaction might take place.

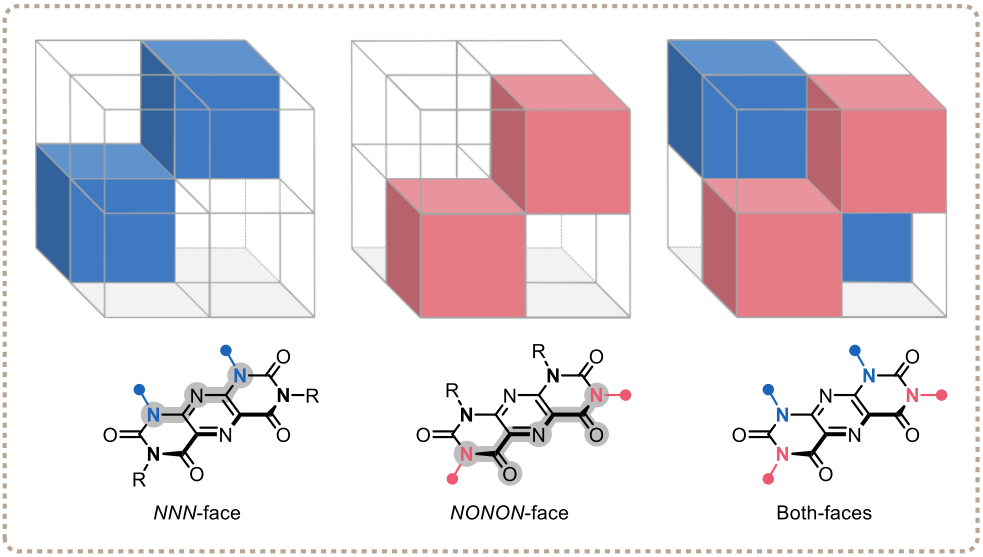

Scheme 11: Theoretical model of chiral PPT photoredox catalysts.

Previous PPTs were limited to 1,3,7,9-tetra alkyl (or aryl) substituents.[21,29] Recent efforts allowed for the selective synthesis of a varied substitution pattern on the PPT photoredox catalyst core.[40] A recently published methodology, describes the synthesis of three novel 3,7-difunctionalized PPTs bearing protected and unprotected alkylcarboxyl groups on the *N*-substituents derived from unnatural amino acid 2-methylalanine on the *NONON*-face. The catalysts were fully characterized by photophysical and electrochemical means and notably remain largely unaffected by the varied substitution pattern.

Although this synthetic procedure was showcased to be robust and scalable, 8 steps were required, and an overall yield of 20% and 13% was achieved, allowing room for improvement (Scheme 12).[40]

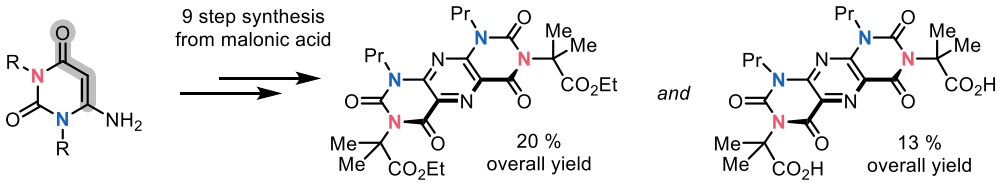

Scheme 12: *NONON*-face functionalized PPTs.

2 Objectives

The primary objective of this thesis is to synthesize the novel *NNN*-substituted PPT framework, which has not been previously investigated (Scheme 13). Subsequently, the aim is to determine whether the photophysical and electrochemical properties of this new PPT are comparable to the excellent properties of the former PPT photocatalysts.

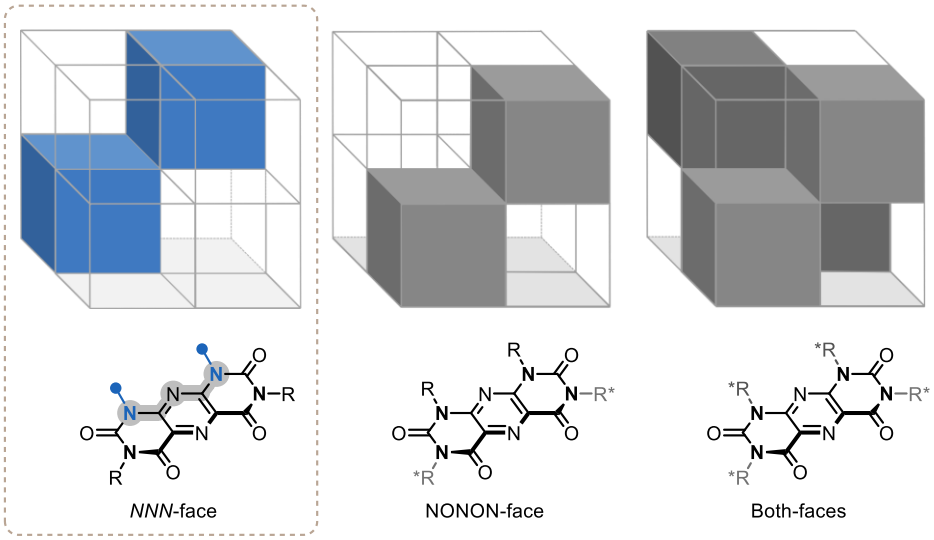

Scheme 13: Target substitution pattern for the thesis.

Previously, the key step in the synthesis of the PPT core was the oxidative dimerization of uracil derivatives, which formed the pyrazine ring and, subsequently, the PPT. Starting from noncommercial complex uracil derivatives, the synthesis of these starting materials can be labour-intensive, and each step is accompanied by material losses.

For this thesis, the approach for the synthesis was rethought, with the potential to simplify and streamline the process significantly. The new retrosynthetic approach first disconnects the nitrogens at the 1 and 9 positions of the PPT **4**, resulting in a pyrazine-2,6-dicarboxamide derivative **3**, which can be further broken down to 2,6-pyrazinedicarboxylic acid **2** and a urea derivative **1** (Scheme 14). Furthermore, the possibility of utilizing this approach to obtain an entirely new class of PPTs by starting from the 2,5-pyrazinedicarboxylic **2a** acid will be explored.

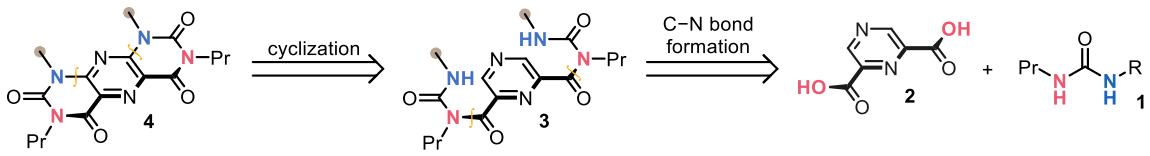

Scheme 14: Retrosynthetical approach to the synthesis of pyrimdopteridines.

3 Results and Discussion

3.1 Synthesis of 1,3-*N*,*N*-disubstituted ureas

The revised synthetic approach for *N*,*N*,*N*-functionalized PPTs **4** through the cyclization of pyridzincarboxamides **3** necessitates the synthesis of 1,3-disubstituted ureas **1**. The urea derivatives will feature a propyl substituent (N, black) on the left side, while the right side will be functionalized with a carboxyalkyl group (N, blue).

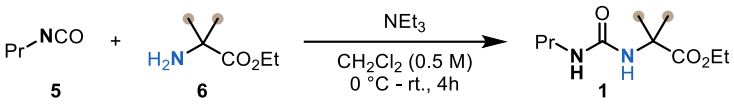

Scheme 15: Synthesis of unsymmetrically substituted ureas.

These ester functionalities serve as valuable handles for subsequent chiral modifications of the PPT frameworks and are derived from *α,α'-gem*-disubstituted artificial amino acids **6**. This approach acknowledges the work of Knowles *et al.*, where *α,α'-gem*-disubstitution significantly influences the τ-angle, subsequently affecting the bite angle and rigidity of the HAT (Hydrogen Atom Transfer) PPT catalyst, which is crucial for the catalyst's performance.[41] Thus, the *α,α'-gem*-disubstitution needs to be carefully considered from the initial stages of synthesis.

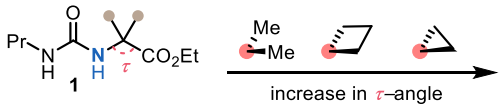

Scheme 16: Comparison of τ-angles in urea derivatives.

The urea derivatives were synthesized following literature-known procedures.[40,42] *α,α'-gem*-disubstituted amino acid hydrochloride salts **6a-6c** and *n*-propylamine **6d** were utilized as nucleophiles in an addition reaction to *n*-propylisocyanate **7** (Table 1).

Table 1: Scope of the herein employed ureas.[a]

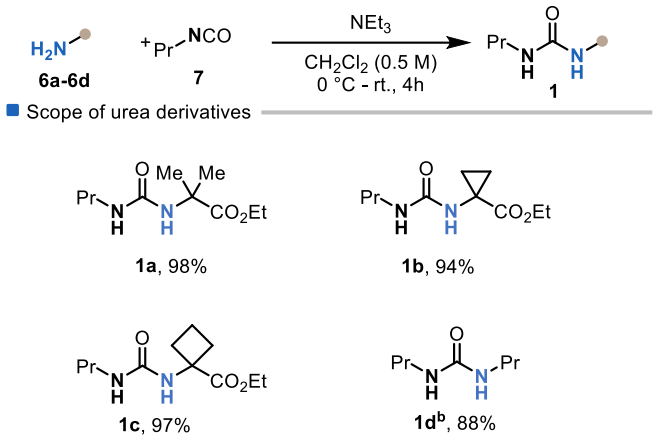

[a]Reactions were run at 10 mmol (**1a**), 1 mmol (**1b**), 1.5 mmol (**1c**) scale using **6** (1 equiv.) **7** (1.1 equiv.) and NEt_3 (1.2 equiv.). [b]**1d** was run at 5 mmol scale using **6d** (1.1 equiv.) and **7** (1.0 equiv.) in tetrahydrofuran. Yields refer to isolated yields after purification.

Four 1,3-dipropyl ureas **1a**-**1d** were successfully synthesized in 88-98% yield. The transformation was complete within 4 h, and the crude product solely requires an acidic workup to yield a pure product on a multigram scale. Noteworthy, the *α,α'-gem*-disubstitution in **1a**-**1c** did not impair the yield of the product. Furthermore, the urea derivative **1d** was synthesized utilizing *n*-propylamine **6d** as a nucleophile for the addition to *n*-propylisocyanate **7** in THF. This yielded the product **1d** in 1h with no further purification required. This underlines the straightforward accessibility of these starting materials.

3.2 Synthesis of dipropylpyrazine dicarboxamides through acylation of urea derivatives

With the urea derivatives **1a-1d** in hand, the pyrazine carboxamide **3** synthesis was approached (Scheme 17).

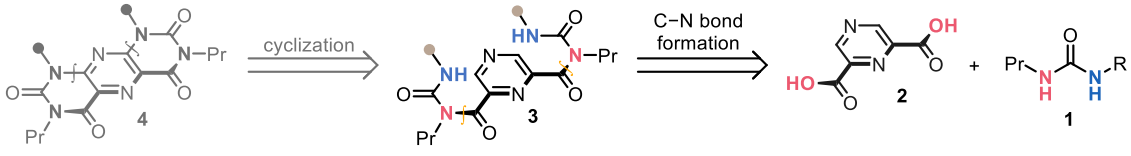

Scheme 17: First reaction step of the synthesis for ester functionalized PPTs.

The commercially available 2,5-and 2,6-pyrazinedicarboxylic acids **2** and **2a** were selected as the starting materials (Scheme 18).

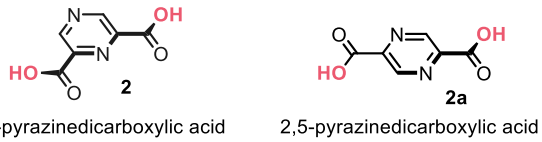

2,6-pyrazinedicarboxylic acid 2,5-pyrazinedicarboxylic acid

Scheme 18: Chosen starting materials for the dipropylpyrazine dicarboxamide synthesis.

However, starting from carboxylic acids, an activation prior to coupling is necessary since the hydroxyl group is considered to be an inadequate leaving group.[43] In literature, common choices for the activation of carboxylic acids include the transformation to the corresponding acyl chlorides or acid anhydrides (Scheme 19). The reactivity of the leaving group is associated with the pK_a of its corresponding acid.[43]A lower pK_a indicates better leaving-group ability and increased reactivity.

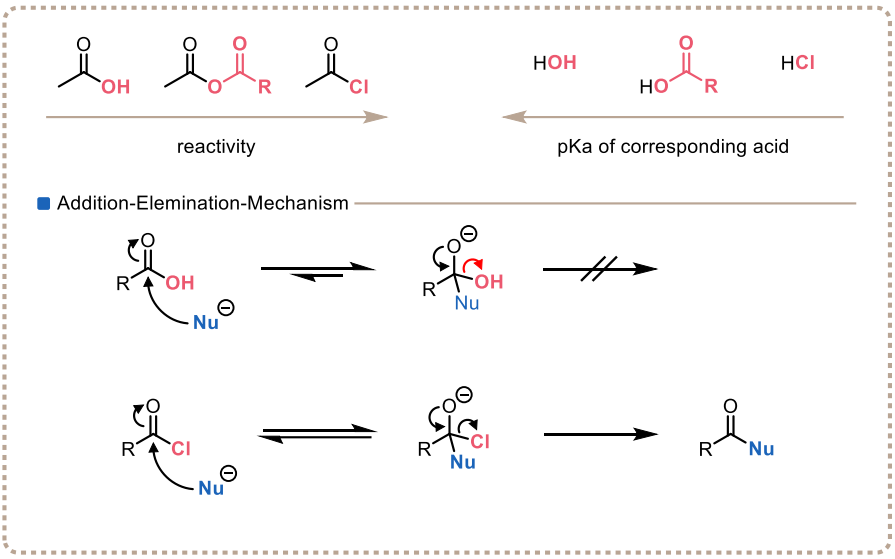

Scheme 19: Reactivity of carboxylic acids and activated derivatives.[43]

In this case, activation via an acyl chloride intermediate was chosen. Not only was there an existing procedure by Verboom *et al*. for synthesizing pyrazine-2,6-dicarbonyl dichloride **8**, but more importantly, acyl chlorides are generally more reactive than the mixed carboxylic acid anhydrides.[44]

To synthesize the diacylchloride, Verboom *et al*. utilize oxalyl chloride in combination with catalytic amounts of dimethylformamide (DMF). The mechanism for the synthesis of acid chloride **8** is shown below (Scheme 20).[44]

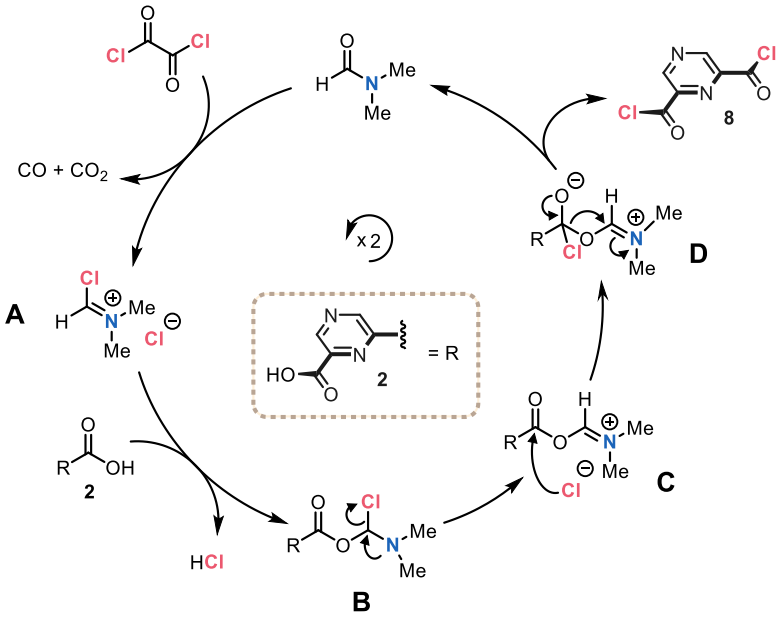

Scheme 20: Proposed mechanism for the DMF-catalyzed formation of Pyrazinedicarbonyl dichloride.

DMF first reacts with the oxalyl chloride to form a Vilsmeier reagent (**A**), releasing carbon monoxide and carbon dioxide, which provides a driving force for this reaction. Subsequently, the carboxylic acid **2** performs a nucleophilic attack on the iminium cation (**B**), liberating a chloride anion, which undergoes a nucleophilic attack on the carbonyl group (**C**). The formed tetrahedral intermediate **D** regenerates DMF upon the formation of the acylchloride **8**. For the chosen pyrazinedicarboxylic acids **2** and **2a**, this reaction must occur twice to attain the desired product **8**.

In practice, the corresponding pyrazinedicarboxylic acid (**2** or **2a**) was suspended in CH_2Cl_2. Then, oxalyl chloride and DMF were added. Once the reaction finished, the solvent and unreacted oxalyl chloride were removed *in vacuo*, and the acid chloride (**8** or **8a**) was redissolved in CH_2Cl_2. After obtaining the solution, it was used without further purification. The reaction was routinely performed on a 0.3 mmol scale and could be scaled up to 2.0 mmol without a considerable decrease in yield.

The enhanced reactivity of acyl chlorides is vital for coupling with poor nucleophiles like urea derivatives. In ureas - as in amides - the lone pair on the nitrogen resides in the p-orbital, achieving optimal stabilization through overlap with the π^* orbital of the carbonyl group, resulting in partial sp^2-hybridization of the nitrogen. However, this interaction reduces the nucleophilicity of the nitrogen, presenting a significant challenge in the coupling reaction. Another obstacle in the employment of unsymmetrically 1,3-disubstituted ureas **1a-1c** is chemoselectivity (Scheme 21).

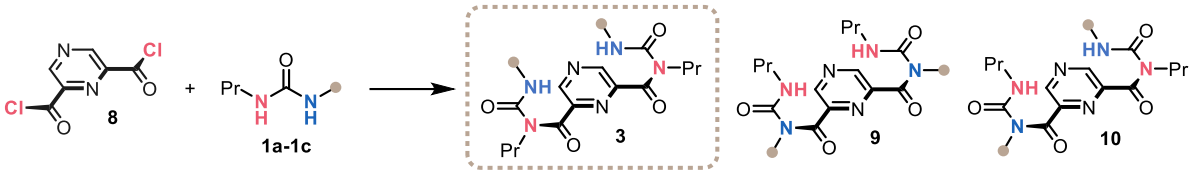

Scheme 21: Possible products and side products concerning chemoselectivity.

The nucleophilic attack can occur through the nitrogen connected to the propyl group **3**, the nitrogen attached to the ester **9**, or both **10**, putatively resulting in product mixtures.

3.2.1 Synthesis of dipropylpyrazine dicarboxamides via acylchlorides

With these challenges in mind, the less expensive 2,5 pyrazinedicarboxylic acid (**2a**) was utilized to carry out three test reactions (Scheme 22). Urea **1a** was employed as a coupling partner.

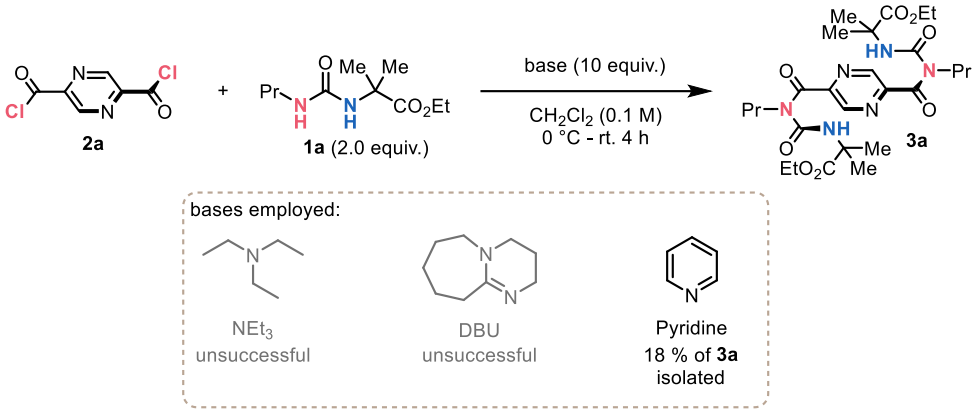

Scheme 22: Initial test reactions for 2,5 dipropylpyrazine dicarboxamides.

The acyl chloride was synthesized according to the general procedure by Verboom *et al*. and added to a mixture of the urea and 10 equivalents of base. The first try resembles the approach by Verboom *et al*. using triethylamine, a nucleophilic base catalyst.[44] Despite them achieving high yields with these conditions utilizing primary amines as nucleophiles, in our hands, using the urea **1a** leads to no conversion to the product according to ^{1}H-NMR spectroscopy of the crude reaction mixture. Likewise, employing 1,8-diazabicyclo(5.4.0)undec-7-ene (DBU) as a base did not lead to the formation of the desired product **3a**. A reaction with pyridine, however, led to a promising conversion of the starting material **1a** according to crude NMR spectra. A fraction of the sample was purified by silica column chromatography, resulting in 15 mg of a pure compound. Analysis of recorded 2D-NMR spectra of the purified material supported the formation of the desired coupling product **3a**, corresponding to 18% isolated yield. Firstly, an asymmetrical species can be ruled out because the pyrazine hydrogen atom signal appears as a single peak at 8.83 ppm instead of two separate signals. Secondly, analysis of the ^{1}H-^{1}H homonuclear correlation spectroscopy (COSY) spectrum, allowed to assign all the protons to the product **3a**. However, there was still the matter of which nitrogen of the unsymmetrically

substituted urea **1a** acted as the preferred nucleophile in this reaction. Here, the ^{1}H-^{13}C heteronuclear multiple bond correlation (HMBC) spectrum provided valuable insights (Scheme 23).

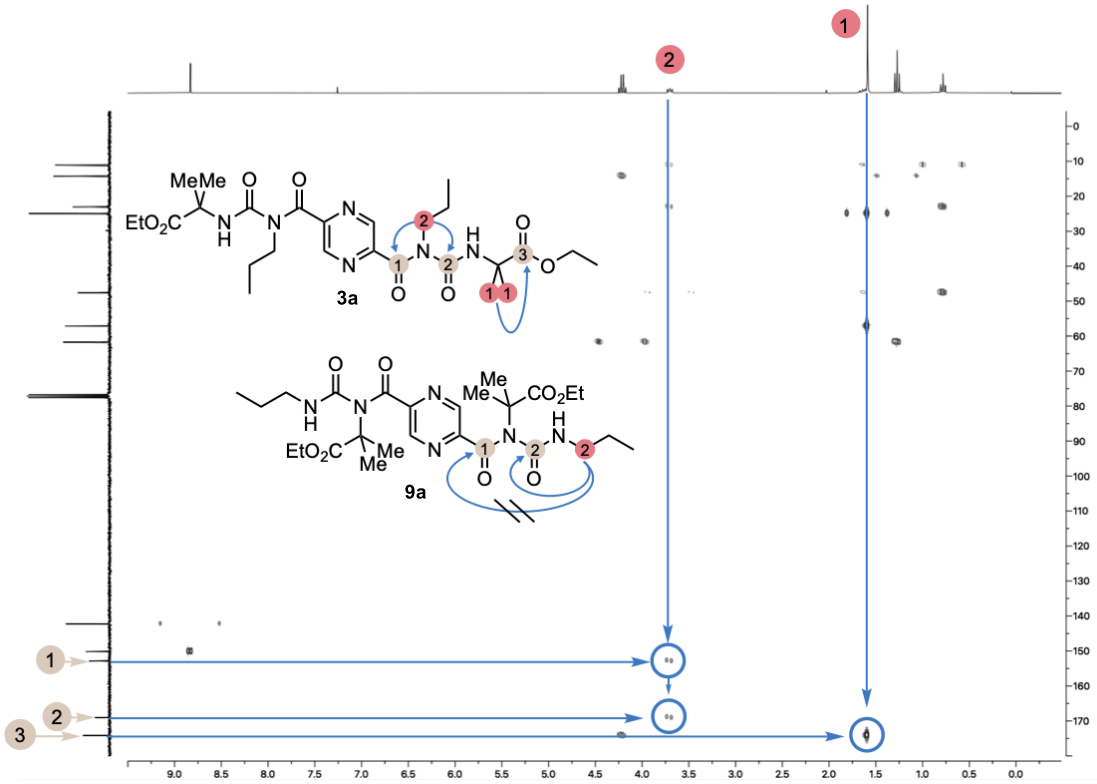

Scheme 23: HMBC spectrum of the isolated pyrazine-2,5-dicarboxamide-derivative.

The peak at 3.76 – 3.65 ppm of the methylene group (Signal 2) belonging to the propyl substituent couples via three bonds to both carbonyl groups at 152.8 and 169.0 ppm (Signal 1 and 2). This coupling is only evident in regioisomere **3a**, would be absent in case of the reverse structure **9a**, providing strong evidence for the formation of the desired product. The formation of this species is in line with the expected reactivity of this urea derivative. The nitrogen connected to the propyl group, is less sterically encumbered as compared to the nitrogen adjacent to the ester functionality. Furthermore, the ester can act as an electron-withdrawing group, reducing the nucleophilicity of the neighbouring nitrogen.

With these promising conditions in hand, the reaction was repeated on 0.1 mmol scale with 2,6-pyrazinedicarboxylic acid (**2**) as the starting material, leading to a good isolated yield of 65% (Table 2, entry 1). Building on these initial findings and seeing that the base has such an essential role in this reaction, a screening of bases was conducted (Table 2).

Table 2: Screening of the coupling between the urea and 2,6-pyrazinedicarbonyl dichloride.[a]

entry	base	yield [%]
1	pyridine	65
2	4-phenylpyridine	66[b]
3	4-methoxypyridine	21
4	4-trifluoromethylpyridine	37
5	4-cyanopyridine	49
6	pyridine-*N*-oxide	16
7	dimethylaminopyridine	-
8	*N*-methylmorpholine	-
9	1-methylimidazole	-
10	pyridazine	-

[a]Reactions were run at 0.1 mmol scale using **2** (1 equiv.), $(COCl)_2$ (3.6 equiv.) and DMF (cat.) to obtain **8**. **8** was used without further purification in the subsequent reaction using **8** (1 equiv.), **1a** (2 equiv.) and **base** (10 equiv.). Yields given refer to isolated yields if not otherwise noted. [b]1H-NMR yield, 4-phenylpyridine as impurity.

Differently substituted pyridines bearing electron-donating or -withdrawing substituents in 4-position resulted in moderately or substantially lower yields (entries 4-6). 4-Phenylpyridine resulted in a comparable NMR-yield, however, the product **3b** could not be separated from 4-Phenylpyridine. Alternative bases, such as dimethylaminopyridine (DMAP) (entry 7), *N*-methylmorpholine (entry 8), 1-methylimidazole (entry 9), and pyridazine (entry 10), resulted in no conversion of the urea **1a** according to the crude ^{1}H-NMR spectra.

Reaction pathways using pyridines or tertiary amines as nucleophilic catalysts for carboxylic acid derivatives have been well-known in the literature since the 1950s.[45] According to the proposed mechanism shown in Scheme 24 below, the role of the base is not only to catch and thus buffer HCl liberation; it also most likely acts as a nucleophilic catalyst.

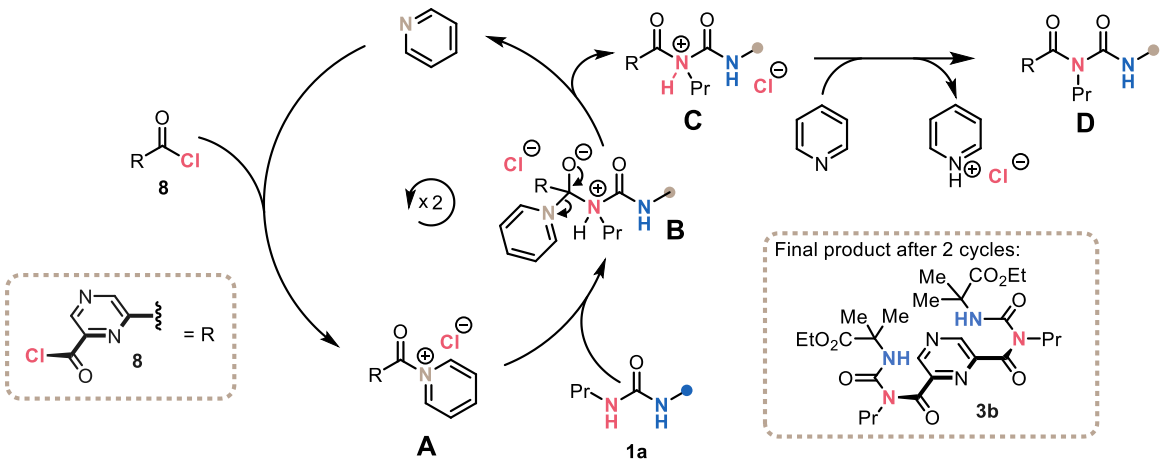

Scheme 24: Proposed mechanism of the reaction of the urea with 2,6-Pyrazinedicarbonyl dichloride.

In the first step, pyridine reacts with diacylchloride to form an acylpyridinium species (**A**), which is then attacked by the urea in the second step (**B**), regenerating pyridine in the third step. Lastly, in the fourth step pyridine also acts as a base, deprotonating the still-protonated intermediate (**C**) to form the final product (**D**). Looking at the results, it is evident that bases with significantly different p*K*a's compared to pyridine failed to match its performance (Scheme 25).

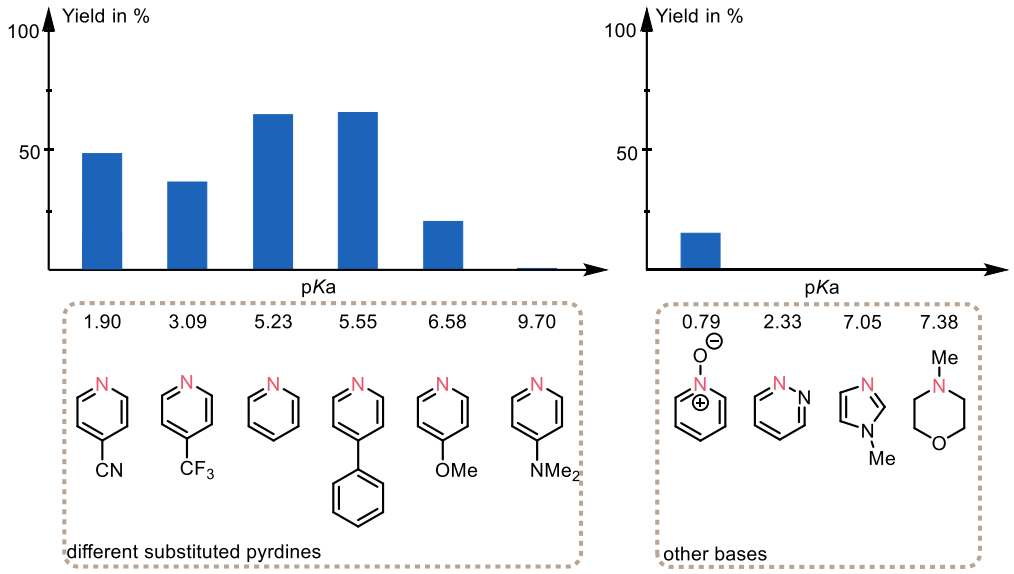

Scheme 25: Yields reached in correlation to the p*K*a of the base additive.[46–53]

DMAP, an otherwise well-established base known for catalyzing reactions in this manner, led to no conversion to the product.[54,55] For instance, DMAP was reportedly 10^4 more active than pyridine in an amine-catalyzed acylation of *m*-chloroaniline with benzoyl chloride.[54] However, the higher reactivity of DMAP when using a weak nucleophile such as the urea derivative **1a** could actually have an adverse effect on the formation of the product. In this case, although the acylpyridinium species (Scheme 25, A) is likely formed, the urea could not be nucleophilic enough to displace DMAP.[56] This possible explanation may also be applied to *N*-methylmorpholine (p*K*a 7.38)[50] and 1-methylimidazole (p*K*a 6.95)[49], which are also drastically more basic than

pyridine.[54] Notably, from this perspective, a direct connection between p*K*a and nucleophilicity cannot be drawn. Among the pyridine derivatives, only 4-phenylpyridine with a p*K*a of 5.55[51] obtained a similar yield of 66%. Given the equal immediate environment from the reaction center to pyridine and its close p*K*a, this result is coherent. 4-Methoxypyridine bearing a +M-substituent is also more basic than pyridine with a p*K*a of 6.62[48] and also performed poorly. Here, the same explanation proposed for DMAP could apply, but with a less extreme effect, seeing that the product still formed, albeit in only 21%. Meanwhile, using electron-withdrawing substituted pyridines like 4-cyanopyridine with a pKa of 1.90[53] and 4-trifluoromethylpyridine with a pKa of 3.09[52] yielded 49% and 37%, respectively. For the less basic derivatives, the formation of the acylpyridinium species may pose a challenge. Another rationale could be that the overall pH of the reaction is overly acidic, which is another crucial challenge of this reaction. This is because the urea derivative (**1a-1c**) is not only a poor nucleophile but can also undergo an intramolecular 5-exo-trig cyclization reaction (Scheme 26).

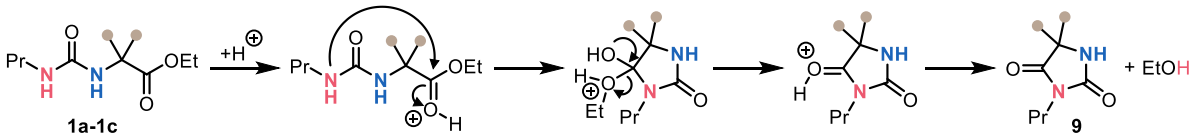

Scheme 26: Mechanism of acid-catalyzed intramolecular 5-exo-trig cyclization reaction of urea derivatives **1a**-**1c**.

This reaction can be catalyzed through acids. The acid-catalyzed reaction for similar substituted ureas is well-known in the literature and could be more likely to happen using less basic pyridines.[47] In some reactions, this side product **9** was coeluted in the column chromatography with the product as a minor impurity, validating its formation. To prove the impact of using less basic pyridines on the generation of the side product, the crude ^{1}H-NMR spectra were analyzed to determine the product-to-side product ratio. However, a definitive conclusion could not be made due to impurities in the crude NMR spectra preventing accurate integration.

The base screening underscores the pivotal role of pyridine in this synthesis process. Between the tested bases, pyridine strikes the optimal balance between p*K*a and nucleophilicity. Pyridine efficiently promotes the reaction and limits unproductive side-product formation. Hence, with the best base in hand, the reaction was optimized further by screening the equivalents of the reactants and the sequence of addition.

Table 3: Screening of equivalents of the reactants and the sequence of addition.[a]

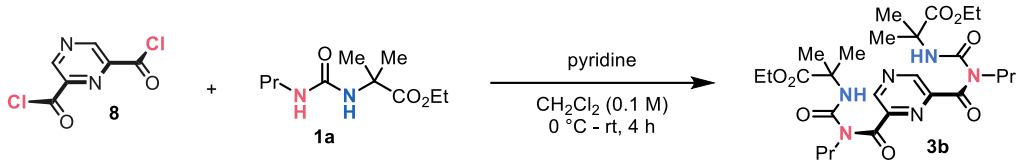

entry	deviation from standard reaction conditions	yield [%]
1	1.2 equiv. **8** and 12 equiv. of pyridine	32
2	1.5 equiv. of **8** and 15 equiv. of pyridine	14
3	Inverse addition[b]	57
4	2.2 equiv. of urea[b]	60
5	3.0 equiv. of urea[b]	75
6	3.0 equiv. of 1a (2 mmol/- gram scale)[b]	74
7	**2.5 equiv. of 1a 20 equiv. of pyridine (1 mmol)[b]**	**81**

[a]Reactions were run at 0.1 mmol scale using **2** (1 equiv.), $(COCl)_2$ (3.6 equiv.) and DMF (cat.) to obtain **8**. **8** was used without further purification in the subsequent reaction using **8** (1 equiv.), **1a** (2 equiv.) and pyridine (10 equiv.). Yields refer to isolated material after purification. Deviations form this procedure are displayed. [b]The altered reagent order was used adding **1a** to a cooled mixture of **8** and pyridine.

Initially, an excess of diacylchloride **8** was employed in entries 1 and 2. To maintain a consistent ratio with diacylchloride **8**, the amount of pyridine was increased accordingly. However, the use of an over-stoichiometric amount of diacylchloride **8** resulted in a poor yield of 30% (entry 1). Further increasing the excess caused the yield to drop to 15% (entry 2). One likely explanation is that using more diacylchloride **8** halts the reaction at the monosubstituted intermediate, seeing that one diacyl chloride **8** has to react with two urea derivatives **1a**.

In all previous trials, the urea derivative **1a** was dissolved in the base first, and subsequently, the reaction mixture was cooled to 0 °C with an ice bath. Secondly, the acyl chloride **8** was slowly added to the reaction mixture. In entry 3 of Table 2, the order of reactants was inverted. This time, the base was directly added to the ice bath-cooled diacylchloride **8** solution, forming a yellow suspension. Then, the urea **1a** was dropped in via a solution in CH_2Cl_2. On a small scale, this method displayed a slightly lower performance but helped to streamline the reaction process in bigger scales.

By employing 2.2 equivalents of urea derivative **1a** with this inverted reactant sequence 60% yield of product **3b** could be isolated (entry 4). Further increasing the employed excess of urea derivative **1a** to 3.0 equiv. achieved the up-until-then best yield of 75% (entry 5). Furthermore, these reaction conditions could also be scaled up to a gram scale with no loss in yield (entry 6).

Nevertheless, employing three equivalents of the urea derivative **1a** is disfavored and should be avoided for complex, highly functionalized urea derivatives intended for incorporation into the substrate scope. Employing 2.5 equivalents of urea **1a** in combination with an increase of pyridine, a very good yield of 81 % could be achieved (entry 7), finalizing the optimization of this reaction.

3.2.2 Scope of synthesized dipropylpyrazine dicarboxamides 3a-3e

Next, the synthesized ureas **1a**-**1d** were subjected to the optimized conditions to explore the generality of the optimized procedure (Table 4).

Table 4: Scope of the synthesized dipropylpyrazine-2,6-dicarboxamides.[a]

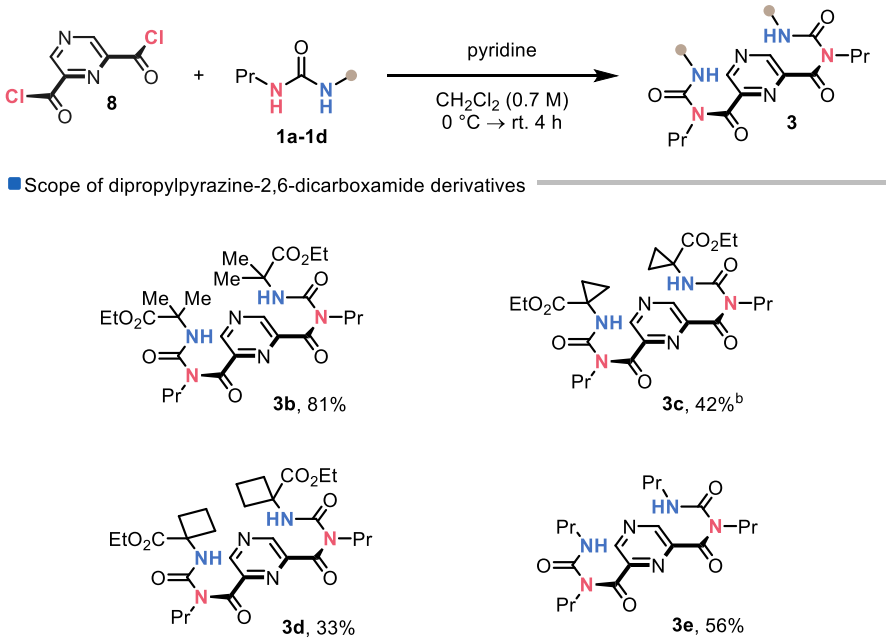

[a]Reactions were run at 1 mmol (**3b**), 0.3 mmol (**3c,3e**), 0.2 mmol (**3d**) scale using **2** (1 equiv.), $(COCl)_2$ (3.6 equiv.) and DMF (cat.) to obtain **8**. **8** was used without further purification in the subsequent reaction using **8** (1 equiv.), **1a** (2.5 equiv.) and pyridine (20 equiv.). Yields refer to isolated material after purification. [b]**3c** was isolated as a mixture of regioisomeres.

Four different dipropylpyrazine-2,6-dicarboxamides **3b**-**3e** were synthesized. The *α,α'-gem*-disubstituted ureas yielded the corresponding carboxamides in 81% bearing *α,α'-gem*-dimethyl substituents **3b**, 46% for the cyclopropyl-substituted pyrazine carboxamide **3c**, and 33% for the cyclobutyl-substituted derivative **3d**. **3c** was isolated as a mixture of regioisomers. The distinct difference between the utilized ureas is the τ-angle. Previous studies by Miller *et al*. revealed that the τ-angle increases from an *α,α'-gem*-dimethyl substitution over cyclobutyl substitution to cyclopropyl substitution.[41,57] With the increase of the τ -angle from the dimethyl-substituted to the cyclobutyl-substituted urea, the yield of the corresponding carboxamides **3b-3d** decreases. The cyclopropyl substituted carboxamides **3c**, bearing the widest τ-angle, leads to a mixture of regioisomers after purification. This was supported by HPLC-MS and ^{1}H and ^{13}C NMR spectroscopy (Figure 1).

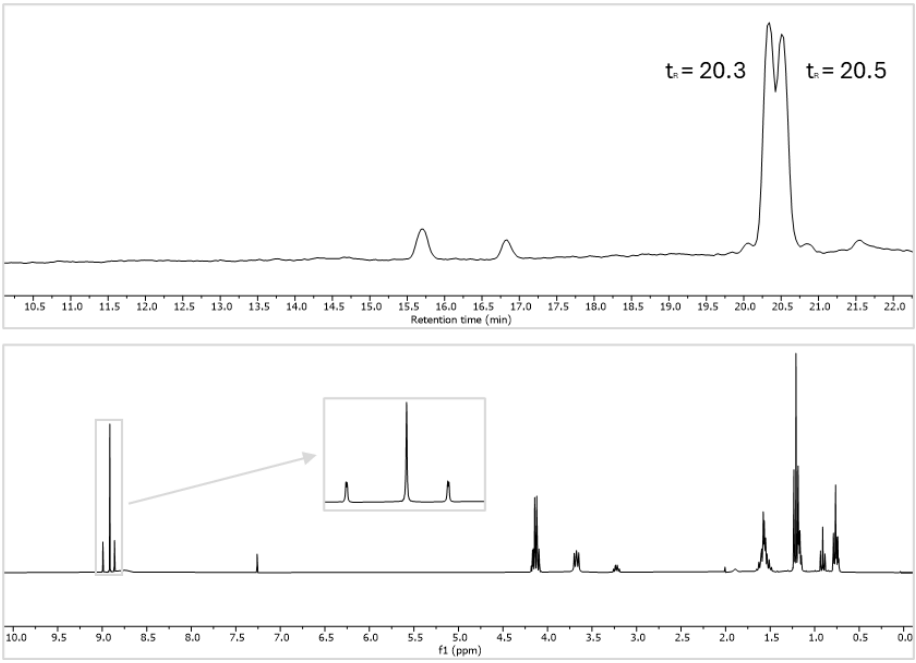

Figure 1: HPLC and ^{1}H NMR spectrum of **3c** and **3c'**.

The chromatogram of the HPLC shows two peaks in quick succession at 20.3 min and 20.5 min with the same m/z-ratio of 583 ($M+Na^+$). Furthermore, the ^{1}H NMR spectrum displays 3 peaks in the aromatic region, whereas otherwise, only one peak can be found for the symmetrical structures. The two additional peaks likely originate from the unsymmetrical substituted pyrazine-2,6-dicarboxamide. The peaks appear as doublets in a one-to-one ratio, which matches the expected pattern. The simplest 1,3-dipropylurea **1d** furnished a moderate yield of 56% of the carboxamide **3e**. At first, this seems unexpected, considering that the nucleophilicity of the alkyl-substituted urea should be comparatively higher. However, it can be speculated that since the urea is symmetrical and both nitrogen atoms are equally nucleophilic, a dimerization could take place, accounting for the diminished yield of the target compound **3e**. In summary, it can be concluded that a high steric demand at one face of the urea bears benefits in terms of regioselectivity, leading to a general advantageous reactivity.

Subsequently, the 2,5-pyrazinedicarboxylic acid **2a** was subjected to the same reaction conditions, employing urea **1a** (Scheme 27).

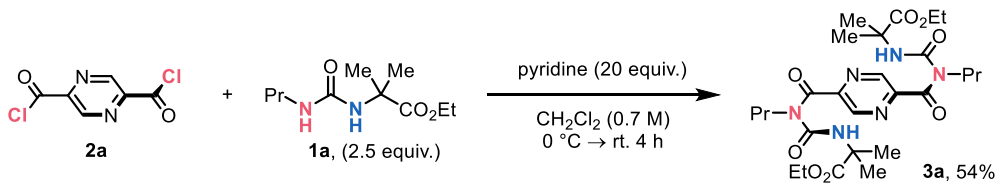

Scheme 27: Exploration of the 2,5-substitutiopattern.

The corresponding 2,5-pyrazine carboxamide **3a** was obtained in an isolated yield of 54%. To our surprise, the yield was roughly 30% less as compared to its 2,6-substituted counterpart **3b**. The

diminished yield is counterintuitive, considering that the substitution patterns theoretically favors the nucleophilic attack of the carbonyl groups.

Further optimization is underway in our laboratories.

3.3 Synthesis of PPTs through cyclization of dipropylpyrazine dicarboxamides

An effective procedure for coupling urea derivatives has been established, although it continues to pose some challenges, as discussed above. Despite these obstacles, it is crucial to advance to the following reaction step to confirm the viability of the proposed synthetic route for the streamlined synthesis of *N*,*N*,*N*-functionalized PPTs (Scheme 28).

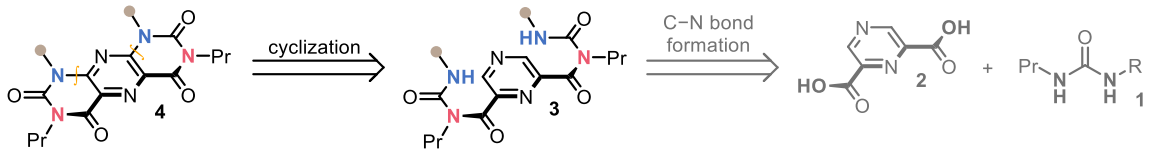

Scheme 28: Second reaction step of the synthesis for ester functionalized PPTs.

The C–N bond formation in the final assembly of the PPT **4**, as shown in Scheme 28, can be envisioned as a coupling reaction between a urea derivative and an electron-deficient aromatic ring. Common methods for achieving this transformation include metal-catalyzed cross-couplings, nucleophilic aromatic substitutions, and Minisci-type reactions, among others.[58–60]

3.3.1 Synthesis of PPTs through metal-catalyzed cross-couplings

One prominent example of metal-catalyzed cross-couplings is the Buchwald-Hartwig coupling.[59] It is a widely used technique for coupling nitrogen species with aromatic systems and typically involves the coupling of an aryl halide or triflate with a secondary or primary amine, most commonly in the presence of a palladium catalyst and a base additive. Before this reaction manifold can be applied, the pyrazine ring has to be converted into an electrophile apt to engage in an oxidative addition step.

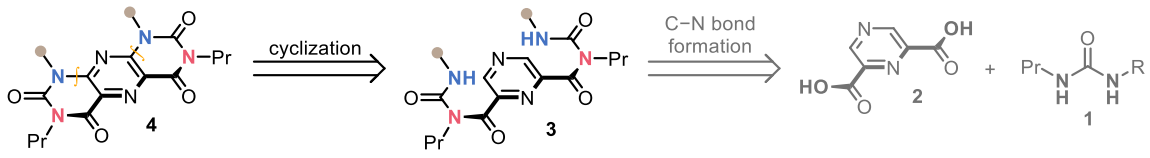

Scheme 29: Cyclisation via Buchwald-Hartwig cross-coupling.

The drawbacks of this method include potential challenges in the transmetallation step due to the relatively low nucleophilicity of the urea nitrogen. Additionally, the use of a base, and therefore a nucleophile, raises concerns about the stability of the ester functionality.

Given these challenges and considerations, bromide was selected as the leaving group due to its relatively high reactivity in Buchwald-Hartwig couplings. Common brominating agents, such as

elemental bromine and N-bromosuccinimide (NBS), were evaluated, with NBS chosen as a milder alternative to bromine (Scheme 30).

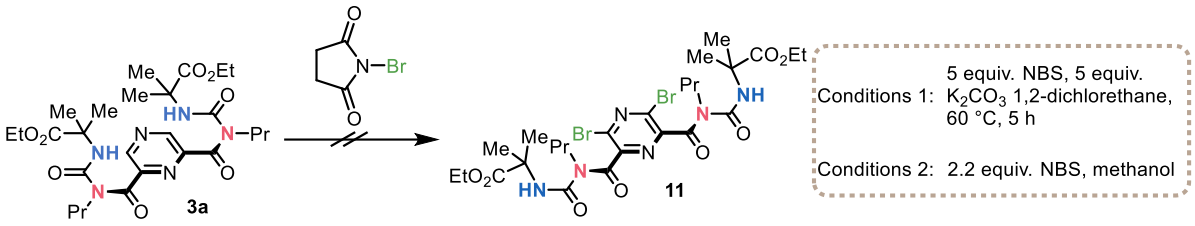

Scheme 30: Bromination of dipropylpyrazine-dicarboxamides with NBS.

Two attempts to brominate the pyrazine derivative **3a** were unsuccessful. In the first attempt, 5 equivalents of NBS and potassium carbonate were used in 1,2-dichloroethane as the solvent. After stirring the reaction mixture for 5 hours at 60 °C, the crude ^{1}H-NMR spectra revealed a complex mixture, and no single species could be isolated even after purification by column chromatography. A second attempt using only NBS in methanol also resulted in a complex mixture of products. These results suggest that NBS may be too reactive for this substrate.

3.3.2 Synthesis of PPTs through a nucleophilic aromatic substitution

The implementation of electron-deficient leaving groups offers an alternative paradigm for the functionalization of aromatic compounds through nucleophilic aromatic substitution (S_NAr).[58] The rationale was to fluorinate the pyrazine ring and then deprotonate the urea using a strong base non-nucleophilic base like NaH to promote the intramolecular nucleophilic addition to form the desired PPT scaffold (Scheme 31). In contrast to aliphatic nucleophilic substitutions, in which fluoride is considered poorly reactive, in aromatic nucleophilic substitutions, more electronegative substituents increase reactivity. Fluoride remains a poor leaving group, but a substitution with fluoride accelerates the addition step (Scheme 31).[43] Not only is the nucleophilic attack on the partially positive carbon atom more favorable due to the presence of electron-withdrawing groups, but the resulting anionic intermediate, known as the Meisenheimer complex (Scheme 31, **A**), is also stabilized.

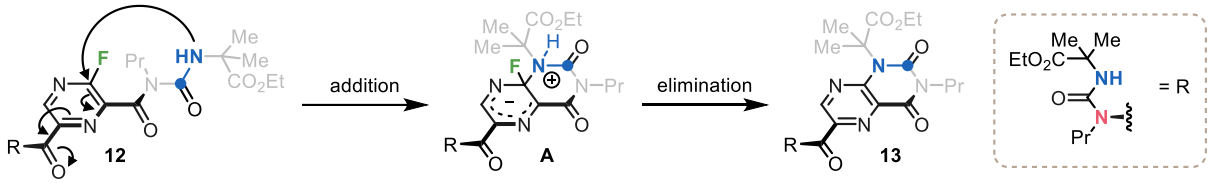

Scheme 31: Mechanism of an aromatic nucleophilic substitution.

The substrate **3b** is equipped with two electron-withdrawing amid functional groups, para, and ortho, to each of the potential fluorine atoms. An electron-withdrawing substituent para or ortho to the leaving group further stabilizes the Meisenheimer complex. In view of this factor, it was concluded that this approach is promising.

Employing fluorine in organic molecules, however, is challenging.[61,62] Conventional deoxyfluorination approaches were deemed inapplicable.[63] Using electrophilic fluorine sources such as fluorine gas is also not feasible due to high toxicity, low selectivity, and high reactivity. However, a procedure published by Hartwig *et al*. for the selective C–H fluorination of pyridines and diazines appeared promising.[64] Hartwig *et al*. utilized commercially available silver(II)fluoride under mild reaction conditions, only needing 1 hour reaction time and no additional heating for the fluorination of sample heteroarenes (Scheme 32).

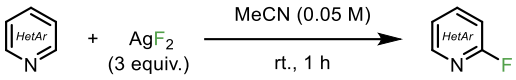

Scheme 32: Fluorination of Pyridines by AgF_2.

Following the general procedure from Hartwig *et al*., 6 equivalents of AgF_2 in 2 ml of MeCN (0.05 M) were employed for a test reaction to convert pyrazine carboxamide **3a** into 3,5-difluoropyrazine **14** (Scheme 33).

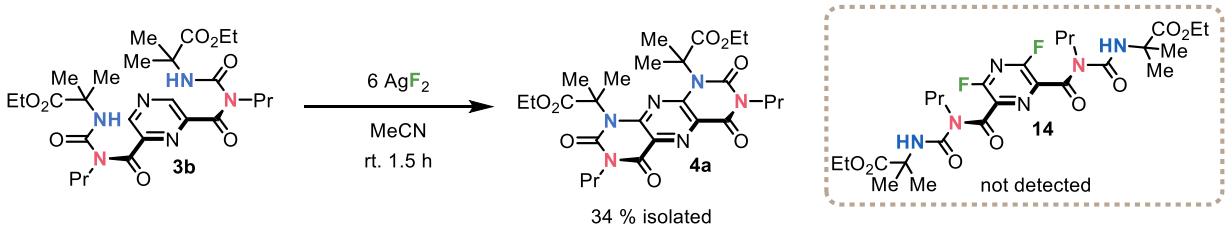

Scheme 33: Initial trial for the fluorination of **3b**.

The reaction was monitored by thin-layer chromatography (TLC) and high-performance liquid chromatography coupled with mass spectrometry (HPLC-MS). Strikingly, after 30 min, a highly UV-sensitive spot with the same R_f value as the starting material appeared. The HPLC-MS spectrum of the crude reaction mixture showed no fluorinated species **14**. However, and more importantly, a mass signal aligning with the mass of the cyclized product **4a** (*m/z* 583 [M+Na$^+$]) was identified. After 60 minutes of reaction time, the HPLC peak intensity increased, with only small traces of remaining starting material. After 1.5 h, the reaction mixture was filtered through a plug of silica, washed with diethyl ether, and subsequently purified by flash chromatography. The highly UV-sensitive spot was isolated in a yield of 34%. Analysis by HRMS and NMR spectroscopy confirmed the presence of the desired cyclization product **4a**.

At first, this reactivity is unexpected. Considering that, in a successive study by Hartwig *et al*., harsh conditions were required when using the previously synthesized fluorinated azines as substrates for intermolecular nucleophilic aromatic substitution reactions.[65] To couple amides, which are structurally similar to ureas, 100 °C and NaH in DMF were needed. NaH is utilized to deprotonate the amide, enhancing its nucleophilicity in the process. The vital distinction is that

the cyclization to **4a** proceeds in an intramolecular fashion. This mechanistic difference could provide a general entropic advantage provided by the two-fold 6-*exo*-trig cyclization.

Assuming the reactions follow the same mechanism as proposed by Hartwig, the following reaction sequence can be postulated (Scheme 34).

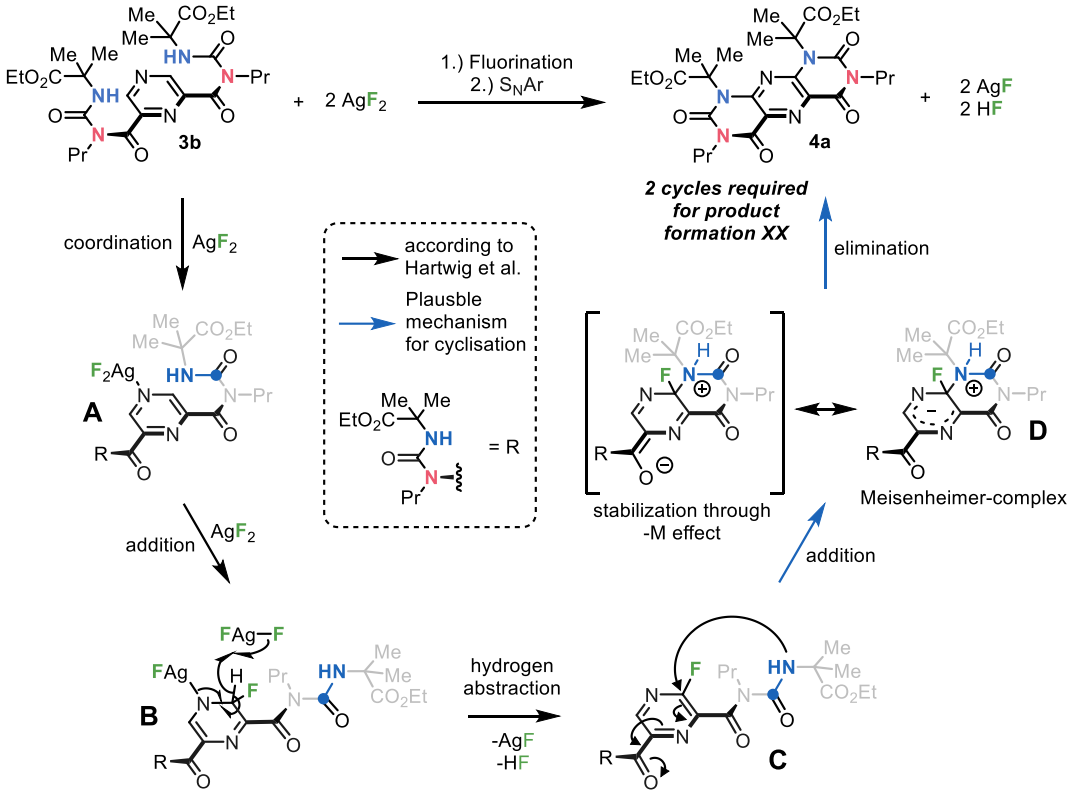

Scheme 34: Plausible reaction mechanism for the formation of **4a**.

The reaction mechanism commences with the coordination of silver(II)fluoride to the nitrogen in the 4-position of the pyrazine unit **A** following a formal addition along the N4-C3 double bond, generating intermediate **B**. Next, the hydrogen atom at C3 is abstracted by a second equivalent of silver(II)fluoride, forming the fluorinated intermediate **C**. The monofluoropyrazine **C** gets rapidly attacked by the free urea nitrogen, forming Meisenheimer complex **D**, which eliminates HF. Repetition of this process at C5 leads to the formation of the desired PPT **4a**.

However, it is noteworthy that no fluorinated species could be detected by HPLC-MS or according to ^{19}F-NMR spectroscopy of the crude reaction mixture. A possible explanation is that upon fluorination, the cyclization could be very rapid.

Yet, it is still surprising that although the substrate is fully consumed, only a 34% yield was isolated. To gain a better understanding of the reaction mechanism and possible side reactions that could be avoided, the reactivity of AgF towards the substrate **3b** was investigated. AgF forms upon oxidation of the substrate and could be reduced further to elemental Ag. Indications for such a reactivity were suggested by a slight silver deposition on the inner wall of the reaction

vessel. The substrate **3b** was stirred in AgF for 90 min and monitored for conversion by ^{1}H-NMR spectroscopy 30 min intervals (Scheme 35).

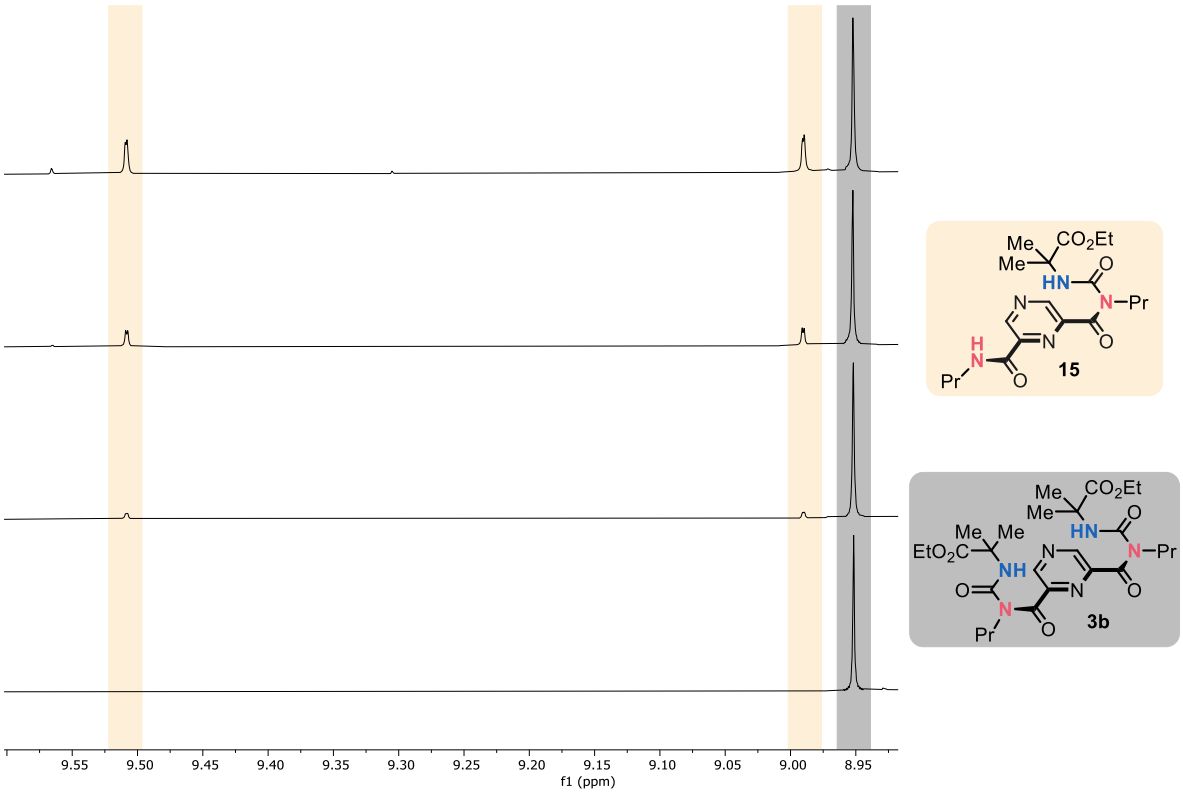

Scheme 35: Reaction monitoring of the conversion of **3b** by ^{1}H-NMR spectroscopy.

If the new species formed is, in fact, the proposed species **15**, substrate and product are in a 0.7/1 ratio, resembling a significant conversion after 90 min.

The fact that AgF can cleave urea derivatives is fascinating and has, to the best of our knowledge, not been reported before. Whether this reactivity is specific to this derivative or could potentially be applied to a broader range of substrates is still under investigation, with promising implications for future applications. Furthermore, the mechanism of this reactivity has yet to be elucidated. Seeing that the origin of the hydrogen of the newly formed species and the fate of the potential formamide counterpart are not apparent.

With this information in hand, a screening was conducted (Table 5). First, the equivalents of AgF_2 were altered (Entry 1-3).

Table 5: Optimization of the cyclization of dipropylpyrazine-dicarboxamide **3b**.[a]

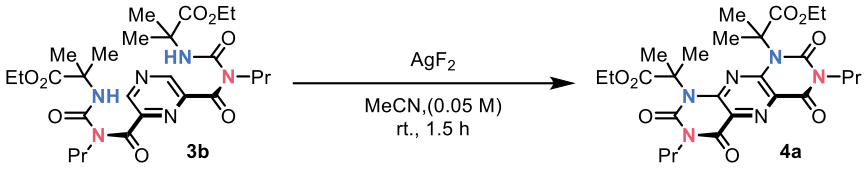

entry	deviation from standard reaction conditions	Yield [%]
1	6 equiv. of AgF_2	34
2	none	42
3	2.0 equiv. of AgF_2	6[b]
4	Additional cooling[c]	33
5	Nitromethane as solvent	nd.
6	CH_2Cl_2 as solvent	nd.
7	Nitromethane as solvent, reflux, on.[d]	traces
8	DCM as solvent, reflux, on.[d]	nd.
9	10 Vol% MeCN in CH_2Cl_2 as solvent	traces
10	4 equiv. NaCl as additve	43

[a]Reactions were run at 0.1 mmol scale using **3b** (1 equiv) and AgF_2 (4 equiv.). If not otherwise noted yields given refer to isolated yields after purification. Deviations form this procedure are displayed. [b] ^{1}H-NMR yield, **3b** as impurity. [c]The reaction mixture was cooled using an NaCl ice bath. [d]The rection mixture was stirred at reflux overnight.

Six equivalents of AgF_2 were utilized in the procedure by Hartwig *et al.*, achieving the initial 34% of **4a**. Lowering the equivalents to four, which is stochiometric, increased the yield to 42 %. Utilizing the AgF_2 in substoichiometric amount led to 6 % of an unpure fraction. The diminished yield of entry three is in line with the proposed reactivity. Furthermore, it seems that using four equivalents diminishes unproductive side reactions, leading to an increased yield. The excess, which Hartwig *et al.* proved necessary for increased yields regarding substrate **3b**, is counterproductive. Given the high reactivity of this transformation, with turnover complete in 1.5 hours, in the next entry, the reaction mixture was cooled to -20 °C. This, however, also led to a diminished yield of 33 %. Next, a solvent screening was conducted. Utilizing CH_2Cl_2 and nitromethane instead of acetonitrile under otherwise identical conditions did not lead to a noticeable turnover of the substrate (Entry 5,6). Additionally, no product could be detected in HPLC-MS. Utilizing these two solvents at reflux did not significantly change the reaction outcome. In both crude NMR spectra, the starting material **3b** still presented the major component despite some impurities present. However, in entry 7, traces of the product could be detected by HPLC-MS. Combining these findings with the results of Hartwig *et al.*, it appears that acetonitrile

is necessary for this transformation. Therefore, the following approach utilized 10 Vol% of MeCN in CH_2Cl_2, seeing that it seems to be inert in the reaction. It was hypothesized that using less MeCN could increase the selectivity by reducing reactivity. However, the hypothesis did not hold up, and only traces of the product could be detected by HPLC-MS. Next, NaCl was utilized as an additive and achieved a 43 % yield of **4a** (entry 10). Considering that AgF is able to facilitate an undesired reaction pathway, it is desirable to remove AgF from the reaction mixture. AgF, compared to the heavier halogen analogs, has a unique position. It is very soluble in water (1800 g/l at 25°C) and also slightly in acetonitrile, which is attributed to the higher calculated ionic character of the silver–fluorine bond.[66,67] The use of NaCl did not affect the yield, suggesting that its solubility in acetonitrile may be too low for this rationale. This concludes the optimization for the time being, isolating the thesis's target compound in a yield of 42 %. This yield corresponds to around 80% for each of the four reaction steps.

With these findings in hand, the 2,5 constitutional isomer was subsequently also subjected to a similar reaction condition of entry 1 Table 5 (Scheme 36).

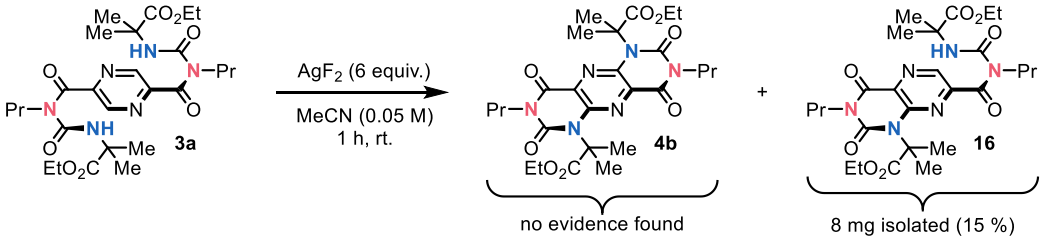

Scheme 36: Reaction of 2,5 pyrazine dicarboxamide **3a** with AgF_2.

Strikingly, **3a** did not match the reactivity of its 2,6-disubstituted counterpart **3b**. In this case, only the half-cyclized species **16** could be isolated. Spectroscopic analysis by HRMS, ^{1}H-NMR, and HPLC-MS supports the formation of the pteridine **16**. The different reactivity of the 2,6- versus the the 2,5-disubstituted pyrazines **3a** and **3b** can have two main reasons, which are illustrated in Scheme 37.

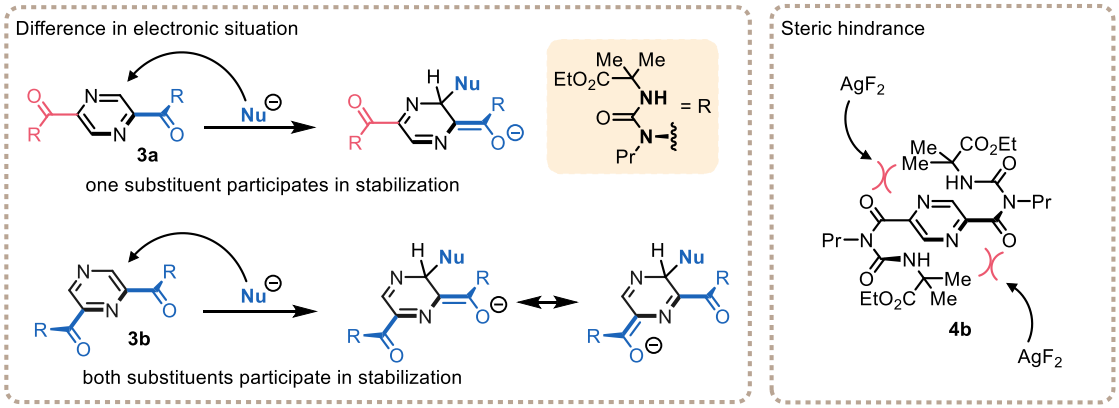

Scheme 37: Possible reason for the difference in reactivity of 2,5- and 2,6-disubstituted pyrazine **3a** and **3b**.

First, in this case of the 2,5-disubstituted pyrazine **3a,** the proposed Meisenheimer intermediate is not stabilized as efficiently as the 2,6-substitution pattern of **3b** (Scheme 37, left). In the 2,5-substitution pattern, only the adjacent carbonyl substituent stabilizes the negative charge of the intermediate in the course of the nucleophilic attack. Secondly, a steric effect could play a role (Scheme 37, right). The adjacent carbons of the nitrogen of the 2,6-disubstituted pyrazine **3b** remain without substitution, creating space for the formation of the amido-silver(II)-fluoride complex. In contrast, within the 2,5-disubstituted pyrazine **3a**, the bulky carbonyl substituents adjacent to pyrazine nitrogen atoms possibly hinder the attack of the aromatic C–H bond.

3.3.3 Towards the electrochemical synthesis of PPT 4a

When performing redox reactions in organic chemistry, it is important to consider the potential of employing synthetic electrochemical methods.[68–70] In fact, electrochemistry, in general, represents a more economical and sustainable alternative to using classical reagents, aligning with the principles of green chemistry.[71] Thus, an electrochemical approach for the conversion of substrate **3b** was investigated, examining a range of reaction conditions throughout the process (Table 6).

Table 6: Investigation of an electrochemical approach utilizing Gr/Gr electrodes.[a]

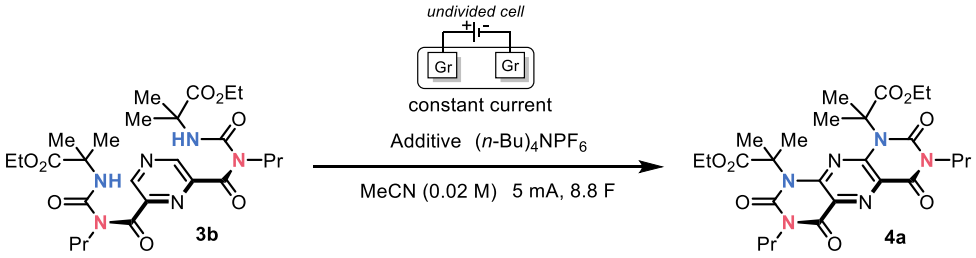

entry	Additive	yield
1	CsF	traces
2	$CsCO_3$	n.d.
3	CsF (10 equiv.)	n.d.

[a]Reactions were run at 0.1 mmol scale using **3b** (1 equiv.) additive (4 equiv.) and TBAPF (5 equiv.). The substrate **3b**, the electrolyte and the additive were given into the reaction vessel. The reaction vessel was purged with argon for 10 min before reaction start.

In initial trials, Tobias Täufer discovered that when using a graphite/graphite electrode system with CsF as an additive and TBAPF as an electrolyte in acetonitrile, a peak in the HPLC-MS showed a mass signal corresponding to the desired product **4a** in the crude reaction mixture. However, the isolation of the observed species was unsuccessful. Subsequently, this procedure was repeated (Table 6, Entry 1). Again, the suspected product could be observed by HPLC-MS. After, the crude reaction mixture was purified by column chromatography. A subsequent extraction with an aqueous NH_4Cl solution allowed the removal of excess electrolyte, yielding 18.4 mg of isolated material. However, the isolated fraction turned out to be a mixture of substances, as evidenced by HPLC-MS and ^1H NMR (Figure 2).

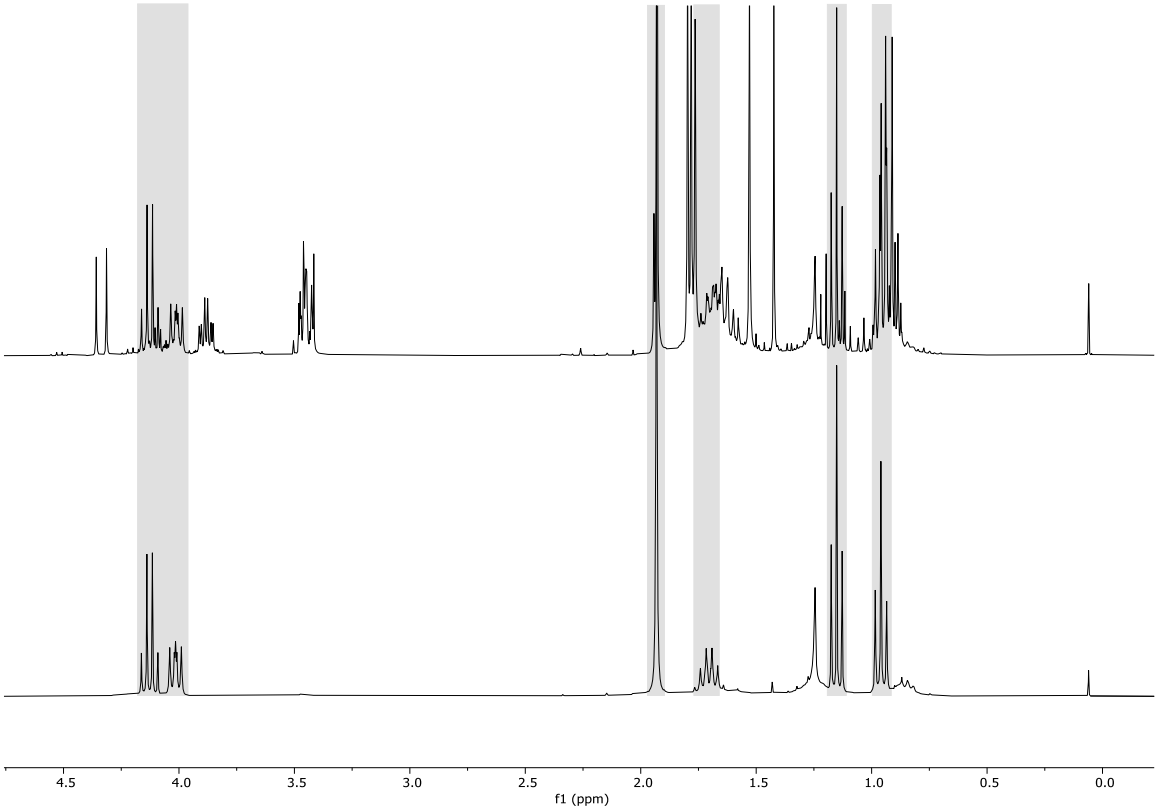

Figure 2: Comparison of isolated fraction of entry 1 (top spectrum) to a pure sample of the desired product **4a** (bottom spectrum) peaks aligning are marked gray.

However, comparing the ^{1}H NMR of the isolated fraction to the pure species **4a**, it can be speculated that the product is indeed formed, indicated by the grey overlay of the peaks in the spectrum (Figure 2). Using $CsCO_3$ instead of CsF, traces of product **4a** were detected (Table 6, entry 2). However, the formation of the same side product as in the case of CsF was observed according to HPLC-MS; therefore, no purification was attempted. It was speculated that the electrolyte overloads the column and hinders adequate purification. Thus, the reaction was repeated utilizing 10 equiv. of CsF, and the reaction mixture was extracted with aqueous NH_4Cl (1 M) prior to further purification (Table 6, entry 3).[72] This effectively removed the electrolyte $TBAPF_6$ from the crude reaction mixture (Figure 3).

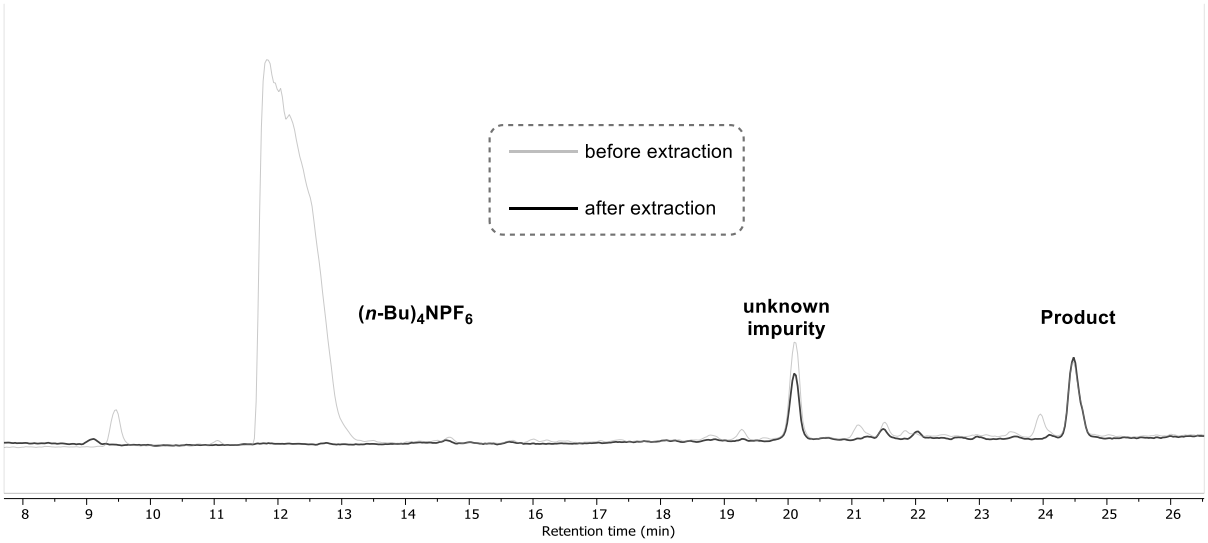

Figure 3: Crude HPLC-chromatogram of before (light gray) and after (black) wash with NH_4Cl solution.

Despite the significant difference in retention times between the unknown impurity and the desired product **4a** (20.1 minutes vs. 24.5 minutes, respectively) on the reversed-phase HPLC, the two substances were inseparable by normal-phase flash column chromatography.

Concluding the preliminary results, the synthesis of the desired PPT **4a** under electrochemical conditions seems feasible. However, the correct reaction setup in combination with the purification protocol has not yet been established and requires further optimization. Application of preparative inversed-phase HPLC could present one solution for better purification.

3.4 Characterization of *N*,*N*,*N*-face difunctionalized PPT 4a

With the targeted compound **4a** in hand the photophysical and electrochemical properties were measured and compared to previously synthesized archetypal PrPPT and *O*,*N*,*O*-face difunctionalized PPT **17**. The results are summarized in Table 7 and Figure 4, below.

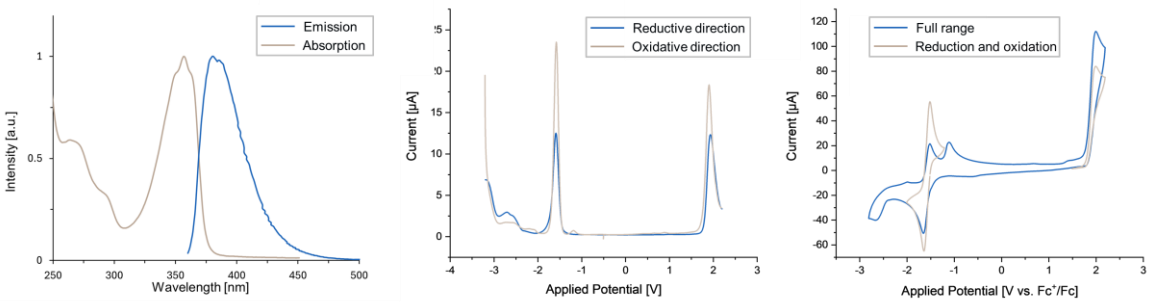

Figure 4: normalized UV-vis absorption/emission spectra (left), DPV (center), CV (left).

Table 7: Photophysical and electrochemical properties of PrPPT, PPT **17** and PPT **4a**.

Compounds	λ_{max}^{abs} [nm]	λ_{max}^{em} [nm]	$E_{0,0}$ [eV]	$E_{1/2}^{red}$ [V vs Fc⁺/Fc][a]	$E_{1/2}^{ox}$ [V vs Fc⁺/Fc][a]	$E_{1/2}^{red}$ [V vs SCE][b]	$E_{1/2}^{ox}$ [V vs SCE][b]	E_{red}^{*} [V vs Fc⁺/Fc][d]	E_{ox}^{*} [V vs Fc⁺/Fc][d]	E_{red}^{*} [V vs SCE][d]	E_{ox}^{*} [V vs SCE][d]
PrPPT[29]	363	385	3.31	-1.59	+1.80	-1.21	+2.18	+1.72	-1.51	+2.10	-1.13
PPT 17[40]	363	390	3.30	-1.57	+1.83	-1.19	+2.21	+1.73	-1.47	+2.11	-1.09
PPT 4a	357	380	3.36	-1.59	+1.92	-1.21	+2.30	+1.77	-1.44	+2.15	-1.06

[a]Potentials were measured using cyclic voltammetry (CV) and differential pulse voltammetry (DPV) relative to Fc⁺/Fc. [b]Referenced to SCE by adding +0.38 V to the value relative to Fc⁺/Fc.[73] [c]$E_{0,0}$ values corresponding to the energy at the intersection of the normalized excitation and emission spectra. [d] Calculated by $E_{red}^{*} = E_{0,0} + E_{1/2}^{red}$. and $E_{red}^{*} = E_{1/2}^{ox} - E_{0,0}$.

The absorption maximum λ_{max}^{abs} was determined at 357 nm in MeCN by UV-Vis absorption spectroscopy. The emission maximum λ_{max}^{em} was determined at 380 nm in MeCN by photoluminescence spectroscopy. The absorption and emission maxima of PPT **4a** show a hypsochromic shift of 6 nm for the local absorption maximum and 5 nm for the emission maximum compared to that of PrPPT. At the same time, a slightly increased stokes shift of 0.21 eV for **4a** compared to 0.19 eV for PrPPT, associated with the slightly increased molecular complexity. The change in absorption and emission maxima of PPT **4a** stands in contrast to that of PTT **17**. PPT **17** displayed an identical absorption maximum as the PrPPT and an increased Stoke's shift of 24 nm, which was equally attributed to the increased molecular complexity.[40] Overall, the small Stokes shift of approximately 20 nm testifies for a rigid molecular structure, indicating minimal energetic loss of the absorbed energy in the excited state. The excited state energy $E_{0,0}$ was determined at the intersection of the normalized absorption and emission spectra

and corresponds to 3.36 eV for **4a**. The electrochemical properties $E_{1/2}^{red}$ and $E_{1/2}^{ox}$ were determined using cyclic voltammetry (CV) and differential pulse voltammetry (DPV). The measurement was referenced to the ferrocene redox couple Fc^{+}/Fc and subsequently converted to the saturated calomel electrode (SCE) reference system by adding +0.38 V to give a broader comparability.[73] PPT **4a** undergoes an irreversible anodic oxidation at +2.30 V vs. SCE and a reversible reduction at approximately -1.21 V vs. SCE in MeCN. The excited state redox potentials E_{red}^{*} and E_{ox}^{*} were calculated according to:

$$E_{red}^{*} = E_{0,0} + E_{1/2}^{red} \quad (1)$$

$$E_{ox}^{*} = E_{1/2}^{ox} - E_{0,0} \quad (2)$$

Based on the analysis, the change in photophysical and electrochemical properties due to *N*-substitution is negligible. Therefore, the excellent excited-state properties with a reduction potential exceeding +2.10 V vs SCE in MeCN are maintained. This observation underscores the hypothesis that the electrochemical and photophysical characteristics are primarily associated with the PPT core and not significantly affected by the *N*-substitution pattern.

4 Summary and Outlook

In summary, a novel synthetic approach for *N*,*N*,*N*-difuctionalized PPT photoredox catalysts was established, resulting in an overall yield of 33% isolated yield for **4a**. Three reaction steps were required to complete this synthesis (Scheme 38).

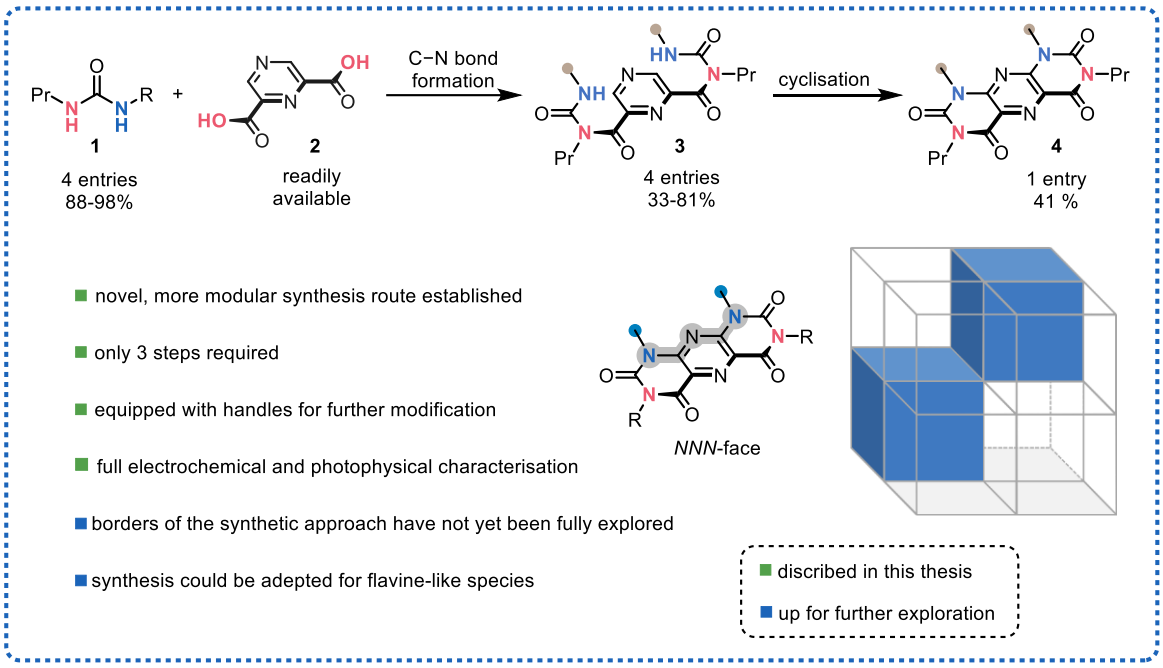

Scheme 38: Summary of the results of the thesis with a selection of prospects.

The first reaction step utilized *α,α'-gem*-disubstituted artificial amino acids **6a-6c**, and propyl amine **6d** as nucleophiles for the addition to propyl isocyanate. Using this method, four urea derivatives **1a-1d** were synthesized with yields between 88-98%.

In the second reaction step, the coupling of the synthesized urea derivatives with 2,5-and 2,6-pyrazinedicarboxylic acids (**2a** and **2**) to form pyrazine dicarboxamides **3** was investigated. Herein, the activation of the carboxylic acid by transformation to an acyl chloride **8** or **8a** in combination with pyridine turned out to be productive. The unique role of pyridine in facilitating the reaction became evident in a screening of bases. Bases with significantly different p*K*a values compared to pyridine other bases were not able or not as efficient in promoting the reaction. A subsequent screening of the equivalents of the reagents concluded the optimization. With optimized conditions in hand, 5 pyrazine dicarboxamides **3a-3e** were synthesized with yields ranging from 33% to 81%. Notably, in the case of utilizing the cyclopropyl functionalized urea derivative **2b**, a challenge regarding the regioselectivity could be identified. Herein, both nitrogen

atoms of the urea **2b** served as nucleophiles, resulting in an inseparable mixture of regioisomers **3c** and **3c'**.

The synthesis of PPTs **4** through cyclization of the pyrazine dicarboxamides **3** represents the third and last step, the synthesis route. In total, three potential reaction pathways were investigated. A transition metal-catalyzed cross-coupling approach was unsuccessful due to a failed synthesis of the suitable starting material **11**, and the synthesis of the desired PPT **4a** under electrochemical conditions could not deliver a pure product. However, a nucleophilic aromatic substitution approach utilizing AgF_2 yielded the target compound **4a** with 41%. This can be seen as a proof of concept that the strived-for pathway is feasible.

Subsequent to the synthesis, an extensive exploration of the photophysical and electrochemical properties of **4a** revealed that the change in photophysical and electrochemical properties due to *N*-substitution on the *NNN*-face of **4a** is negligible. In combination with the previous work of the group of Pospech, this underscores the crucial role of the heteroarene core in governing the excellent excited state properties of PPTs.[40]

Seeing that the change in photophysical and electrochemical properties of **4a** is minor, the next step will be to investigated if the catalytic activity is also not affected by *N*-substitution. Therefore, the synthesized PPT **4a** ought to be tested in a model reaction, like the oxidative annulation of 2-phenyl benzoic acid **17** (Scheme 39)

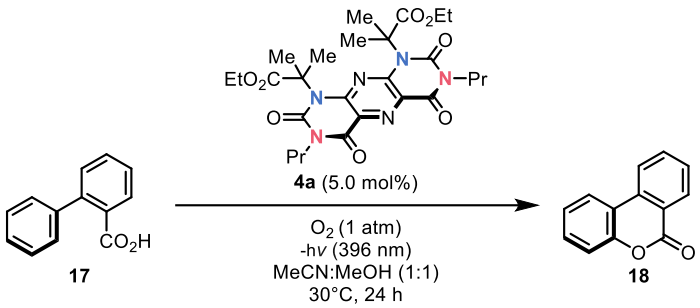

Scheme 39: Test of the catalytic activity of PPT **4a** in the oxidative annulation of 2-phenyl benzoic acid.[33]

Furthermore, this work presents a solid foundation for exploring the boundaries of the described synthetic pathway further. For example, with a now better understanding of the coupling of urea derivatives with pyrazinedicarbonyl dichloride, the scope of this reaction pathway can be significantly broadened. Additionally, the use of isocyanic acid **19** instead of propyl isocyanate **7** could enhance the desired regioselectivity by reducing steric hindrance, resulting in an even more modular synthetic approach (Scheme 40).

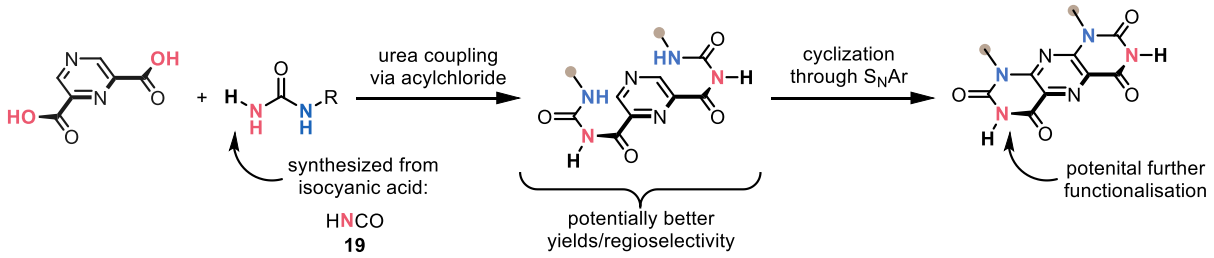

Scheme 40: Synthesis route started from isocyanic acid synthesized ureas.

Additionally, starting from 2-quinoxalinecarboxylic acid (**20**), the synthetic approach could also be adapted for the synthesis of flavine-like structures (**22**) (Scheme 41).

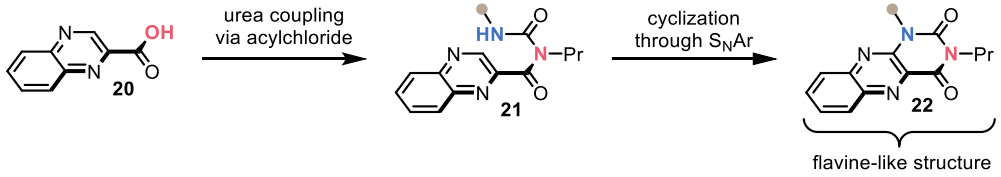

Scheme 41: Adapted synthesis route for flavine-like structures.

5 Experimental Section

5.1 General Remarks

All reactions involving moisture- or air-sensitive reagents or products were performed under an atmosphere of dry argon using standard Schlenk techniques and pre-dried glassware. Syringes for handling of dry solvents or liquid reagents were flushed with dry argon prior to use. All chemicals were purchased from commercial suppliers and used as received.

Solvents

Commercially available dry solvents were purchased from SIGMA-ALDRICH and ACROS ORGANICS. For most reactions, these were directly used without further purification.

Reagents

AgF_2 was purchased from BLDpharm and stored in a glove box.

Chromatography

Analytical thin layer chromatography (TLC) was performed with pre-coated TLC sheets from MACHERY-NAGEL (Layer: 0.2 mm combination layer kieselgur/silica gel with fluorescent indicator UV_{254}). The plates were visualized under ultraviolet light (254 nm or 366 nm). For non-fluorescent samples, a vanillin stain (15 g vanillin in 250 ml EtOH and 2.5 ml conc. H_2SO_4) was utilized. Chromatographic purification of products was accomplished by flash column chromatography on MERCK silica gel, grade 60 (0.063-0.200 mm, 70–230 mesh ASTM).

Vacuum

Following pressures were measured on the VARIAN SD-200 Type 350C VDE530 vacuum pump and are not corrected: membrane pump vacuum (MPV): 10 mbar, oil pump vacuum (OPV): 0.01 mbar.

Electrosynthesis

The electrochemical synthesis was carried out using the ElectraSyn 2.0 system (IKA). Electrodes and other accessories regarding the electrochemical reactions were also obtained from ElectraSyn (IKA).

5.2 Analytical Methods

Infrared Spectroscopy

Infrared spectra were recorded using an Alpha FT-IR-Spectrometer (BRUKER). Liquid and solid probes were measured neat, with absorption given in wave numbers (cm^{-1}), and were recorded in the range of 4000–400 cm^{-1}. The following abbreviations were used for characterization: s (strong), m (medium), w (weak).

Mass Spectrometry

Mass spectra were measured on an Agilent 6890/5973 (GC-MS), Agilent 1200/6210 Time-of-Flight (LC-MS), or Agilent 1260 Infinity/ 6125B (HPLC/MS). The respective mass-to-charge ratios are detected, and the intensities normalized to the base peak (I = 100) are given in brackets. High-resolution mass spectra (HRMS) were recorded on Thermo Electron MAT 95-XP (EI) or Agilent 1200/6210 Time-of-Flight (ESI). Electron ionization (EI) spectra were performed at 70 eV using methane as the carrier gas, with a time-of-flight (TOF) mass analyzer. Electrospray ionization (ESI) spectra were performed using a time-of-flight (TOF) mass analyzer.

Melting Points

Melting points were measured using a BÜCHI 400 melting point apparatus. Reported values are uncorrected.

Nuclear magnetic resonance

Nuclear magnetic resonance (NMR) spectra were recorded at 300 or 400 MHz (^{1}H NMR) and 75 or 125 MHz (^{13}C NMR) on an AV 400 (BRUKER), AV 300 (BRUKER) or Fourier 300 (BRUKER) instrument. Chemical shifts are reported as δ-values in ppm relative to the solvent residual peak.

	^{1}H NMR	^{13}C NMR
$CDCl_3$	7.26 ppm	77.16 ppm
DMSO-d_6	2.50 ppm	39.52 ppm

All spectra were recorded at ambient temperature. The signals were assigned on the basis of experimental data (chemical shifts, coupling constants, integrals) and characterized using the following abbreviations: s = singlet, d = doublet, t = triplet, q = quartet, p = pentet, h = hextet, m = multiplet, dd = double doublet, ddd = double doublet of doublets, td = triple doublet, dt = double triplet, qt = quadruple triplet, dq = double quartet and reported as (multiplicity; coupling constant;

integration). All coupling constants are given in Hertz (Hz). All spectra were recorded with 1024 Scans.

X-Ray

Data were collected on a BRUKER Kappa APEX II Duo diffractometer using Cu-Kα radiation. The structures were solved by direct methods (SHELXS-97: Sheldrick, G. M. Acta Cryst. 2008, A64, 112.) and refined by full-matrix least-squares procedures on F2 (SHELXL-2018: Sheldrick, G. M. *Acta Cryst.* **2015**, C71, 3.). Mercury (Macrae, C. F., Edgington, P. R., McCabe, P., Pidcock, E., Shields, G. P., Taylor, R., Towler, M., van de Streek, J. *J. Appl. Cryst.* **2006**, 39, 453.) was used for graphical representation. Displacement ellipsoids correspond to 30% probability. Hydrogen atoms are omitted for clarity.

Photophysical Measurements

The absorption spectra were measured with a UV/Vis absorption spectrophotometer UV5 Bio (METTLER TOLEDO). All emission spectra were recorded with a Cary Eclipse Fluorescence Spectrophotometer (Varian) with an excitation wavelength (λ_{Ex}) of 350 nm. The samples were dissolved in acetonitrile (MeCN; UVASOL®-Quality) and placed in 10 mm quartz cuvettes (HELLMA ANALYTICS). All pyrimidopteridines (PPTs) were measured with an optical density of around 0.1 at 360 nm.

Cyclic Voltammetry (CV) and Differential Pulse Voltammetry (DPV)

All electrochemical investigations were performed at room temperature in dried acetonitrile p.A. (VWR) under an Argon atmosphere with 0.1 M tetrabutylammonium hexafluorophosphate (Fluka) as conducting salt using an Autolab (PGSTAT 204, Metrohm). A glassy carbon disk electrode (d = 2 mm) was used as the working electrode, a Pt-electrode as the counter electrode, and an Ag/AgCl/LiCl sat. in EtOH-system as the reference electrode (all electrodes: Metrohm). All potentials mentioned in this paper were measured with respect to this reference system and were checked by using the ferrocenium/ferrocene-internal reference system (potential of Fc^+/Fc: 0.54 V [vs. Ag/AgCl/LiCl sat. in EtOH]. The potentials reported relative to the Fc^+/Fc redox couple was converted to SCE by adding 0.38 V. The CV scans were done three times at a scan rate of 50, 100 & 250 mV s^{-1}. The measurements were performed with a 10 mM compound dissolved in the electrolyte.

Differential pulse voltammetry was measured using a step potential of 5 mV, modulation amplitude of 25 mV, modulation time of 0.05 s, and interval time of 0.05 s.

5.3 General Procedures

5.3.1 General procedure for the synthesis of the urea derivatives (GP1)

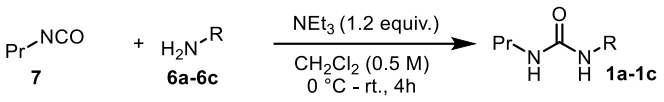

A flask was charged with the corresponding amino hydrochloride salt **6a-6c** (10 mmol, 1.0 equiv.) and dissolved in dichloromethane (CH_2Cl_2, 0.5 M) under ambient atmosphere. The reaction mixture was cooled to 0 °C using an ice bath, and triethylamine (12 mmol, 1.2 equiv.) was added while stirring. Propyl isocyanate **7** (11 mmol, 1.1 equiv.) was then added dropwise to the cooled reaction mixture. The mixture was stirred for 4 hours, gradually warming to ambient temperature. After completion, the reaction was quenched by adding 1 M aqueous HCl solution, and the mixture was extracted three times with CH_2Cl_2 (20 mL). The combined organic layers were washed with brine, dried over anhydrous sodium sulfate (Na_2SO_4), and filtered. The solvent was removed under reduced pressure using a rotary evaporator, yielding the product **1a**-**1c**.

5.3.2 General procedure for the synthesis of the pyrazine carboxamides (GP2)

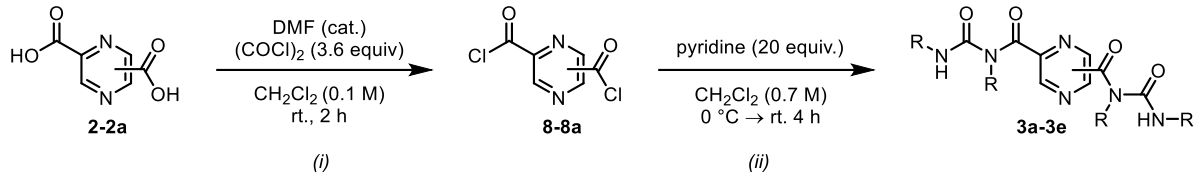

(i) 2,6-pyrazinedicarbonyl dichloride (**8**) and 2,5-pyrazinedicarbonyl dichloride (**8a**) were synthesized according to a literature-known procedure.[44] The corresponding pyrazinedicarboxylic acid **2** or **2a** (1.0 mmol, 1.0 equiv.) was suspended in CH_2Cl_2 (0.1 M) (Scheme 42). Afterwards, oxalyl chloride (3.6 mmol, 3.6 equiv.) and catalytic amounts of DMF (catalytic amounts) were added, and the reaction was stirred for 2 h at ambient temperature, resulting in a clear solution. The solvent and unreacted oxalyl chloride were removed *in vacuo*. The crude acid chloride (**8** or **8a**) was redissolved in CH_2Cl_2 (0.1 M). The obtained solution was used without further purification with an assumed concentration of 0.1 M.

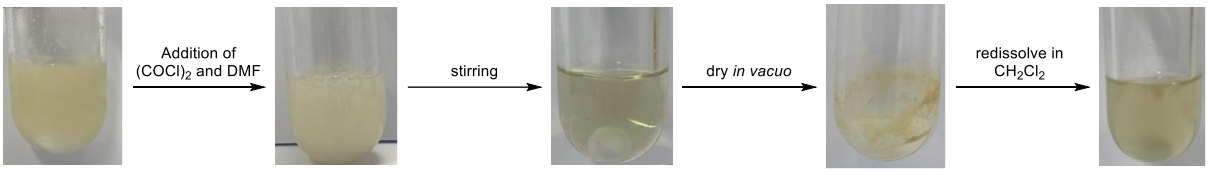

Scheme 42: Reaction sequence utilizing 2,6-Pyrazinedicarbonyl dichloride.

(ii) The acid chloride (**8** or **8a**) solution was cooled to 0 °C, and pyridine (20 mmol, 20 equiv.) was added. Subsequently, the corresponding urea **1a-1d** (2.5 mmol, 2.5 equiv.) was dissolved in CH_2Cl_2 (0.5 M) and added to the stirring solution in the course of 15 min at 0 °C. After an additional 15 min, the reaction mixture was allowed to warm to ambient temperature and stirred for 4 h. The crude mixture was then concentrated *in vacuo* and directly purified by column chromatography.

5.4 Experimental Data

5.4.1 Synthesis of the urea derivatives

Synthesis of ethyl 2-methyl-2-(3-propylureido)propanoate (1a)

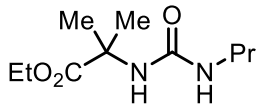

1a

Following the general procedure GP1, using of ethyl 2-amino-2-methylpropanoate hydrochloride **6a** (10 mmol) afforded the title compound **1a** (2.13 g, 9.8 mmol, 98%) as a colorless crystalline solid, after washing with brine and drying **1a** over anhydrous sodium sulfate.

R_f = 0.39 (*n*-pentane:ethyl acetate = 1:1, Vanillin stain)

m.p. = 69-72 °C

^{1}H NMR ($CDCl_3$, 300 MHz): δ = 5.29 (bs, 2H) 4.17 (q, J = 7.1 Hz, 2H), 3.13 – 3.04 (m, 2H), 1.66 – 1.47 (m, 8H), 1.25 (t, J = 7.1 Hz, 3H), 0.91 (t, J = 7.4 Hz, 3H).

^{13}C NMR ($CDCl_3$ 75 MHz): δ = 175.7, 157.9, 61.5, 56.4, 42.4, 25.8, 23.4, 14.2, 11.4.

MS (EI): *m/z* (%) = 143 (51), 84 (11), 58 (100).

HRMS (ESI-TOF): *m/z* $[M+Na]^+$ calcd. for $C_{10}H_{20}N_2O_3$+Na^+: 239.1366; found: 239.1366.

IR (ATR, neat, cm^{-1}): 3335(w), 2965(w), 2930(w), 2874(w), 1730(m), 1677(w), 1626(s), 1562(s), 1455(m), 1382(w), 1362(w), 1284(m), 1223(s), 1144(s), 1112(m), 1024(m), 880(w), 844(w), 775(w), 619(m), 467(w), 405(w).

The analytic data agrees with those reported in literature.[40]

NMR spectra of compound 1a

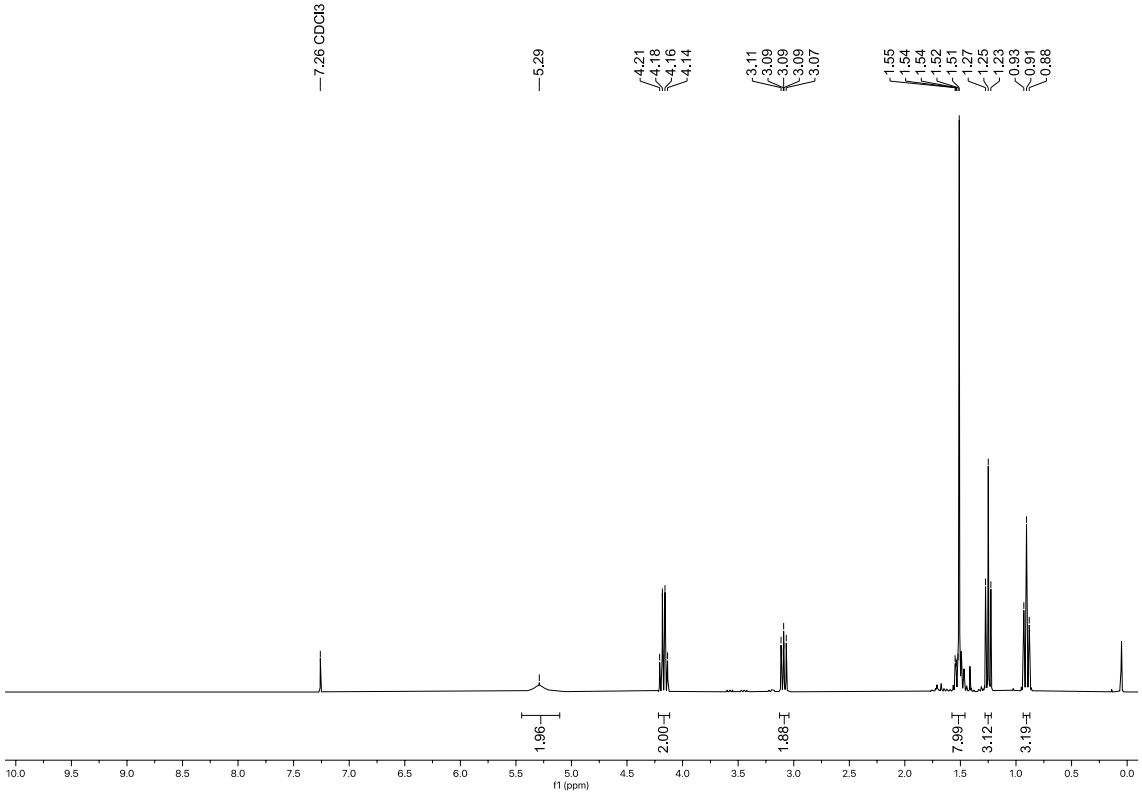

NMR spectrum 1. ^{1}H NMR ($CDCl_3$, 300 MHz).

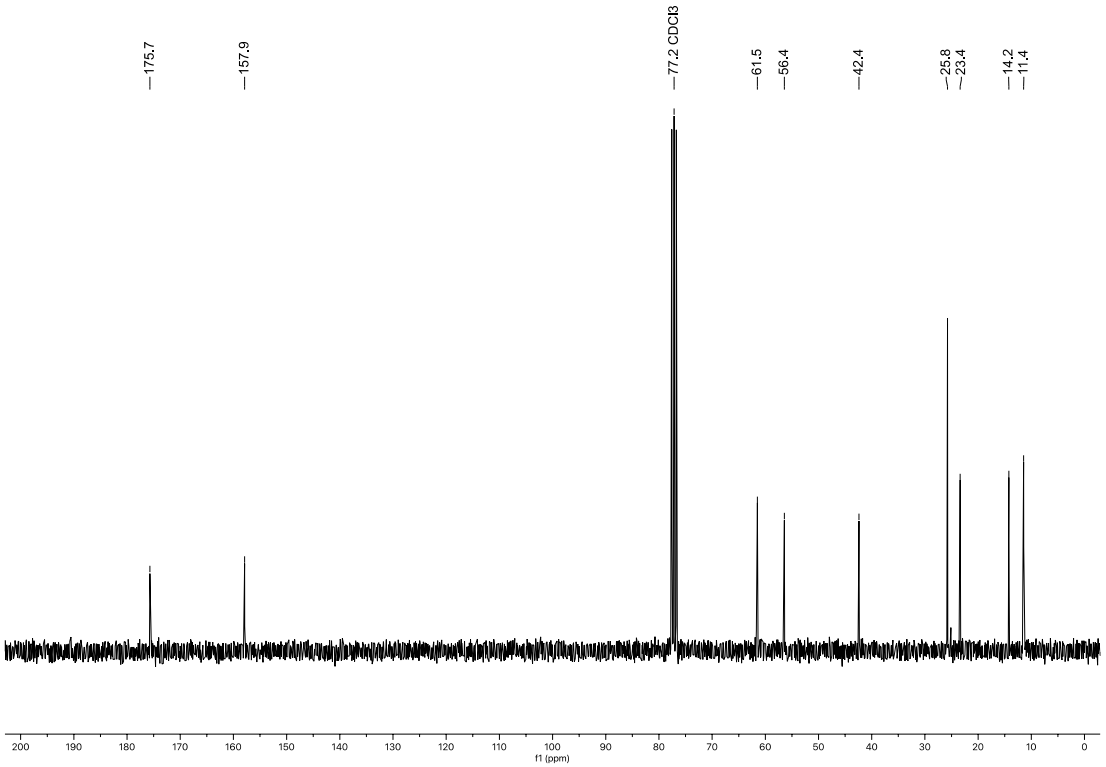

NMR spectrum 2. ^{13}C NMR ($CDCl_3$ 75 MHz).

Synthesis of ethyl 1-(3-propylureido)cyclopropane-1-caboxylate (1b):

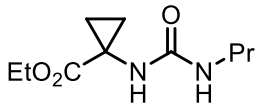

1b

Following general procedure GP1, using ethyl 1-aminocyclopropane-1-carboxylate hydrochloride **6b** (1.0 mmol) afforded the title compound **1b** (202.1 mg, 0.94 mmol, 94%) as a colorless crystalline solid, after washing with brine and drying **1b** over anhydrous sodium sulfate.

R_f = 0.25 (*n*-pentane:ethyl acetate = 1:1, Vanillin stain)

m.p. = 70-73 °C

^{1}H NMR (300 MHz, $CDCl_3$): δ = 5.73 (s, 1H), 5.24 (s, 1H), 4.10 (q, *J* = 7.1 Hz, 2H), 3.16 – 3.07 (m, 2H), 1.54 – 1.41 (m, 4H), 1.20 (t, *J* = 7.1 Hz, 3H), 1.16 – 1.10 (m, 2H), 0.87 (t, *J* = 7.4 Hz, 3H).

^{13}C NMR (75 MHz, $CDCl_3$): δ = 173.6, 159.0, 61.4, 42.0, 34.3, 23.5, 18.1, 14.2, 11.4.

MS (EI): *m/z* (%) = 168 (13), 140 (10), 129 (37), 100 (100.0), 83 (30), 55 (19).

HRMS (ESI-TOF): *m/z* $[M+Na]^+$ calcd for $C_{10}H_{18}N_2O_3+Na^+$: 237.1209; found: 237.1214.

IR (ATR, neat, cm^{-1}): 3326(w), 2963(w), 2934(w), 2875(w), 1724(s), 1633(s), 1567(s), 1461(w), 1440(m), 1410(w), 1370(m), 1337(m), 1300(s), 1260(s), 1176(s), 1114(m), 1066(w), 1028(s), 984(w), 929(w), 865(w), 826(w), 753(m), 626(s), 493(m), 409(w).

NMR spectra of compound 1b

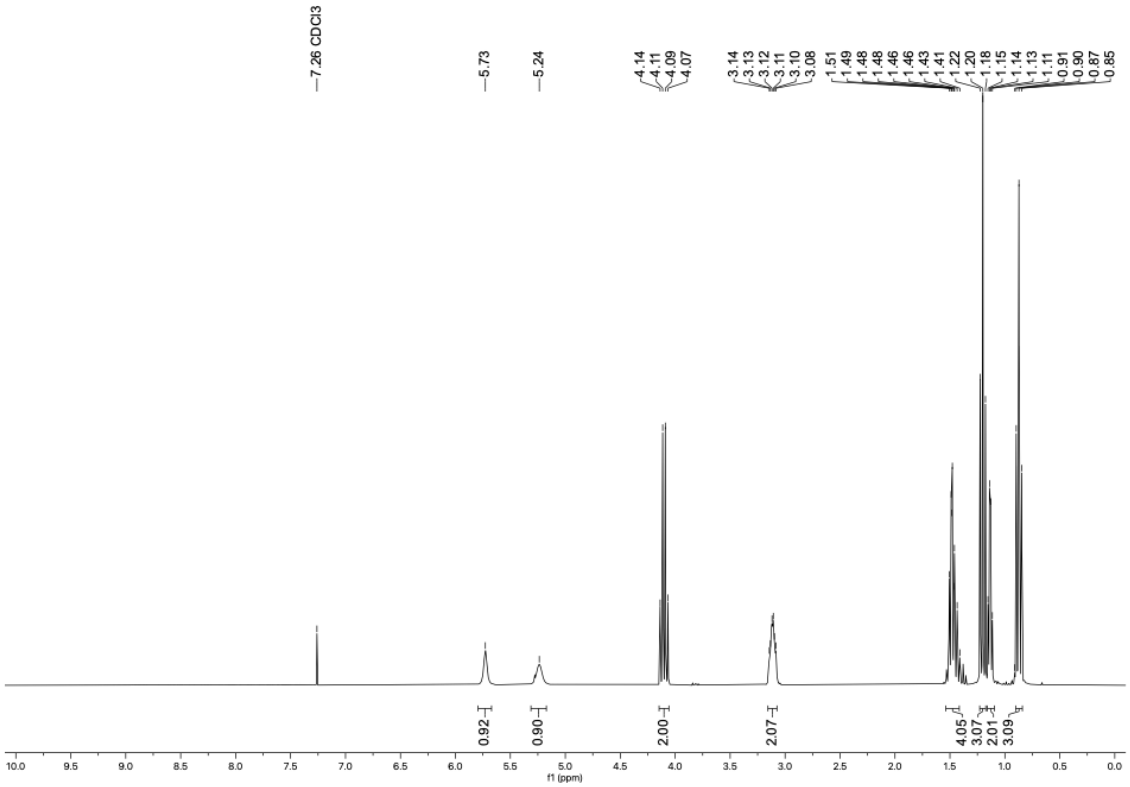

NMR spectrum 3. ^{1}H NMR (300 MHz, $CDCl_3$).

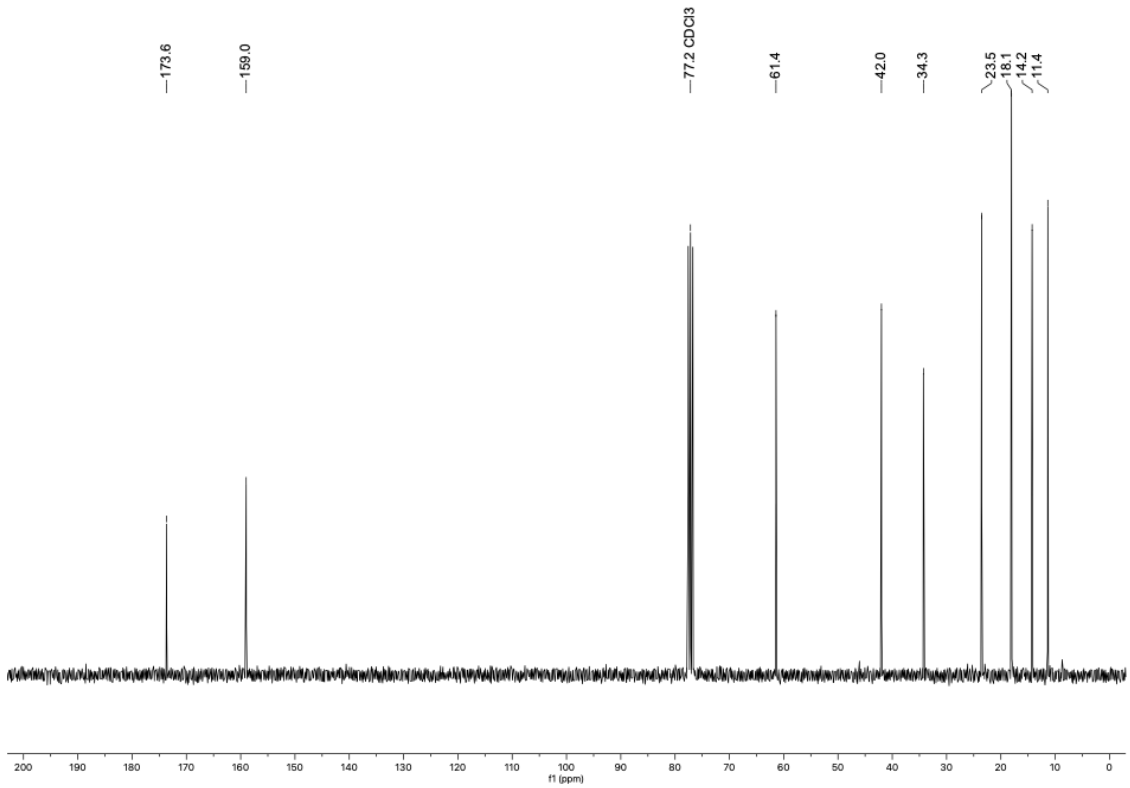

NMR spectrum 4. ^{13}C NMR (75 MHz, $CDCl_3$).

Synthesis of ethyl 1-(3-propylureido)cyclobutane-1-caboxylate (1c)

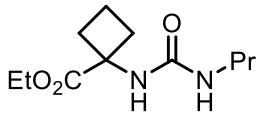

1c

Following the general procedure, using ethyl 1-aminocyclobutane-1-carboxylate hydrochloride **6c** (1.5 mmol) afforded the title compound **1c** (333,4 mg, 1.46 mmol, 97%) as a colorless crystalline solid after washing with brine and drying **1c** over anhydrous sodium sulfate.

R_f = 0.28 (*n*-pentane:ethyl acetate = 1:1, Vanillin stain)

m.p. = 50-51°C

^{1}H NMR (400 MHz, $CDCl_3$) δ = 5.60 (s, 1H), 5.12 (t, *J* = 5.8 Hz, 1H), 4.18 (q, *J* = 7.1 Hz, 2H), 3.13 – 3.03 (m, 2H), 2.64 – 2.51 (m, 2H), 2.28 – 2.17 (m, 2H), 2.05 – 1.90 (m, 2H), 1.46 (h, *J* = 7.4 Hz, 2H), 1.26 (t, *J* = 7.1 Hz, 3H), 0.87 (t, *J* = 7.4 Hz, 3H).

^{13}C NMR (101 MHz, $CDCl_3$) δ = 175.0, 158.0, 61.3, 58.4, 42.1, 31.8, 23.6, 15.4, 14.2, 11.4.

MS (EI): *m/z* (%) = 200 (86), 154 (84), 148 (43), 115 (95), 71 (100)

HRMS (ESI-TOF): *m/z* $[M+Na]^+$ calcd for $C_{11}H_{20}N_2O_3$+Na^+: 251.1366; found: 251.1369.

IR (ATR, neat, cm^{-1}): 3394 (w), 3280 (w), 2959 (w), 2934 (w), 2872 (w), 1724 (s), 1633 (s), 1549 (s), 1506 (w), 1459 (w), 1440 (w), 1366 (w), 1303 (s), 1243 (m), 1220 (s), 1198 (m), 1143 (m), 1101 (s), 1025 (m), 923 (w), 875 (w), 829 (w), 776 (w), 701 (w), 617 (m), 503 (w).

NMR spectra of compound 1c

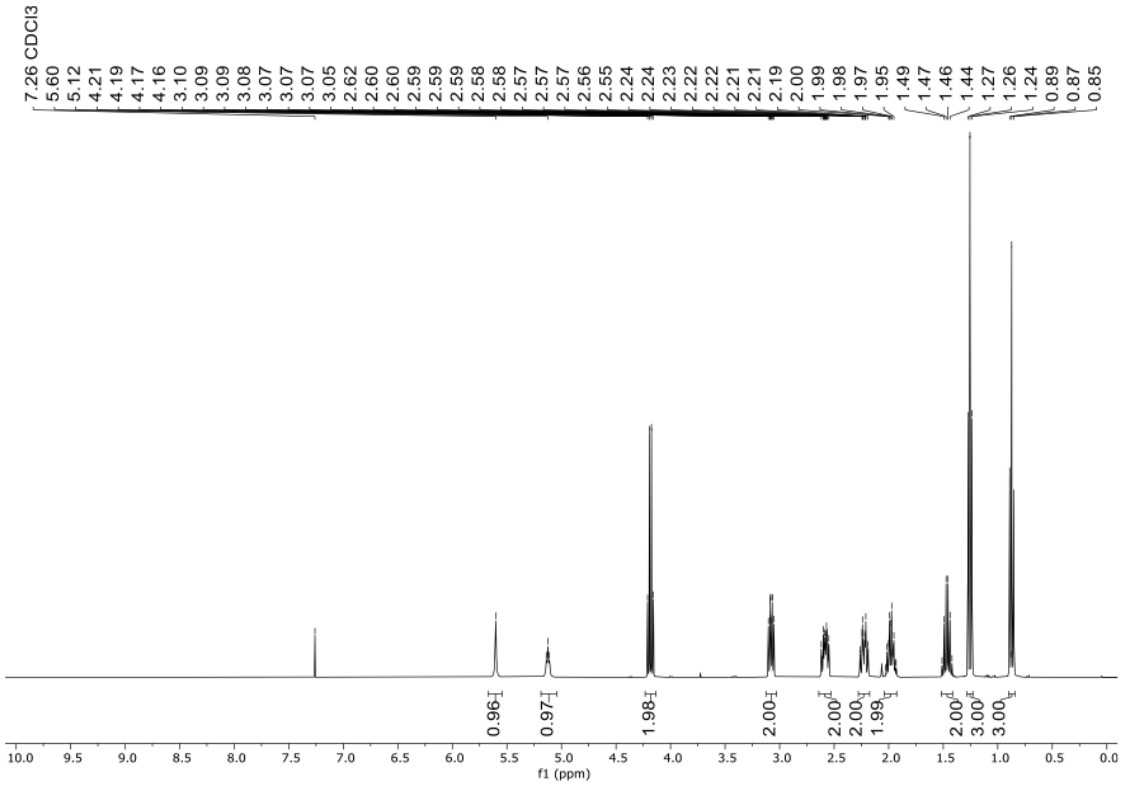

NMR spectrum 5. ^{1}H NMR (400 MHz, $CDCl_3$).

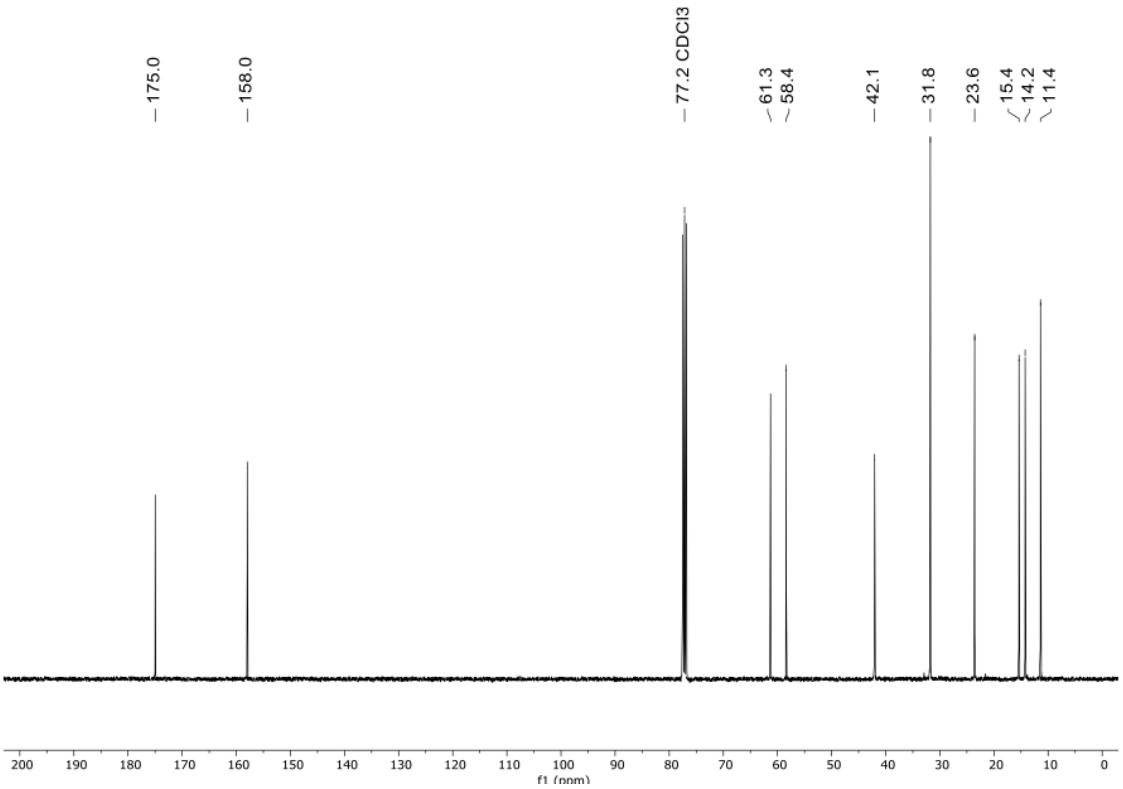

NMR spectrum 6. ^{13}C NMR (101 MHz, $CDCl_3$**).**

Synthesis of 1,3-dipropylurea (1d)

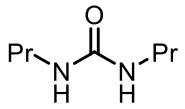

1d

The title compound **1d** was synthesized following a literature known procedure.[42] *n*-Propylamin **6d** (452 µl, 5.5 mmol, 1.1 equiv.) was dissolved in THF (4.0 ml) and the reaction mixture was cooled by an ice bath. Subsequently, the *n*-propylisocyanat **7** (468 µl, 5.0 mmol, 1 equiv.) was dropwise added to the cooled solution and the mixture was stirred for 1 hour, gradually warming to ambient temperature. After the reaction finished, the solvent was removed under reduced pressure using a rotary evaporator, yielding the title compound **1d** (636.0 mg, 4.4 mmol, 88%) as a colorless crystalline solid.

R_f = 0.13 (*n*-pentane:ethyl acetate = 1:1, Vanillin stain)

m.p. = 103-105 °C

^{1}H NMR (300 MHz, DMSO-d6) δ = 5.75 (t, *J* = 5.8 Hz, 2H), 2.97 – 2.87 (m, 4H), 1.44 – 1.26 (m, 4H), 0.82 (t, *J* = 7.4 Hz, 6H).

^{13}C NMR (75 MHz, DMSO-d6) δ = 158.1, 41.1, 23.3, 11.3.

MS (EI): *m/z* (%) = 144 (48) [M^+], 58 (19), 56 (23), 55 (18), 44 (16), 43 (24), 41 (18), 30 (100), 28 (14).

HRMS (ESI-TOF): *m/z* $[M+H]^+$ calcd for $C_7H_{16}N_2O+H^+$: 145.1336; found: 237.145.1334.

IR (ATR, neat, cm-1): 3327(w), 2960(m), 2931(w), 2870(m), 1691(w), 1622(s), 1578(s), 1460(m), 1374(w), 1313(w), 1236(s), 1157(m), 1072(w), 891(w), 756(w), 592(s), 436(w).

The analytic data agrees with those reported in literature [42]

NMR spectra of compound 1d

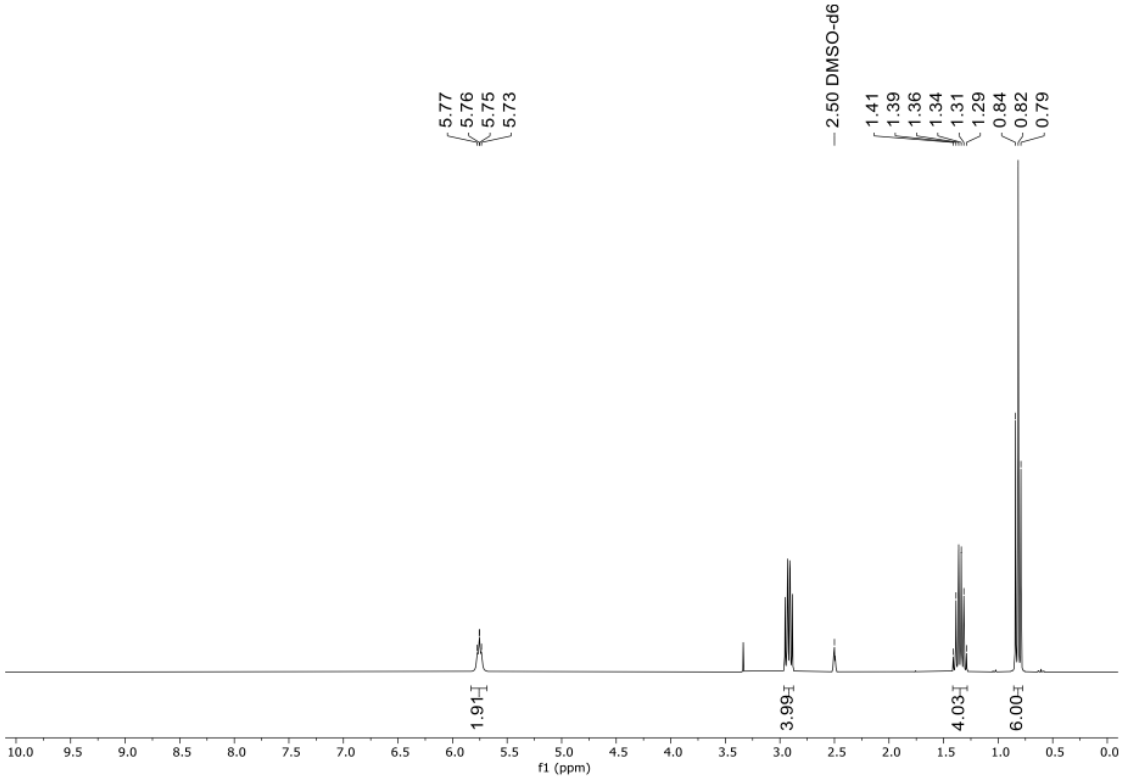

NMR spectrum 7. ^{1}H NMR (300 MHz, DMSO-d6).

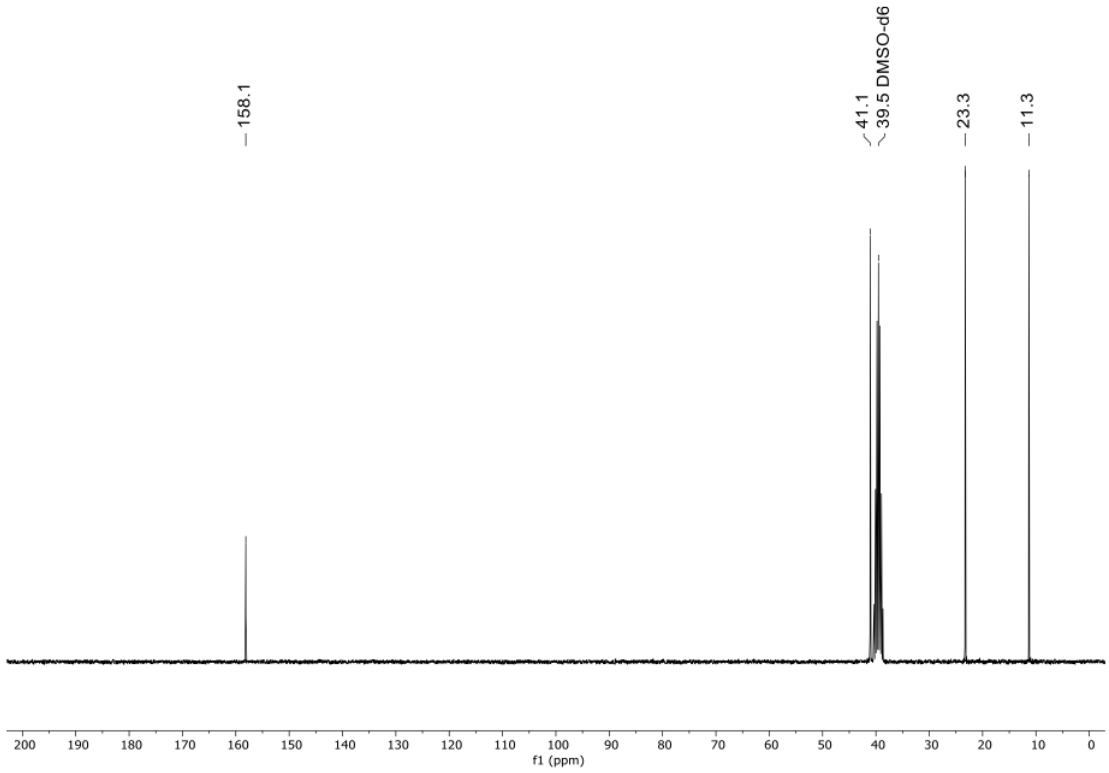

NMR spectrum 8. ^{13}C NMR (75 MHz, DMSO-d6).

5.4.2 Synthesis of dipropylpyrazine dicarboxamides

Synthesis diethyl 2,2'-((((pyrazine-2,5-dicarbonyl)bis(propylazanediyl))-bis(carbonyl))bis(azanediyl))bis(2-methylpropanoate) (3a)

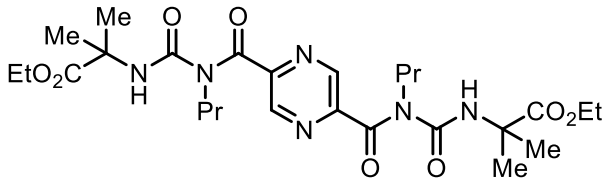

3a

Following the general procedure GP2, using 2,5-pyrazinedicarboxylic acid (**2a**) (50.4 mg, 0.3 mmol) afforded the title compound **3a** (91.7 mg, 0.16 mmol, 54%) as a yellow solid after purification by column chromatography (*n*-pentane:ethyl acetate = 2:1).

R_f = 0.69 (*n*-pentane:ethyl acetate = 1:1, UV)

m.p. = 122-125 °C

^{1}H NMR (300 MHz, $CDCl_3$) δ = 8.83 (s, 2H), 4.21 (q, *J* = 7.1 Hz, 4H), 3.76 – 3.65 (m, 4H), 1.68 – 1.57 (m, 16H), 1.27 (t, *J* = 7.1 Hz, 6H), 0.78 (t, *J* = 7.4 Hz, 6H).

^{13}C NMR (75 MHz, $CDCl_3$) δ = 174.2, 169.0, 152.8, 150.1, 142.3, 61.7, 57.1, 47.6, 24.9, 23.0, 14.2, 11.1.

MS (ESI): *m/z* (relative intensity) 587 (100) [M+Na^+], 408 (33), 251 (20).

HRMS (ESI-TOF): *m/z* [M+Na]$^+$ calcd for $C_{26}H_{40}N_6O_8$+Na^+: 587.2800; found: 587.2812.

IR (ATR, neat, cm^{-1}): 3336(w), 2963(w), 2936(w), 2879(w), 1740(m), 1660(s), 1520(s), 1462(m), 1372(m), 1350(w), 1275(s), 1244(s), 1218(m), 1197(m), 1152(s), 1112(m), 1079(s), 1026(s), 982(w), 935(w), 922(m), 889(w), 858(m), 796(m), 780(m), 759(m), 744(m), 573(m), 431(s).

NMR spectra of compound 3a

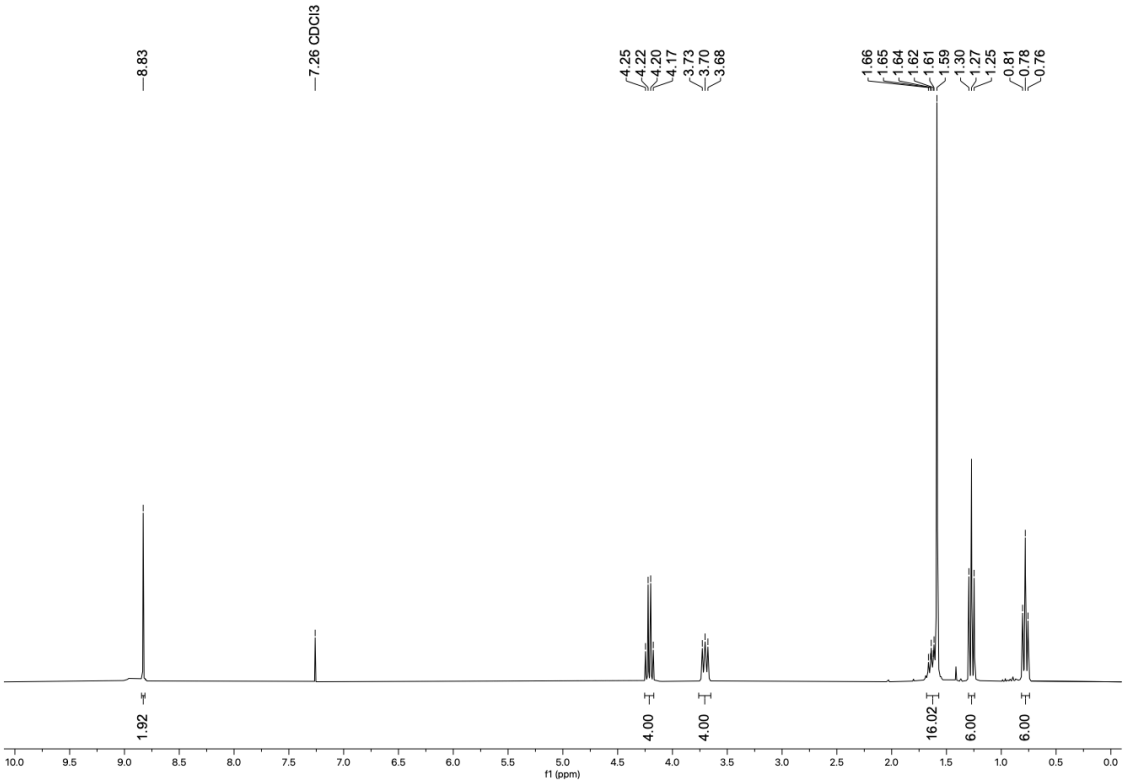

NMR spectrum 9. ^{1}H NMR (300 MHz, $CDCl_3$).

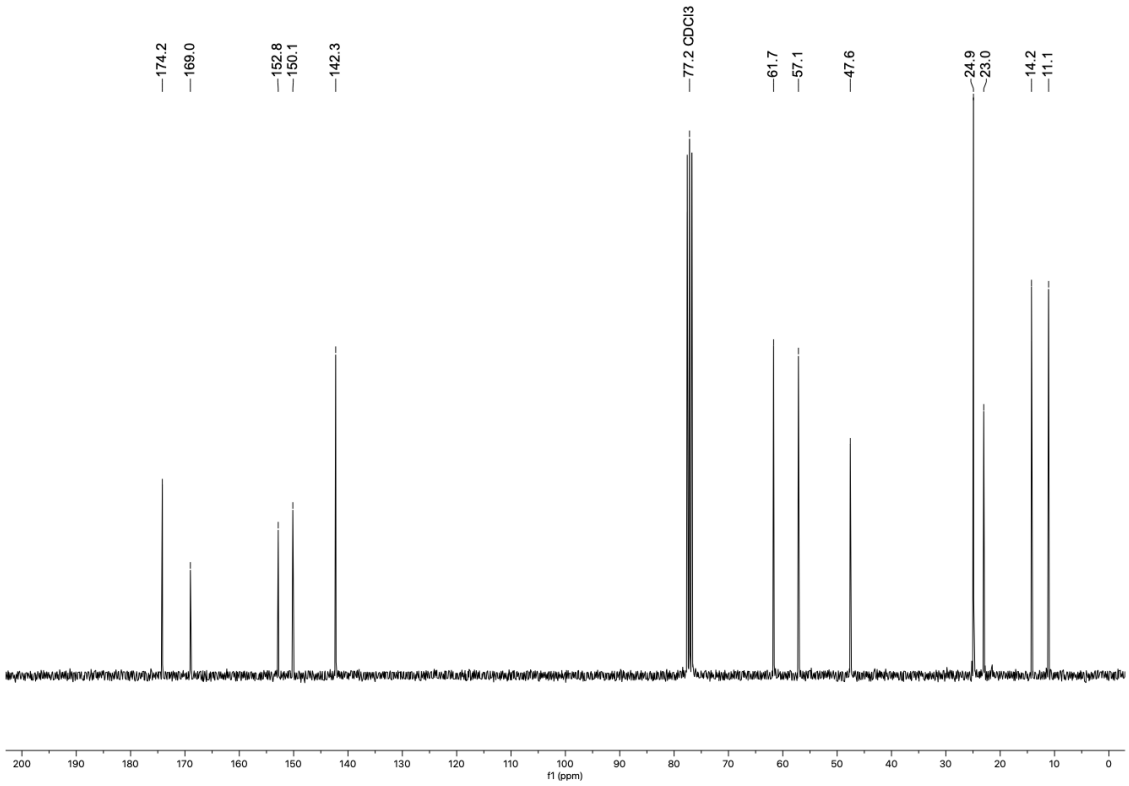

NMR spectrum 10. ^{13}C NMR (75 MHz, $CDCl_3$).

Synthesis of diethyl 2,2'-((((pyrazine-2,6-dicarbonyl)bis(propylazanediyl))-bis(carbonyl))bis(azanediyl))bis(2-methylpropanoate) (3b)

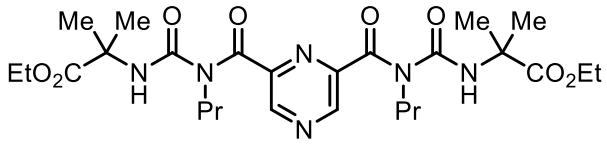

3b

Following the general procedure, using 2,6-pyrazinedicarboxylic acid (**2**) (168.1 mg, 1.0 mmol) afforded the title compound **3b** (456 mg, 0.8 mmol, 81%) as a yellow viscous oil after purification by column chromatography (*n*-pentane:ethyl acetate = 2:1)

R_f = 0.70 (*n*-pentane:ethyl acetate = 1:1, UV)

m.p. = viscous oil at rt.

^{1}H NMR (300 MHz, $CDCl_3$) δ = 8.95 (s, 2H), 4.21 (q, *J* = 7.1 Hz, 4H), 3.72 – 3.63 (m, 4H), 1.63 – 1.53 (m, 16H), 1.27 (t, *J* = 7.1 Hz, 6H), 0.77 (t, *J* = 7.4 Hz, 6H).

^{13}C NMR (75 MHz, $CDCl_3$) δ = 174.2, 168.8, 152.7, 147.4, 145.0, 61.7, 57.1, 47.5, 24.9, 23.1, 14.2, 11.1.

MS (ESI): *m/z* (relative intensity) 587 [M+Na^+],434 (7), 408 (33), 251 (20).

HRMS (ESI-TOF): *m/z* [M+Na]+ calcd for $C_{26}H_{40}N_6O_8$+Na^+: 587.2800; found: 587.2813.

IR (ATR, neat, cm^{-1}): 3306(w), 2966(w), 2876(w), 1707(s), 1655(m), 1514(s), 1455(m), 1382(m), 1364(m), 1282(m), 1241(m), 1201(m), 1147(s), 1080(s), 1017(s), 862(w), 767(m), 712(w), 546(m), 420(m).

NMR spectra of title compound 3b

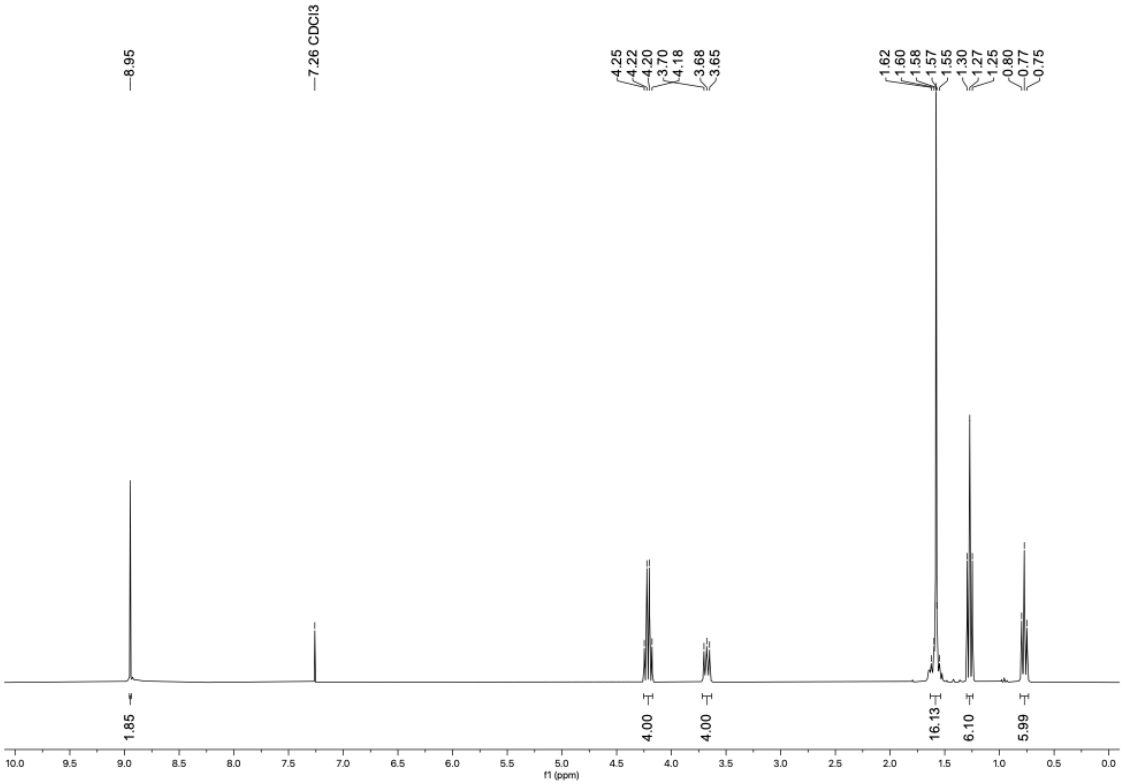

NMR spectrum 11. ^{1}H NMR (300 MHz, $CDCl_3$).

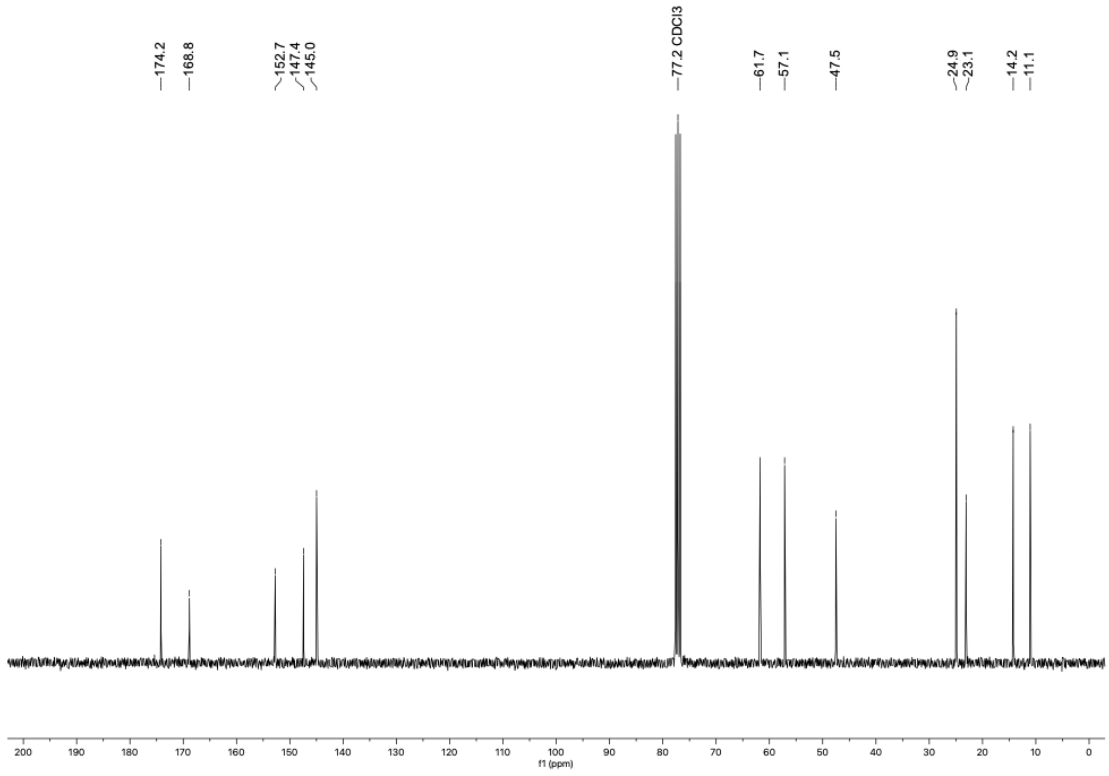

NMR spectrum 12. ^{13}C NMR (75 MHz, $CDCl_3$).

Synthesis of diethyl 1,1'-((((pyrazine-2,6-dicarbonyl)bis(propylazanediyl))bis (carbonyl))bis(azanediyl))bis(cyclopropane-1-carboxylate) (3c)

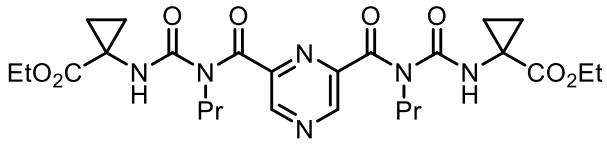

3c

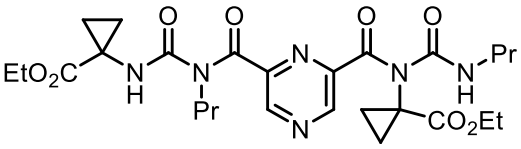

3c'

Following the general procedure, using 2,6-pyrazinedicarboxylic acid (**2**) (50.4 mg, 0.3 mmol) afforded the title compound **3c** (71.3 mg, 0.13 mmol, 42%) as an inseparable mixture of the title compound **3c** and its regioisomer **3c'** after purification by column chromatography (*n*-pentane:ethyl acetate = 2:1)

R_f = 0.52 (*n*-pentane:ethyl acetate = 1:1, UV)

m.p. = viscous oil at rt.

^{1}H NMR (300 MHz, $CDCl_3$) δ = 8.99 (d, *J* = 0.5 Hz, 1H), 8.91 (s, 2H), 8.86 (d, *J* = 0.5 Hz, 1H), 4.18 – 4.07 (m, 8H), 3.71 – 3.63 (m, 5H), 3.23 (td, *J* = 7.1, 5.7 Hz, 2H), 1.66 – 1.47 (m, 15H), 1.27 – 1.14 (m, 19H), 0.91 (t, *J* = 7.4 Hz, 3H), 0.76 (td, *J* = 7.4, 3.3 Hz, 9H).

^{13}C NMR (75 MHz, $CDCl_3$) δ = 172.0, 172.0, 171.6, 168.9, 168.8, 155.0, 154.9, 154.1, 147.3, 147.1, 146.9, 145.0, 144.9, 144.8, 62.1, 61.6, 61.5, 47.7, 47.4, 42.6, 39.6, 34.5, 34.5, 22.9, 22.9, 22.7, 17.7, 14.2, 14.1, 11.4, 11.0.

HPLC (Agilent, SB-C18, Water(0.1 formic acid)/MeOH 95:5 → 0:100, 30 min,0.3 ml/min, ESI): **3c** t_R = 20.3, **3c'** t_R = 20.5.

3c MS (ESI): *m/z* (relative intensity) 583 [M+Na^+],432 (9), 406 (17), 300 (8), 251 (5).

3c' MS (ESI): m/z (relative intensity) 583 [M+Na^+], 502(11), 406 (8), 300 (9).

HRMS (ESI-TOF): *m/z* [M+Na]+ calcd for $C_{26}H_{36}N_6O_8$+Na^+: 583.2487; found: 587.2493.

NMR spectra of 3c and 3c' (mixture of isomers)

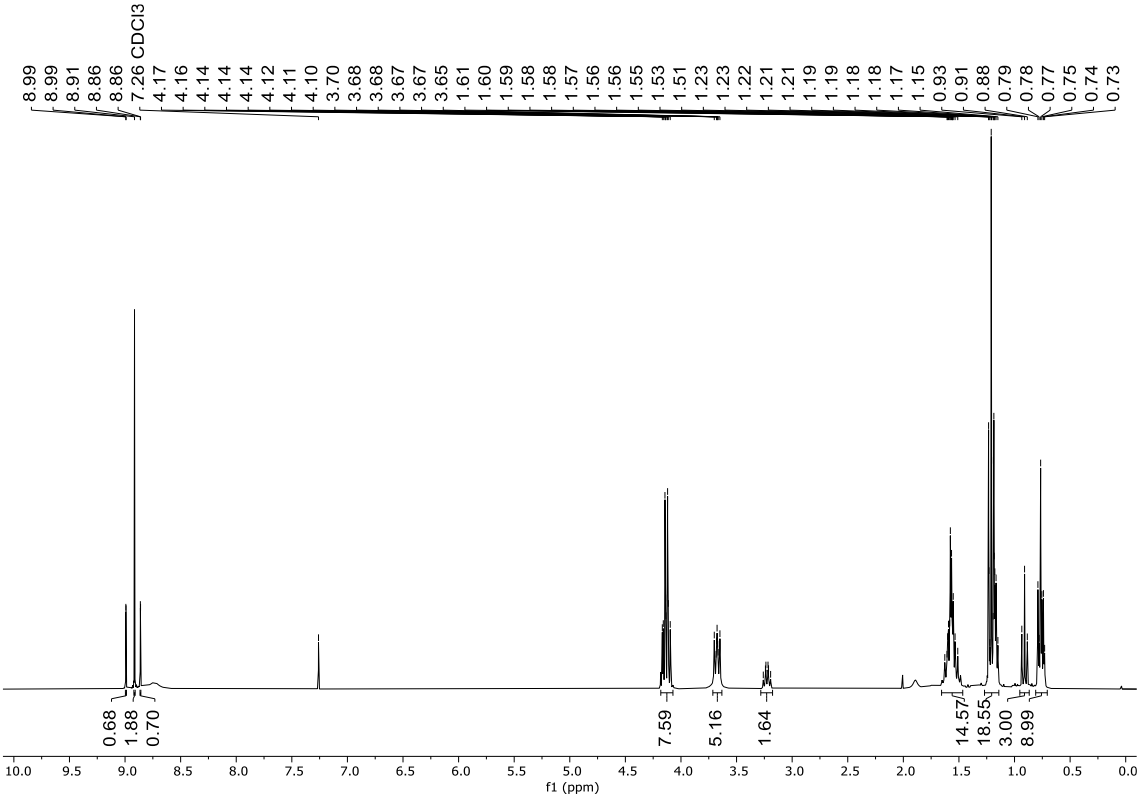

NMR spectrum 13. ^{1}H NMR (300 MHz, $CDCl_3$).

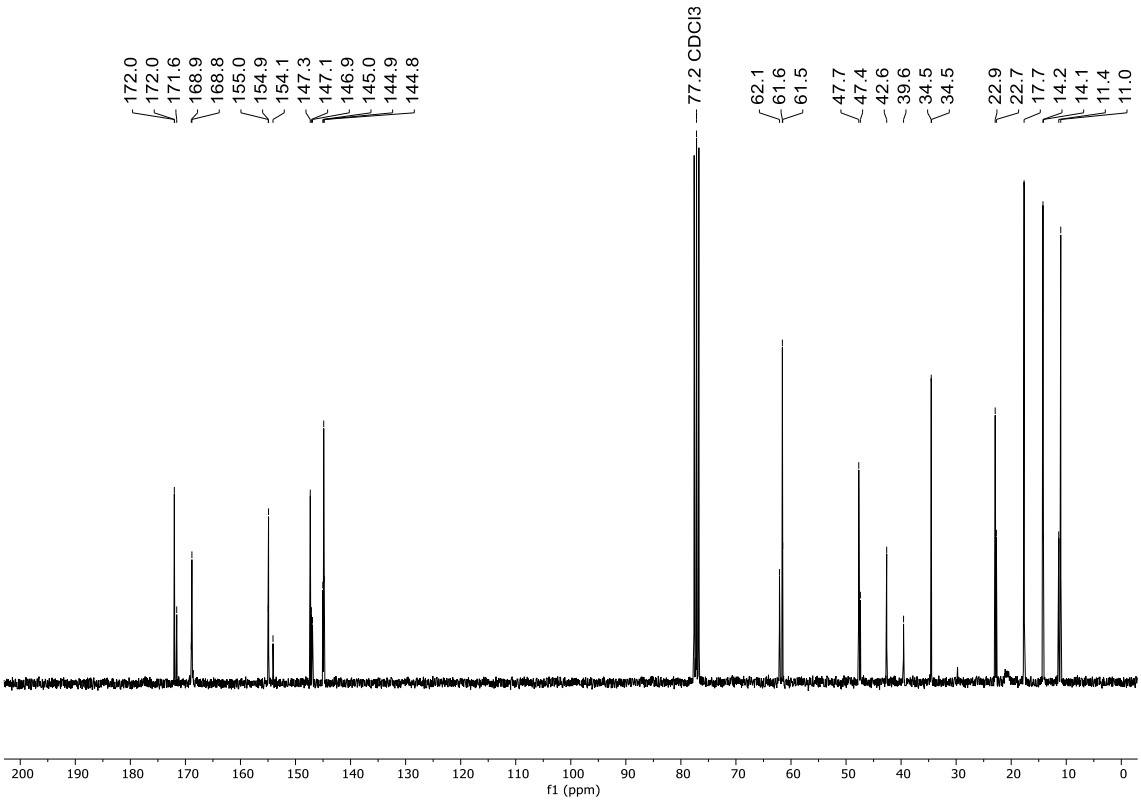

NMR spectrum 14. ^{13}C NMR (75 MHz, $CDCl_3$).

Synthesis of diethyl 1,1'-((((pyrazine-2,6 dicarbonyl)bis(propylazanediyl))bis-(carbonyl))bis(azanediyl))bis(cyclobutane-1-carboxylate) (3b)

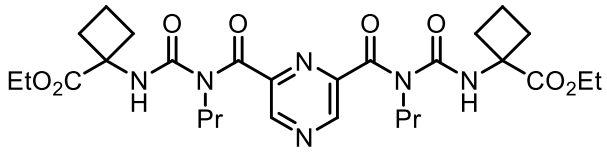

3b

Following the general procedure GP2, using 2,6-pyrazinedicarboxylic acid (**2**) (33.6 mg, 0.2 mmol) afforded the title compound **3b** (39.0 mg, 0.07 mmol, 33%) as a yellow viscous oil after purification by column chromatography (*n*-pentane:ethyl acetate = 2:1)

R_f = 0.65 (*n*-pentane/ethyl acetate = 1:1, UV)

m.p. = viscous oil at rt.

^{1}H NMR (400 MHz, $CDCl_3$) δ = 8.96 (s, 2H), 4.24 (q, *J* = 7.1 Hz, 4H), 3.74 – 3.64 (m, 4H), 2.73 – 2.61 (m, 4H), 2.45 – 2.33 (m, 4H), 2.14 – 2.01 (m, 4H), 1.64 – 1.54 (m, 4H), 1.29 (t, *J* = 7.1 Hz, 6H), 0.77 (t, *J* = 7.4 Hz, 6H).

^{13}C NMR (101 MHz, $CDCl_3$) δ = 173.2, 168.8, 153.1, 147.3, 145.1, 61.6, 58.9, 47.6, 31.5, 23.1, 15.4, 14.3, 11.1.

MS (ESI): *m/z* (relative intensity) 611 [M+Na^+], 446 (8), 420 (17), 251 (8).

HRMS (ESI-TOF): *m/z* [M+Na]$^+$ calcd for $C_{28}H_{40}N_6O_8$+Na^+: 611.2800 found; 611.2795

IR (ATR, neat, cm^{-1}): 3322(w), 2958(w), 2925(w), 2874(w), 2851(w), 1700(s), 1653(s), 1558(w), 1506(s), 1457(m), 1366(s), 1307(s), 1200(s), 1103(s), 1017(s), 876(w), 769(m), 731(m), 668(m), 565(m), 420(s), 401(m).

NMR spectra of compound 3b

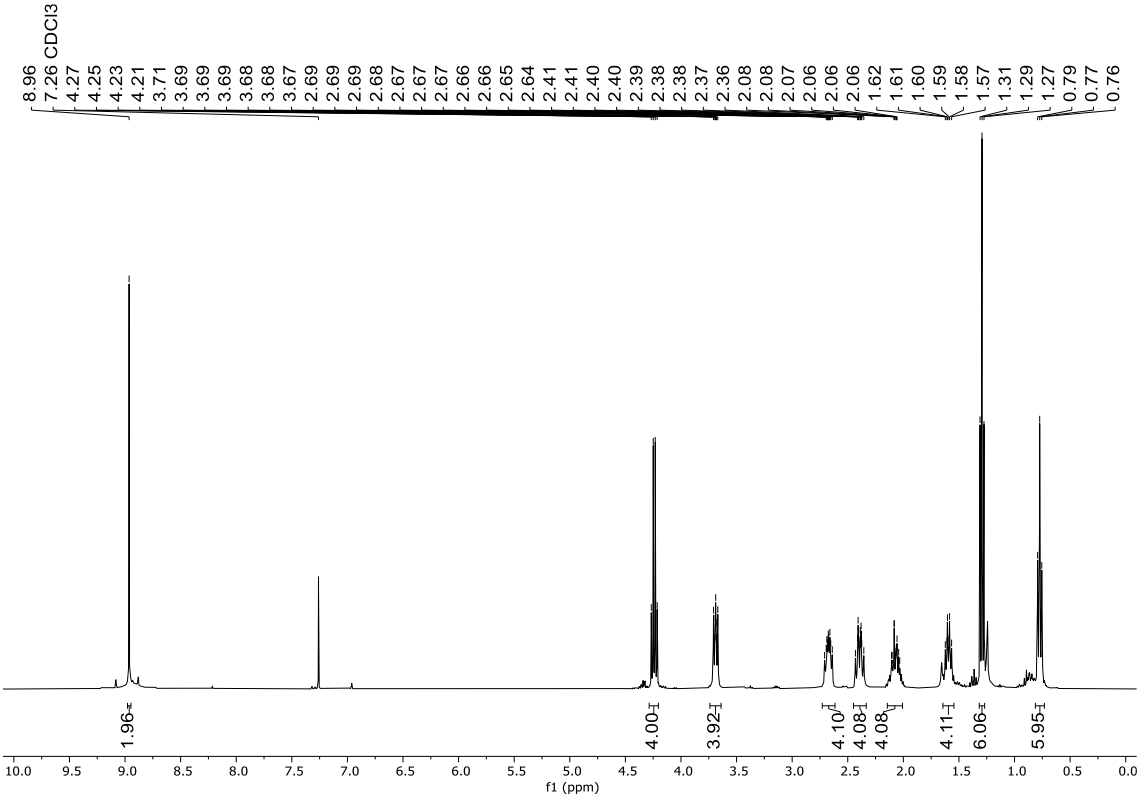

NMR spectrum 15. ^{1}H NMR (400 MHz, $CDCl_3$).

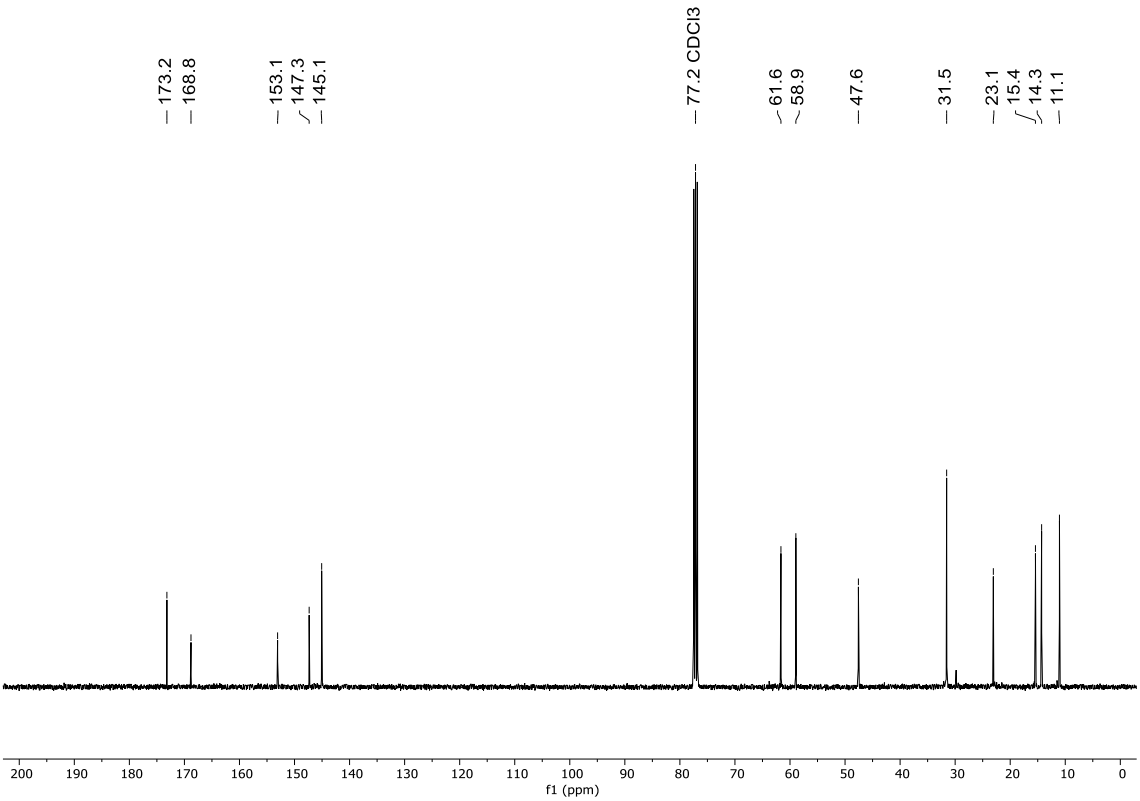

NMR spectrum 16. ^{13}C NMR (101 MHz, $CDCl_3$).

Synthesis of N^2,N^6-dipropyl-N^2,N^6-bis(propylcarbamoyl)pyrazine-2,6-dicarboxamide (3d)

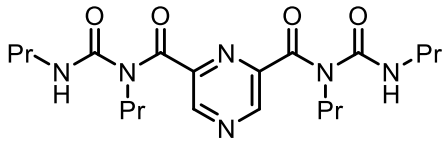

3d

Following the general procedure GP2, using 2,6-pyrazinedicarboxylic acid **2** (50.4 mg, 0.3 mmol) afforded the title compound **3d** (68.4 mg, 0.17 mmol, 56%) as a yellow solid after purification via column chromatography (*n*-pentane:ethyl acetate = 2:1)

R_f = 0.66 (*n*-pentane:ethyl acetate = 1:1, UV)

m.p. = 84-85 °C

^{1}H NMR (400 MHz, $CDCl_3$) δ = 8.92 (s, 2H), 8.42 (s, 2H), 3.75–3.61 (m, 4H), 3.30 (m, *J* = 7.1, 5.6 Hz, 4H), 1.67–1.52 (m, 8H), 0.96 (t, *J* = 7.4 Hz, 6H), 0.77 (t, *J* = 7.4 Hz, 6H).

^{13}C NMR (101 MHz, $CDCl_3$) δ = 168.9, 154.2, 147.6, 144.8, 47.7, 42.6, 23.2, 22.8, 11.5, 11.1.

MS (ESI): *m/z* (relative intensity) 443 [M+Na^+], 362 (24), 251 (7).

HRMS (ESI-TOF): *m/z* [M+Na]$^+$ calcd for $C_{20}H_{32}N_6O_4$+Na^+: 443.2377; found: 443.2385.

IR (ATR, neat, cm^{-1}): 3285(w), 2963(w), 2935(w), 2874(w), 1707(w), 1686(s), 1636(s), 1530(s), 1457(w), 1436(m), 1401(m), 1377(m), 1362(m), 1324(w), 1301(w), 1283(m), 1244(s), 1188(m), 1097(s), 1019(m), 974(w), 915(w), 889(w), 778(m), 768(w), 714(m), 655(m), 637(m), 598(w), 557(w), 507(w), 471(w), 425(m).

NMR spectra of compound 3d

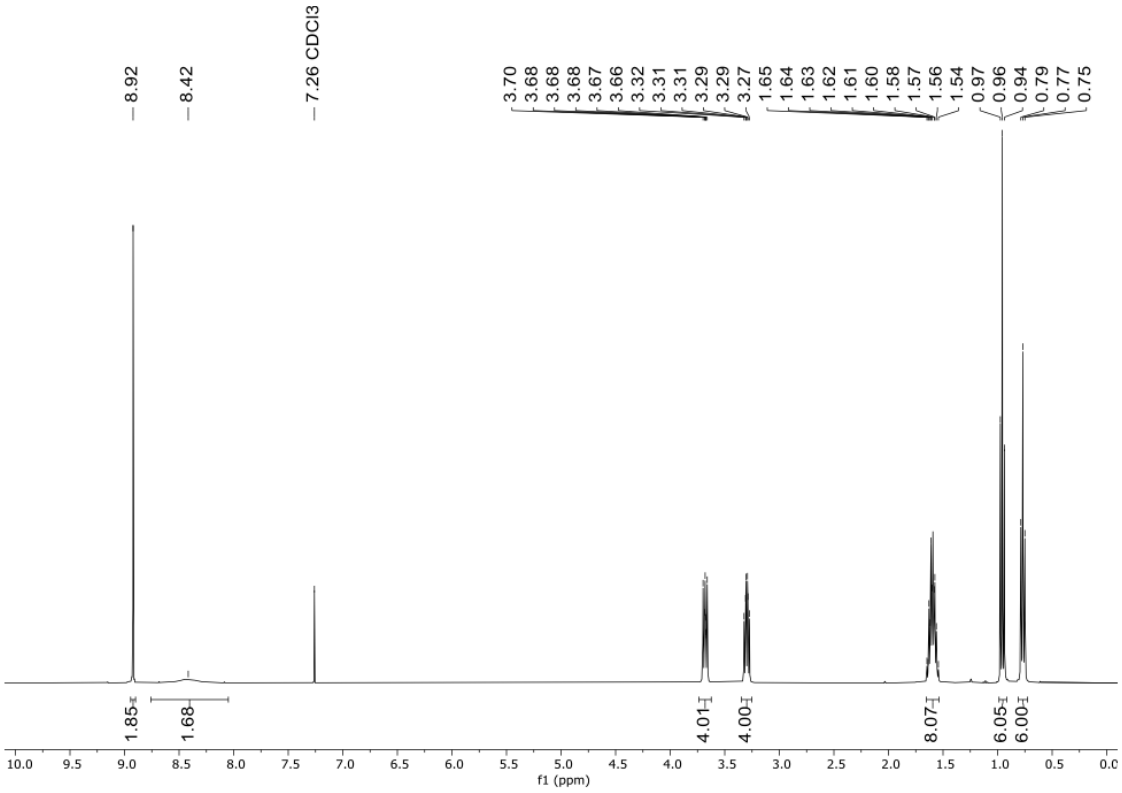

NMR spectrum 17. ^{1}H NMR (400 MHz, $CDCl_3$).

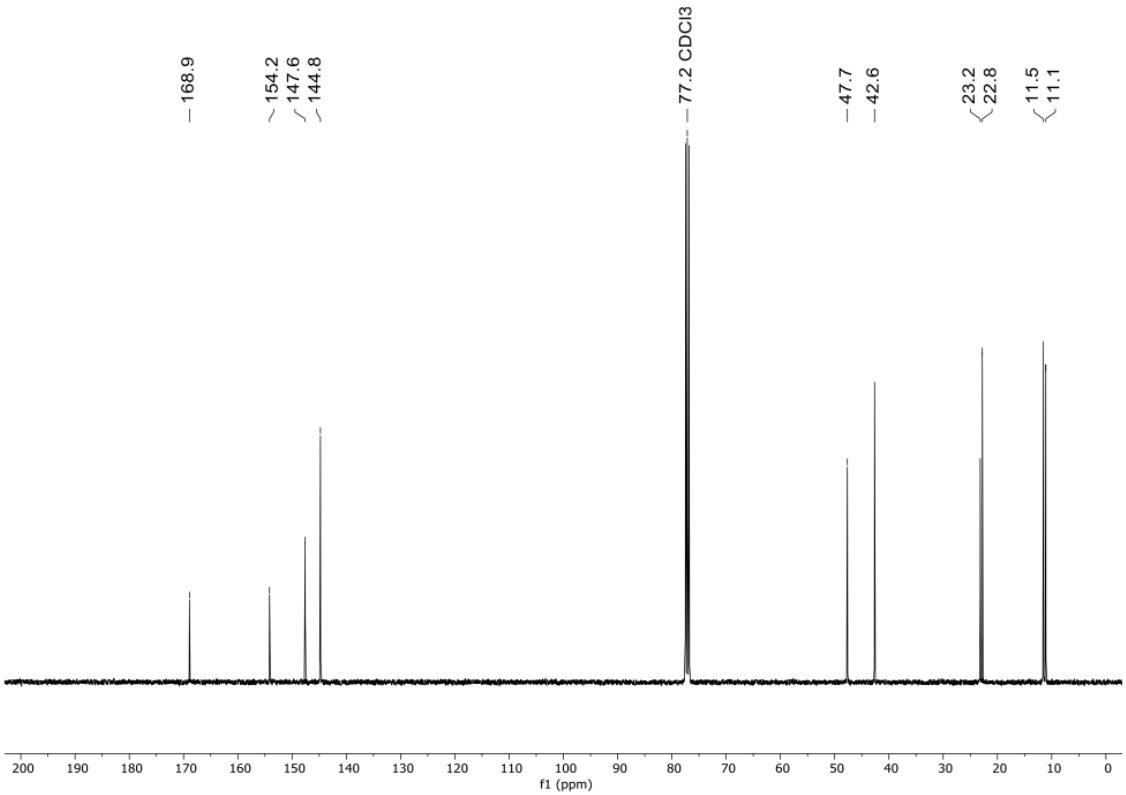

NMR spectrum 18. ^{13}C NMR (101 MHz, $CDCl_3$).

Crystallographic data of 3d

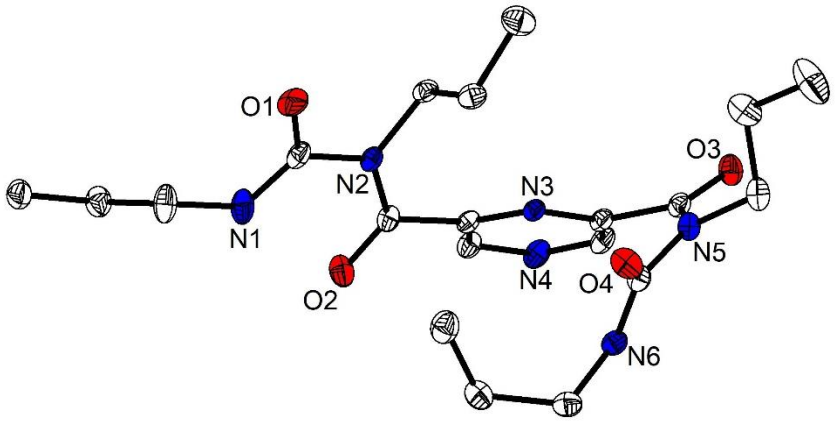

Table 8: Crystallographic data and refinement for **3d**.

chemical formula	$C_{20}H_{32}N_6O_4$
formula weight (g/mol)	420.51
crystal system, space group	Monoclinic, P 2_1/n
T (K)	150(2)
unit cell dimensions: a, b, c (Å)	*a*=8.8906(10), *b*=22.877(3), *c*=11.3070(13)
unit cell dimensions: α, β, γ (°)	α =90, β =104.467(2), γ =90
V (Å3)	2226.8(4)
Z	4
absorption coefficient μ (mm^{-1})	0.089
F (000)	904.0
crystal size (mm3), crystal habit	0.535·0.468·0.461, colorless, block
transmission Tmin, Tmax	0.618, 0.745
reflections collected	4372
independent reflections	4372
reflections with I > 2σ(I)	3859
goodness-of-fit on F2	1.093
final R indices [I > 2σ(I)]	R_1= 0.0448
final R indices [all data]	R_1=0.1215
no. of parameters	283
Δρmax, Δρmin (e $Å^{-3}$)	0.275, -0.193
R.M.S. deviation from mean (e $Å^{-3}$)	0.041

5.4.3 Synthesis of pyrimidopteridines through Carboxamide cyclization

Synthesis of diethyl 2,2'-(2,4,6,8-tetraoxo-3,7-dipropyl-3,4,7,8-tetrahydro-pyrimido[5,4-*g*]pteridine-1,9(2H,6H)-diyl)bis(2-methylpropanoate) (4a)

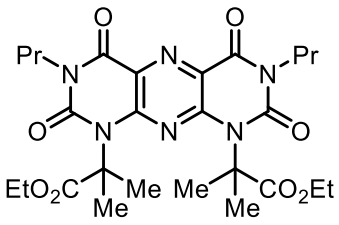

4a

Dipropylpyrazine-dicarboxamide (**3b**) (56.5 mg,0.1 mmol, 1.0 equiv.) was dissolved in MeCN (2 ml). AgF_2 (58.4 mg, 0.4 mmol, 4.0 equiv.) was quickly added to the rapidly stirring solution at ambient temperature. After stirring for 90 min, the crude reaction mixture was quenched by air and filtered through a plug of silica, rinsed Et_2O (5.0 mL). The resulting mixture was concentrated *in vacuo* and purified by column chromatography (*n*-pentane:ethyl acetate = 2:1), yielding the title compound **4a** (23.8 mg, 0.04 mmol, 42%) as a brown solid.

R_f = 0.69 (*n*-pentane:ethyl acetate = 1:1, UV)

m.p. = 95-98°C

^{1}H NMR (300 MHz, $CDCl_3$) δ = 4.13 (q, *J* = 7.1 Hz, 4H), 4.06 – 3.95 (m, 4H), 1.93 (s, 12H), 1.82 – 1.61 (m, 4H), 1.15 (t, *J* = 7.1 Hz, 6H), 0.96 (t, *J* = 7.4 Hz, 6H).

^{13}C NMR (75 MHz, $CDCl_3$) δ = 172.3, 157.7, 150.6, 148.3, 124.8, 66.0, 61.9, 44.3, 29.8, 24.8, 21.0, 14.1, 11.3.

MS (ESI): *m/z* (relative intensity) 583 [M+Na^+], 561 (59) [M+H^+], 332 (6).

HRMS (ESI-TOF): *m/z* [M+Na]$^+$ calcd for $C_{26}H_{36}N_6O_8$+Na^+: 583.2487; found: 583.2477.

IR (ATR, neat, cm^{-1}): 2962(w), 1735(m), 1719(m), 1700(m), 1696(m), 1685(s), 1675(s), 1672(s), 1669(s), 1648(w), 1560(m), 1554(s), 1550(s), 1545(s), 1419(m), 1388(m), 1272(m), 1139(m), 755(m), 507(m).

NMR spectra of compound 4a

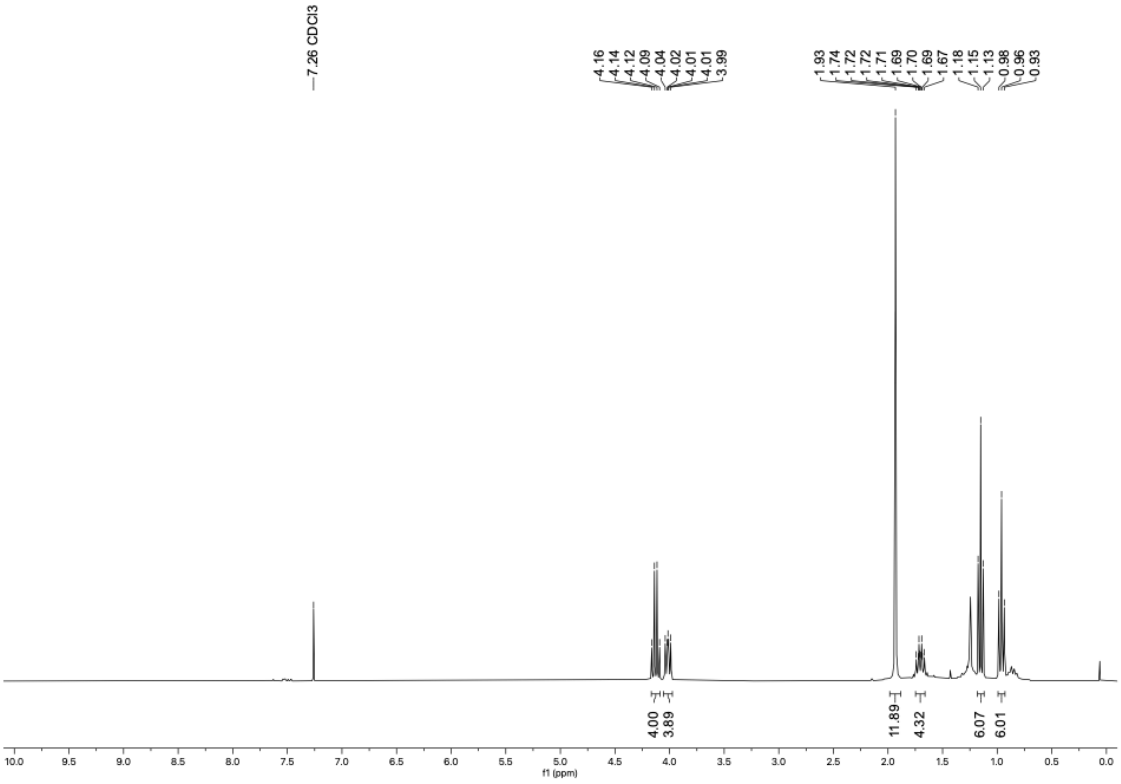

NMR spectrum 19. ^{1}H NMR (300 MHz, $CDCl_3$).

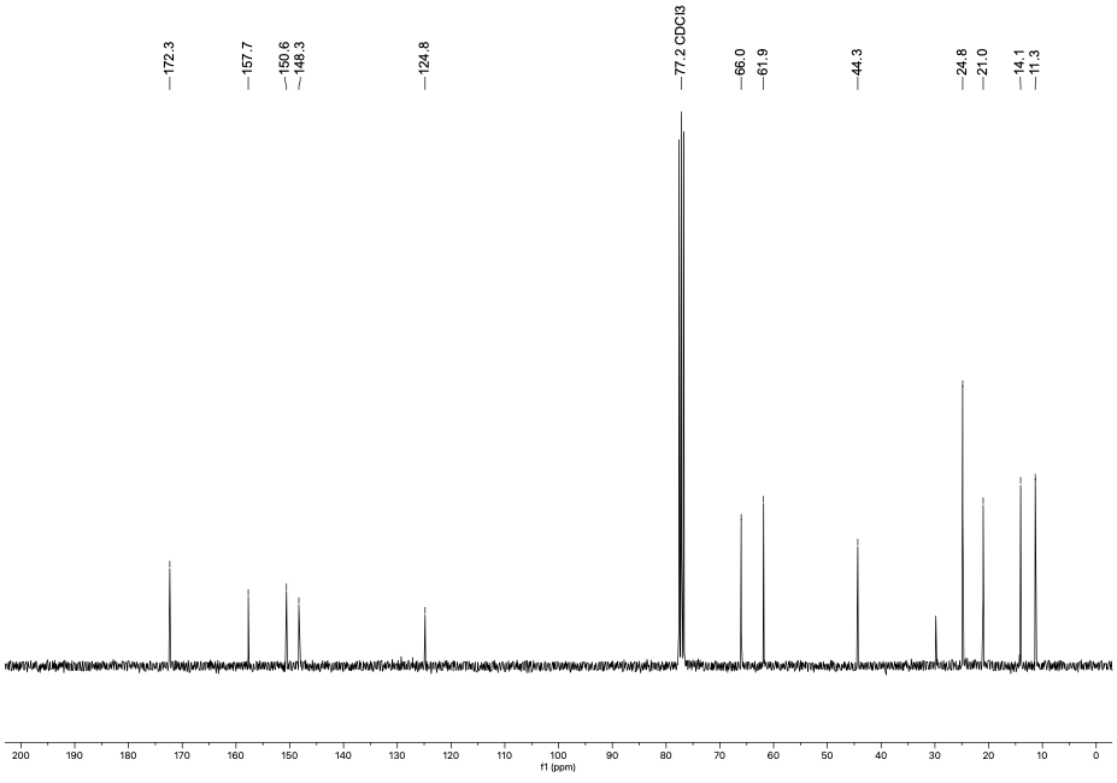

NMR spectrum 20. ^{13}C NMR (75 MHz, $CDCl_3$).

Synthesis of ethyl 2-(3-(1-(1-ethoxy-2-methyl-1-oxopropan-2-yl)-2,4-dioxo-3-propyl-1,2,3,4-tetrahydropteridine-7-carbonyl)-3-propylureido)-2-methylpropanoate (16)

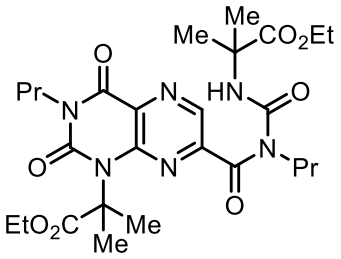

16

Dipropylpyrazine-dicarboxamide (**3a**) (56.5 mg,0.1 mmol, 1.0 equiv.) was dissolved in MeCN (2.0 ml). AgF_2 (86.0 mg, 0.6 mmol, 6.0 equiv.) was quickly added to the rapidly stirring solution at ambient temperature. After stirring for 60 min, the crude reaction mixture was quenched by air and filtered through a plug of silica, rinsed Et_2O (5.0 mL). The resulting mixture was concentrated *in vacuo* and purified by column chromatography (*n*-pentane:ethyl acetate = 2:1), yielding the title compound **16** (8.1 mg, 0.01 mmol, 14%) as an impure brown solid.

R_f = 0.79 (*n*-pentane/ethyl acetate = 1:1, UV)

MS (ESI): *m/z* (relative intensity) 585 [M+Na^+], 563 (81) [M+H^+].

HRMS (ESI-TOF): *m/z* [M+Na]$^+$ calcd for $C_{26}H_{38}N_6O_8$+Na^+: 585.2643; found: 585.2645.

NMR spectra of isolated fraction

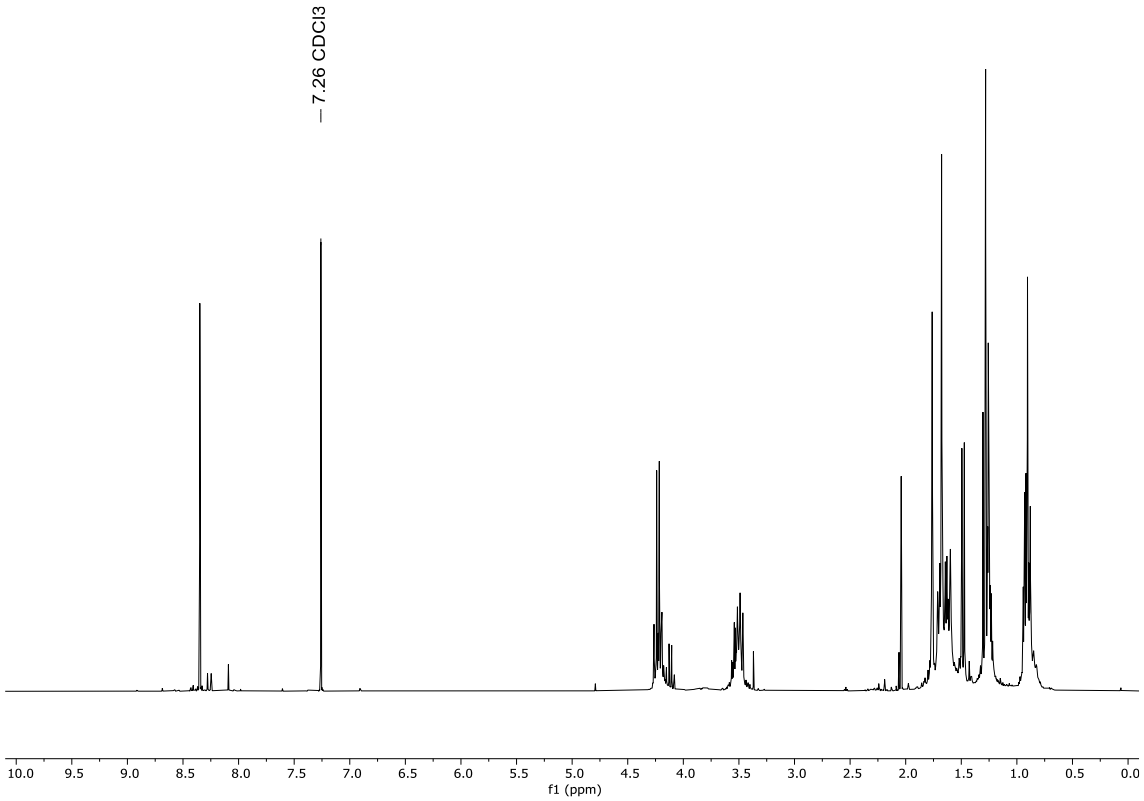

NMR spectrum 21. ^{1}H NMR (300 MHz, $CDCl_3$).

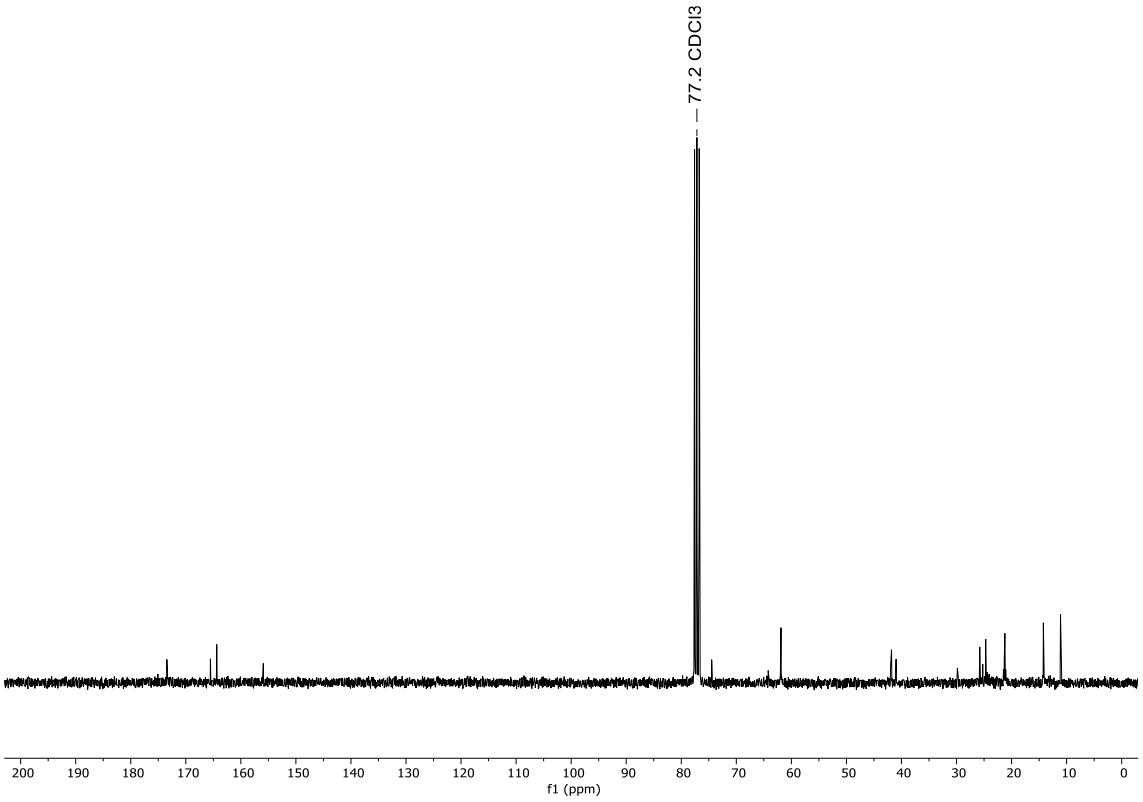

NMR spectrum 22. ^{13}C NMR (75 MHz, $CDCl_3$).

5.5 Electrochemical and photophysical characterization of PPT 4a

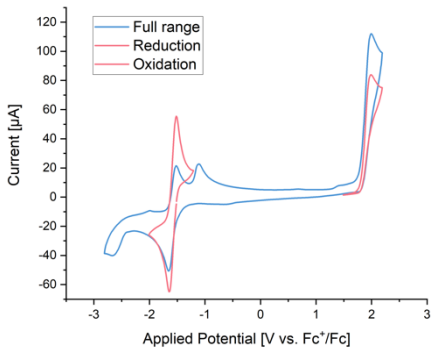

Figure 5: Full cyclic voltammogram of compound **4a** with oxidation and reduction event (red)

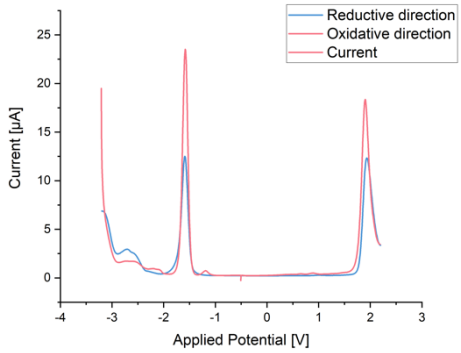

Figure 6: Differential puls voltammogram of **4a** in oxidative (red) and reductive direction (blue)

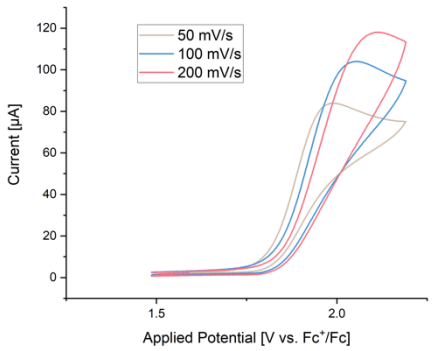

Figure 7: Cyclic voltammogram of the reduction event of **4a** with different scan rates

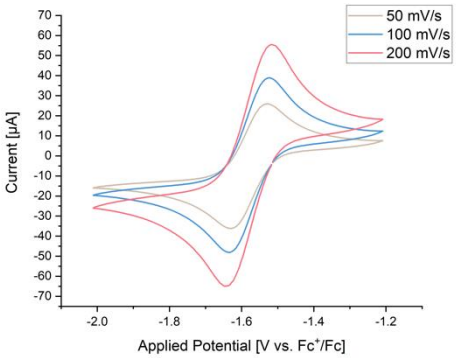

Figure 8: Cyclic voltammogram of the oxidation event of **4a** with different scan rates

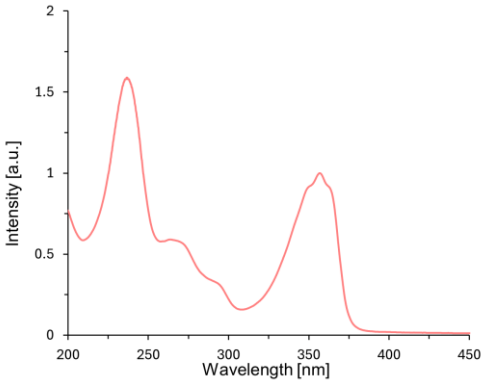

Figure 9: Emission spectrum of **4a** normalized to 1.

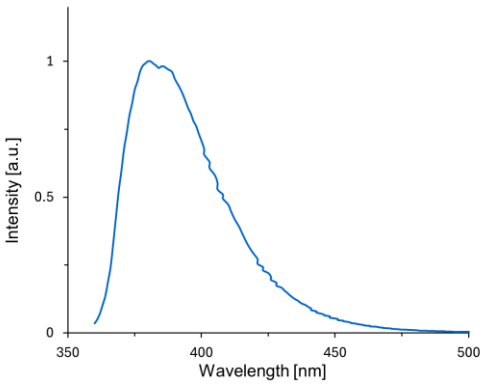

Figure 10: Absorption spectrum of **4a** normalized to 1.

6 References

[1] C. E. Wayne, R. P. Wayne, *Photochemistry*, Oxford Universitry Press, New York, **1996**.

[2] N. A. Romero, D. A. Nicewicz, *Chem. Rev.* **2016**, *116*, 10075–10166.

[3] S. E. Braslavsky, *Pure Appl. Chem.* **2007**, *79*, 293–465.

[4] T. Bortolato, S. Cuadros, G. Simionato, L. Dell'Amico, *Chem. Commun.* **2022**, *58*, 1263–1283.

[5] C. K. Prier, D. A. Rankic, D. W. C. MacMillan, *Chem. Rev.* **2013**, *113*, 5322–5363.

[6] S. A. Matlin, G. Mehta, H. Hopf, A. Krief, *Eur. J. Inorg. Chem.* **2019**, *2019*, 4170–4173.

[7] B. M. Hockin, C. Li, N. Robertson, E. Zysman-Colman, *Catal. Sci. Technol.* **2019**, *9*, 889–915.

[8] G. Noirbent, F. Dumur, *Catalysts* **2020**, *10*, 953.

[9] E. Speckmeier, T. G. Fischer, K. Zeitler, *J. Am. Chem. Soc.* **2018**, *140*, 15353–15365.

[10] R. Brimioulle, D. Lenhart, M. M. Maturi, T. Bach, *Angew. Chem., Int. Ed.* **2015**, *54*, 3872–3890.

[11] K. B. Sharpless, *Angew. Chem., Int. Ed.* **2002**, *41*, 2024–2032.

[12] R. Noyori, *Angew. Chem., Int. Ed.* **2002**, *41*, 2008–2022.

[13] W. S. Knowles, *Angew. Chem., Int. Ed.* **2002**, *41*, 1998–2007.

[14] I. Hargittai, *Struct. Chem.* **2022**, *33*, 303–305.

[15] C. Jiang, W. Chen, W.-H. Zheng, H. Lu, *Org. Biomol. Chem.* **2019**, *17*, 8673–8689.

[16] N. Y. Shin, J. M. Ryss, X. Zhang, S. J. Miller, R. R. Knowles, *Science* **2019**, *366*, 364–369.

[17] X. Huang, E. Meggers, *Acc. Chem. Res.* **2019**, *52*, 833–847.

[18] L. Zhang, E. Meggers, *Acc. Chem. Res.* **2017**, *50*, 320–330.

[19] F. Pecho, Y. Sempere, J. Gramüller, F. M. Hörmann, R. M. Gschwind, T. Bach, *J. Am. Chem. Soc.* **2021**, *143*, 9350–9354.

[20] T. Akiyama, J. Itoh, K. Yokota, K. Fuchibe, *Angew. Chem., Int. Ed.* **2004**, *43*, 1566–1568.

[21] A. Petrosyan, R. Hauptmann, J. Pospech, *Eur. J. Org. Chem.* **2018**, *2018*, 5237–5252.

[22] T. Hering, B. Mühldorf, R. Wolf, B. König, *Angew. Chem., Int. Ed.* **2016**, *55*, 5342–5345.

[23] Y. Maki, M. Sako, I. Oyabu, T. Murase, Y. Kitade, K. Hirota, *J. Chem. Soc. Chem. Commun.* **1989**, 1780–1782.

[24] M. Sako, K. Shimada, K. Hirota, Y. Maki, *Tetrahedron Lett.* **1986**, *27*, 3877–3880.

[25] M. Sako, S. Ohara, K. Shimada, K. Hirota, Y. Maki, *J. Chem. Soc., Perkin Trans. 1* **1990**, 863–868.

[26] M. Sako, K. Hirota, Y. Maki, *Chem. Pharm. Bull.* **1990**, *38*, 2069–2071.

[27] Y. Maki, M. Sako, I. Oyabu, T. Murase, Y. Kitade, K. Hirota, *J. Chem. Soc., Chem. Commun.* **1989**, 1780–1782.

[28] Y. Maki, I. Oyabu, S. Ohara, M. Sako, Y. Kitade, K. Hirota, *Chem. Pharm. Bull.* **1989**, *37*, 3239–3242.

[29] T. Taeufer, M. A. Argüello Cordero, A. Petrosyan, A.-E. Surkus, S. Lochbrunner, J. Pospech, *ChemPhotoChem* **2021**, *5*, 999–1003.

[30] R. Hauptmann, A. Petrosyan, F. Fennel, M. A. Argüello Cordero, A.-E. Surkus, J. Pospech, *Chem. – Eur. J.* **2019**, *25*, 4325–4329.

[31] T. Taeufer, R. Hauptmann, F. El-Hage, T. S. Mayer, H. Jiao, J. Rabeah, J. Pospech, *ACS Catal.* **2021**, *11*, 4862–4869.
[32] F. El-Hage, C. Schöll, J. Pospech, *J. Org. Chem.* **2020**, *85*, 13853–13867.
[33] A. Petrosyan, L. Zach, T. Taeufer, T. S. Mayer, J. Rabeah, J. Pospech, *Chem. – Eur. J.* **2022**, *28*, e202201761.
[34] T. S. Mayer, T. Taeufer, S. Brandt, J. Rabeah, J. Pospech, *J. Org. Chem.* **2023**, *88*, 6347–6353.
[35] A. M. D. P. Nicholas, D. R. Arnold, *Can. J. Chem.* **1982**, *60*, 2165–2179.
[36] T. Sato, in *Compr. Organomet. Chem. II*, Elsevier, Oxford, **1995**, pp. 355–387.
[37] M. Patel, R. Kumar, K. Kishor, T. Mlsna, C. U. Jr. Pittman, D. Mohan, *Chem. Rev.* **2019**, *119*, 3510–3673.
[38] M. J. Genzink, J. B. Kidd, W. B. Swords, T. P. Yoon, *Chem. Rev.* **2022**, *122*, 1654–1716.
[39] W. Yao, E. A. Bazan-Bergamino, M.-Y. Ngai, *ChemCatChem* **2022**, *14*, e202101292.
[40] J. Pospech, J. Fessler, H. D. Xuan, S. Brandt, T. Täufer, A. Kruse, S. Lochbrunner, *Synthesis* **2024**, DOI 10.1055/a-2403-2247.
[41] B. G. Hejna, J. M. Ganley, H. Shao, H. Tian, J. D. Ellefsen, N. J. Fastuca, K. N. Houk, S. J. Miller, R. R. Knowles, *J. Am. Chem. Soc.* **2023**, *145*, 16118–16129.
[42] E. Comeo, P. Trinh, A. T. Nguyen, C. J. Nowell, N. D. Kindon, M. Soave, L. A. Stoddart, J. M. White, S. J. Hill, B. Kellam, M. L. Halls, L. T. May, P. J. Scammells, *J. Med. Chem.* **2021**, *64*, 6670–6695.
[43] J. Clayden, N. Greeves, S. Warren, *Organic Chemistry*, OUP Oxford, **2012**.
[44] N. I. Nikishkin, J. Huskens, S. A. Ansari, P. K. Mohapatra, W. Verboom, *New J. Chem.* **2013**, *37*, 391–402.
[45] M. L. Bender, *Chem. Rev.* **1960**, *60*, 53–113.
[46] H. H. Jaffé, G. O. Doak, *J. Am. Chem. Soc.* **1955**, *77*, 4441–4444.
[47] I. Nicolas, O. Jeannin, D. Pichon, M. Fourmigué, *CrystEngComm* **2016**, *18*, 9325–9333.
[48] J. N. Phillips, *J. Chem. Soc.* **1956**, 1294–1304.
[49] M. L. Bender, B. W. Turnquest, *J. Am. Chem. Soc.* **1957**, *79*, 1656–1662.
[50] H. K. Hall, *J. Phys. Chem.* **1956**, *60*, 63–70.
[51] A. R. Katritzky, P. Simmons, *J. Chem. Soc.* **1960**, 1511.
[52] A. Hajduk, N. Ulrich, *Electrophoresis* **2023**, *44*, 1353–1360.
[53] S. F. Mason, *J. Chem. Soc.* **1959**, 1247–1253.
[54] G. Höfle, W. Steglich, H. Vorbrüggen, *Angew. Chem., Int. Ed. Engl.* **1978**, *17*, 569–583.
[55] A. C. Spivey, S. Arseniyadis, *Angew. Chem., Int. Ed.* **2004**, *43*, 5436–5441.
[56] F. Brotzel, B. Kempf, T. Singer, H. Zipse, H. Mayr, *Chem. – Eur. J.* **2007**, *13*, 336–345.
[57] A. J. Metrano, N. C. Abascal, B. Q. Mercado, E. K. Paulson, A. E. Hurtley, S. J. Miller, *J. Am. Chem. Soc.* **2017**, *139*, 492–516.
[58] S. Caron, E. McInturff, *Pract. Synth. Org. Chem.*, John Wiley & Sons, **2020**, pp. 231–246.
[59] R. Dorel, C. P. Grugel, A. M. Haydl, *Angew. Chem., Int. Ed.* **2019**, *58*, 17118–17129.
[60] R. S. J. Proctor, R. J. Phipps, *Angew. Chem., Int. Ed.* **2019**, *58*, 13666–13699.
[61] Y. Y. See, M. T. Morales-Colón, D. C. Bland, M. S. Sanford, *Acc. Chem. Res.* **2020**, *53*, 2372–2383.
[62] R. Szpera, D. F. J. Moseley, L. B. Smith, A. J. Sterling, V. Gouverneur, *Angew. Chem., Int. Ed.* **2019**, *58*, 14824–14848.
[63] W.-L. Hu, X.-G. Hu, L. Hunter, *Synthesis* **2017**, *49*, 4917–4930.

[64] P. S. Fier, J. F. Hartwig, *Science* **2013**, *342*, 956–960.
[65] P. S. Fier, J. F. Hartwig, *J. Am. Chem. Soc.* **2014**, *136*, 10139–10147.
[66] W. Tyrra, *Heteroat. Chem.* **2002**, *13*, 561–566.
[67] J. C. Bailar, H. J. Emeléus, R. Nyholm, A. F. Trotman-Dickenson, *Comprehensive Inorganic Chemistry*, Pergamon Press, Oxford, **1973**.
[68] C. Schotten, T. P. Nicholls, R. A. Bourne, N. Kapur, B. N. Nguyen, C. E. Willans, *Green Chem.* **2020**, *22*, 3358–3375.
[69] C. Zhu, N. W. J. Ang, T. H. Meyer, Y. Qiu, L. Ackermann, *ACS Cent. Sci.* **2021**, *7*, 415–431.
[70] C. Kingston, M. D. Palkowitz, Y. Takahira, J. C. Vantourout, B. K. Peters, Y. Kawamata, P. S. Baran, *Acc. Chem. Res.* **2020**, *53*, 72–83.
[71] B. A. Frontana-Uribe, R. D. Little, J. G. Ibanez, A. Palma, R. Vasquez-Medrano, *Green Chem.* **2010**, *12*, 2099–2119.
[72] R. Bartholomäus, F. Dommershausen, M. Thiele, N. S. Karanjule, K. Harms, U. Koert, *Chem. – Eur. J.* **2013**, *19*, 7423–7436.
[73] V. V. Pavlishchuk, A. W. Addison, *Inorg. Chim. Acta* **2000**, *298*, 97–102.